

Preparation and *in-situ* Spectroscopic Characterization of High-Energy Density Lithium-Sulphur Batteries

DISSERTATION

zur Erlangung des akademischen Grades

**Doctor rerum naturalium
(Dr. rer. nat.)**

vorgelegt

**dem Bereich Mathematik und Naturwissenschaften
der Technischen Universität Dresden**

von

M. Sc. Olga Grätz

geboren am 06.11.1991 in Chisinau, Republik Moldau

Verteidigt am: 21.01.2020

Gutachter: Prof. Dr. M. Stamm

Gutachter: Prof. Dr. L. Ionov

Die Dissertation wurde in der Zeit von 11/2015 bis 10/2019 im Leibniz-Institut für Polymerforschung Dresden e.V. angefertigt.

1 ACKNOWLEDGEMENTS

While working on this thesis, I received vast help and support, that I am extremely grateful for.

First of all, I would like to thank Prof. Manfred Stamm for the precious opportunity to conduct this project under his supervision, as well as for the numerous advices and tips that have given me inspiration. I also greatly appreciated his patience and understanding. I want to express my gratitude towards Prof. Leonid Ionov for his encouragement and tips well as Dr. Petra Uhlmann for the great working atmosphere within the group. I am, as well, very grateful to the Leibniz Institute for Polymer Research for allowing me to conduct this work and offering me all the necessary conditions and to the Technical University of Dresden for the opportunity to prepare this work and for the administrative guidance.

The scientific work relies to a great extent on the analytical work, so I wish to thank everyone who helped me out. Dr. Dieter Fischer and Julia Muche offered me great support in conducting Raman spectroscopy and interpreting the results, without mentioning the ample access to the measuring device. Michael Göbel provided SEM, EDX and X-ray analyses and interpretations, Dr. Victoria Albrecht performed the physisorption analyses, Dr. Hartmut Komber conducted NMR spectroscopy and Kerstin Arnhold carried TGA measurements out. Dr. Alexander Münch granted me access to the contact angle and UV-VIS measurement devices and gave me ample introduction to the work with said devices.

I also wish to thank the DFG project partners for the work we did together and for the numerous discussions during which new ideas were born. I had the chance to observe their work and learn about the methods they used.

I am extremely grateful to Janett Forkel for the ease with which she resolved all my administrative and organisational difficulties, as well as for her presence and availability. Also, I want to thank the battery group: Dr. Anne Freitag, Dr. Ivan Raguzin, Dr. Anna Urbanski, Dr. Soumyadip Choudhury, Dr. Mazen Azizi and Dr. Kathrin Müller for their help and the numerous advices I received during these years. I am glad to call them friends.

This work has been made possible through the financial support received from the Deutsche Forschungsgemeinschaft (DFG Project ISIBAT No 330114). Also, I am grateful to Celgard and Freudenberg for the received samples, that permitted me to conduct the experiments.

Finally, I would like to express my profound gratitude towards my friends and family. My parents guided and supported me through my entire life, and it is thanks to them that I became a person capable of undertaking such a project. My husband has always been there for me and believed in me even then, when I didn't. My dear friends, Daniela, Alina, Claire, Marion, Madeleine, Claudia, Anna, Juliane, Martin and many others are the people that shared with me both the good and bad moments of my life, making it full and worth living.

This work is, to a great extent, the achievement all of these amazing people. Thank you.

2 TABLE OF CONTENTS

1	Danksagung/Acknowledgements.....	I
2	Table of Contents	1
2.1	<i>LIST OF ABBREVIATIONS</i>	<i>VI</i>
3	Motivation and Aim	1
3.1	<i>MOTIVATION.....</i>	<i>1</i>
3.2	<i>AIM</i>	<i>3</i>
4	Theoretical Background.....	5
4.1	<i>BATTERIES AND ACCUMULATORS</i>	<i>5</i>
4.1.1	Working Principle	5
4.1.2	Comparison of Battery Types	6
4.1.2.1	Lead-acid.....	7
4.1.2.2	Nickel-based batteries	8
4.1.2.3	Lithium-Ion (Li-Ion)	9
4.1.2.4	Lithium-Sulphur	11
4.1.2.5	Lithium-Air	11
4.2	<i>LITHIUM-SULPHUR CELL.....</i>	<i>12</i>
4.2.1	Mechanism	12
4.2.2	Problems to Be Solved.....	14
4.2.2.1	Insulating Nature of Sulphur	14
4.2.2.2	Volume Variation throughout the Cycling.....	15
4.2.2.3	Dendrite Growth at the Anode Surface.....	15
4.2.2.4	Polysulphide shuttle	15
4.2.3	Battery components.....	17
4.2.3.1	Cell casing	17
4.2.3.2	Cathode	18
4.2.3.3	Separator	19
4.2.3.4	Electrolyte.....	20
4.2.3.1	Anode.....	22
4.3	<i>IN-SITU ANALYSIS OF LITHIUM-SULPHUR BATTERIES</i>	<i>24</i>
4.3.1	Methods	24
4.3.1.1	XRD	24

IV

4.3.1.2 SEM	25
4.3.1.3 UV-Vis.....	25
4.3.1.4 HPLC	25
4.3.1.5 NEXAFS	26
4.3.2 Raman Spectroscopy.....	26
4.3.2.1 Theory behind Raman Spectroscopy	26
4.3.2.2 Developments in the domain of Raman spectroscopy - problems and solutions	29
4.3.2.3 Choice of Analysis Conditions	31
4.3.2.4 Theoretical calculation of Raman spectra.....	33
4.3.2.5 Overview of Literature handling Lithium Polysulphide Analysis by Raman Spectroscopy	33
5 Experimental Part	42
5.1 MATERIALS.....	42
5.2 CELL COMPONENT FABRICATION AND CELL ASSEMBLY	43
5.2.1 Cathode.....	43
5.2.2 Electrolyte	44
5.2.3 Electrochemical Cells	44
5.3 RAMAN SPECTROSCOPY.....	45
5.3.1 Cell for In-Situ, In-Operando Measurements.....	45
5.3.2 Analysis Setup	46
5.4 MATERIAL AND PERFORMANCE ANALYSIS.....	47
5.4.1 Scanning Electron Microscopy (SEM).....	47
5.4.2 Thermogravimetric Analysis (TGA)	48
5.4.3 Gas Sorption Analysis.....	48
5.4.4 Electrical Conductivity.....	49
5.4.5 Contact Angle Measurement	49
5.4.6 Galvanostatic Charge-Discharge	50
6 Results and Discussion.....	51
6.1 ADJUSTMENT OF STANDARD CELL.....	51
6.1.1 Binder and Current Collector	51
6.1.2 Separator.....	54
6.2 IN-SITU AND IN-OPERANDO ANALYSIS.....	58

6.2.1	Analysis of Cell Components and Polysulphide Solutions	58
6.2.2	Modified Swagelok® Cell	59
6.2.2.1	First Swagelok® Cell Modification	59
6.2.2.2	Second Swagelok® Cell Modification.....	61
6.2.3	Modified Coin Cell	66
6.2.3.1	Test of the Electrochemical Performance of the Modified Cell	66
6.2.3.1	Raman analysis: results and interpretation.....	67
6.2.3.1	Comparison of the Results Obtained by Raman and NEXAFS Spectroscopy.	71
6.3	<i>RESORCINOL-FORMALDEHYDE BASED CARBON MATERIALS</i>	75
6.3.1	Processing Conditions.....	76
6.3.1.1	Drying of the Gels	76
6.3.1.1	Pyrolysis of the gels	77
6.3.2	Obtained Results	78
6.4	<i>SEPARATOR MODIFICATION</i>	90
6.4.1	Polyethersulphone as Separator Material.....	90
6.4.2	Functionalization of the Celgard Separators	95
7	Summary and Outlook.....	99
7.1	<i>SUMMARY</i>	99
7.2	<i>OUTLOOK</i>	102
8	References	104
9	Appendix	110
9.1	<i>SUPPLEMENTARY DATA</i>	110
9.2	<i>TABLE OF FIGURES</i>	110
9.3	<i>TABLE OF TABLES</i>	113
10	Erklärung gemäß §5 Abs. 1 Punkt 5	114

2.1 LIST OF ABBREVIATIONS

BSE	Backscattered electrons
CCD	Charge coupled device
CMC	Carboxymethyl cellulose
CRS	Coherent Raman scattering
CV	Cyclovoltammetry
DFT	Density functional theory
DME	Dimethoxyethane
DOD	Depth of discharge
DOL	Dioxolane
EDX	Energy-dispersive X-ray spectroscopy
EIS	Electrochemical impedance spectroscopy
HPLC	High-performance liquid chromatography
IL	Ionic liquid
LiBOB	Lithium bis(oxalate)borate
Li-ion	Lithium-ion
LiPS	Lithium polysulfide
Li-S	lithium-sulphur
LiTFSI	Lithium bis(trifluoromethanesulfonyl)imide
NEXAFS	Near edge X-ray absorption fine structure
Ni-Cd	Nickel-cadmium
NMP	N-Methyl-2-Pyrrolidone
OCV	Open circuit voltage
PE	Polyethylene

VII

PP	Polypropylene
PTFE	poly(tetrafluoroethylene)
PVDF	polyvinylidene fluoride
QMD	Quantum mechanical dispersion
SE	Secondary electrons
SEI	Solid electrolyte interface
SEM	Scanning electron microscopy
SoC	State of charge
TEGDME	Triethylene glycol monomethyl ether
THF	Tetrahydrofurane
XANES	X-ray absorption near edge structure
XRD	X-ray diffraction

3 MOTIVATION AND AIM

3.1 MOTIVATION

Energy is one of the main resources of the modern world. If several hundred years ago humanity relied on working animals and on biofuels, the present way of life requires a much higher amount of energy. In effect, the energy consumption has been growing exponentially over the past 150 years, as one can see in data gathered from US (**Figure 3.1**).¹

Some researchers call the present “Anthropocene”: a human-dominated epoch.² The amount of energy used nowadays for human activities is comparable to the sum of the biological processes involved in the food production for the whole humankind.³

One can roughly divide all energy sources available on Earth into three categories - fossil, nuclear and renewable. The fossil and nuclear fuels are, correspondingly, non-renewable.

The extensive use of fossil fuels, in the last century and nowadays, poses major problems. Although there are large amounts of coal, natural gas and petroleum still available on Earth, they are still finite and, at the rate at which we presently consume them, they will be depleted within a couple of generations. This not only implies that the humanity of the future will not have this energy source at hand anymore; it also might lead to a collapse of the chemical industry, pharmaceuticals and polymer materials. Additionally, the issue of the pollution cannot be understated: polluted air (household and ambient) is held responsible for 6,4 millions of deaths worldwide in 2015, the toll being almost as high as that of tobacco⁴; it is also highly detrimental for the environment. Last but not least comes the global warming issue. During the Little Ice Age in the average temperature in the Northern Hemisphere only changed by less than 0.5K,⁴ while still having major repercussions. At present, the researchers predict a 2K temperature variation in the most optimistic of the cases,⁵ which will lead to drastic environmental, economic and geopolitical problems. Even though this grim prospect might be unavoidable without swift and

Energy consumption in the United States (1776-2015)

quadrillion Btu

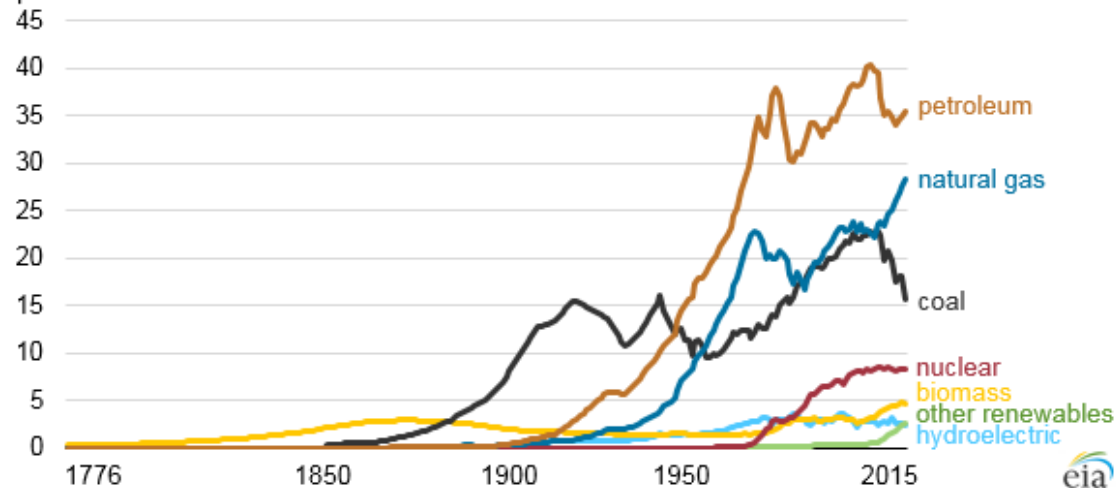


Figure 3.1 Energy consumption of the US over time, illustrating the never-ending growth of the amount of energy necessary for the functioning of the society

drastic changes, the consequences may be at least softened by more conscient behaviour and the adoption of alternative energy sources.

The renewable energy sources are biomass, hydropower, sunlight, wind, tides and geothermal heat. Solar and wind energy have seen constant growth over the past decades. By 2018, they account for almost 30% of the electricity produced in Germany.⁶ Since the energy provided is mechanical (wind) or light (solar), it cannot be kept in a container until need arises, like the fossil fuels for example. That is why the situations of high demand and low supply (in the absence of sunlight or wind), as well as high supply and low demand (for example in the early morning hours, when the wind is strong, but the people are still asleep), are frequent and problematic. This “green” energy has to be stored and released when need arises in order to be competitive. Another problem is the routing of said energy to the consumers, which is generally solved by the construction of a so called “super grid”. Additionally, a further problem is the fact that transportation accounts for a third of the global energy consumption and the vast majority of the vehicles function off fossil fuels. The alternative, electric cars, are at the moment unable to compete in the points of price and comfort.

So, it became apparent, that one of the main challenges of our time is the storage of clean energy, and the scientific and industrial communities have already come up with a considerable amount of solutions for this problem. All of these solutions, however, have their ups and downs.

As it can be seen in **Figure 3.2**⁷, the electrochemical energy storage, which encompasses all battery types, only accounts for 1% of the global energy storage. Nonetheless, it is vital for the situations in which mobility is required – contrary to a pumped hydro plant, a battery can be

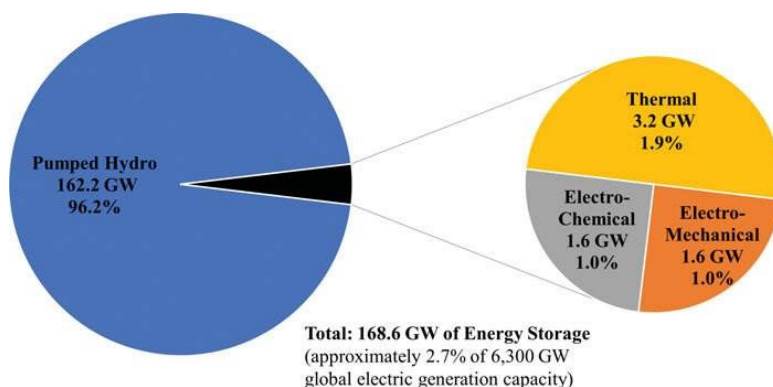


Figure 3.2 Energy storage compared by their share on overall energy stored sorted by type

produced in almost any size and thus placed anywhere. This hold potential for all the electronic devices, the electric cars, planes and boats.

The topic of my thesis, the lithium-sulphur battery, has very promising properties in this regard. For example, it has a theoretic capacity which is over six times higher than that of the present leader, the lithium-ion battery. Other benefits include the fact that the used sulphur is non-toxic to humans or the environment, very cost-effective and abundant.¹

3.2 AIM

The ultimate goal of this work is, as ambitious as it sounds, to enhance the properties of Li-S batteries in order to combat some of the downsides. To do this, the work is divided into several parts.

In order to find out where the problem lies and how it can be handled, one has to obtain a thorough understanding of the processes taking place inside the battery, how they are influenced by different parameters and how they correlate with the cell's performance. To do this, together with the project partners, we undertook a thorough in-situ, in operando study of the Li-S cell. In my capacity I was responsible for designing an in-situ cell, conducting Raman spectroscopy and interpreting the obtained results. The benefits of this study include gaining intrinsic information, the development of an analysis method which could be used routinely and the possibility to tailor cell modifications based on the newly acquired data.

One of the main reasons for the performance loss faced by Li-S batteries is the polysulphide shuttle: the migration of active material away from the cathode. The most promising approach to limit this effect consists in prohibiting the soluble polysulphides to leave the cathode in the first place, which can be achieved by tailoring the encapsulating material. There already exists a large

¹ a more thorough comparison with other battery systems will be undertaken in the chapter 4.1.2

variety of carbons for the use in the Li-S cathodes, but not all of them can be realistically used on an industrial scale because of the complexity of their synthetical protocols. In this part, I undertook a study of carbon derived from resorcinol-formaldehyde aerogel as a possible cathode material, since it is a material that is already well-known and involves a easily scalable protocol.

Contrarily to the cathode materials, other cell components are not as widely researched upon. The separator, whose main purpose is to prohibit any contact between the two electrodes, can also perform a side-job: that of stopping the lithium polysulphides from diffusing away from the cathode and all the way to the anode. For this reason, as a third part of this work, the focus was set on two approaches to improve on the separator. One of them consisted of coating a commercial separator with a polymer hindering the passage of the polysulphides by reducing the overall porosity and via physicochemical interactions. The other was based on the chemical modification of said commercial separators so that they slow the polysulphides down solely by physicochemical interactions.

4 THEORETICAL BACKGROUND

4.1 BATTERIES* AND ACCUMULATORS

The first “true” battery** was invented by Alessandro Volta in 1800 and consisted of superposed zinc and copper plates, separated by a piece of cardboard. It was soaked in an aqueous salt solution. A few decades later, John Frederic Daniell presented his improvement upon the voltaic pile, which was quickly adopted by the industry.⁸ It is still known and, in a way, used today: the easy to build battery is perfect for the teaching of electrochemistry in schools.

4.1.1 Working Principle

The functioning of any battery is linked with the conversion of chemical energy to electrical energy. When a redox reaction occurs, an electron transfer has to take place (**Equation 1**).



The voltaic cell is then constructed in such a way, that the chemical reaction proceeds on two planes. On one side, there is the electron transfer, which occurs indirectly, through a specifically designated channel. Thus, an electric current is generated. On the other side, there is the ionic exchange, which takes place directly in the cell and is ensured by a carefully chosen electrolyte.

The cell can be divided into two half-cells, each consisting of an electrode (anode or cathode) and electrolyte (**Figure 4.1A**). Its electromotive force, also called open-circuit voltage (OCV), represents the difference between the potentials of the electrode active materials. For example, for the case of the Cu-Zn cell, it is of 1.1 V. The real voltage of the cell is affected by its internal resistance and differs from the OCV.

There are several properties that characterize the cell’s performance. First, there is the nominal voltage, stated earlier. It is sometimes also referred to as “tension”, which is a more figurative term. Then, there is the power, expressed in Watt, which represents the rate of energy transfer, calculated by multiplying voltage and current, and lastly there is the power density

* The name “battery” is prone to error. The term has been coined by Benjamin Franklin and referred to several cells (Leyden jars) connected together, in analogy to the military notion. Nonetheless, in this work I will be using the words “battery” and “cell” interchangeably, knowing that I have only been studying single electrochemical cells. Besides, one makes the difference between primary, non-rechargeable and secondary, rechargeable, batteries, also known as accumulators.

** There might be an earlier battery, the Baghdad battery, of approximately two thousand years old, but it is only an assumption that the set of artefacts has once been a galvanic cell. ¹⁵⁶

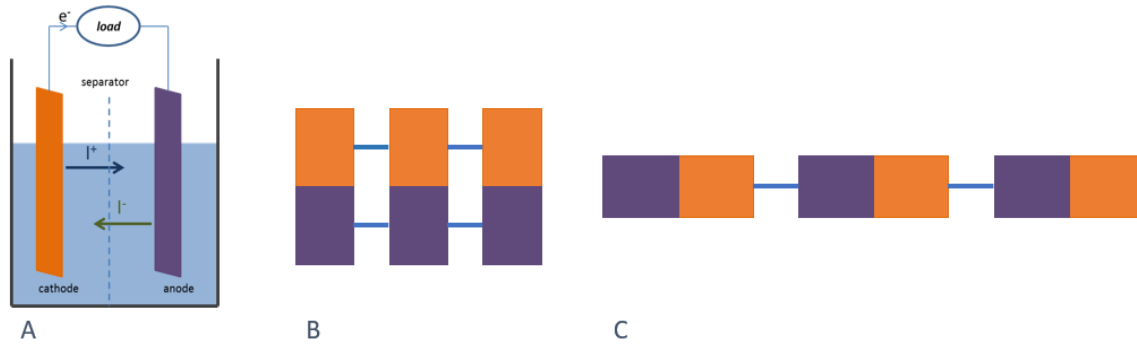


Figure 4.1 Schematic representation of a battery cell and the connection possibilities of several cells: (A); parallel connection (B); series connection (C).

($\text{W}\cdot\text{m}^{-3}$) – the amount of power per unit of volume and the specific power ($\text{W}\cdot\text{kg}^{-1}$) – the amount of power per unit of weight. It represents the loading capability of the battery.

The charge stored by the cell is given by the capacity ($\text{A}\cdot\text{h}$). It is directly linked to the amount of active material: the cell will function for as long as an electrochemical reaction can occur. The energy density ($\text{J}\cdot\text{m}^{-3}$) represents the amount of energy stored per unit of volume and the specific energy – the amount stored per unit of mass ($\text{J}\cdot\text{kg}^{-1}$).

As it was stated before, single cells can consequently be connected into packs. If one needs higher currents, the cells will be connected in parallel (**Figure 4.1B**). For higher voltages, they will be connected in series (**Figure 4.1C**).

4.1.2 Comparison of Battery Types

Since the need for energy sources has been steadily increasing over the past centuries, extensive research has been undertaken in the domain of battery development. A wide variety of cells are already in use, others are still under development. In order to better place the lithium-sulphur (Li-S) battery amongst them, some of the more common batteries, along with their characteristics will be discussed in this chapter.

First of all, the batteries are differentiated into two major categories - primary and secondary. The primary batteries are only used once and discarded after discharge. Their advantages revolve around the comfort of use – accessibility, freedom from utility power, long shelf life. This is why they are, and will continue to, being used for military, rescue or medical applications. They, nonetheless, have a major disadvantage, which is the damage to the environment. Primary batteries are source of hazardous waste and, besides, their manufacture takes typically 50 times more energy than they can ultimately store.⁹ Although attempts are made to recharge primary batteries, this undertaking is still in its beginnings.

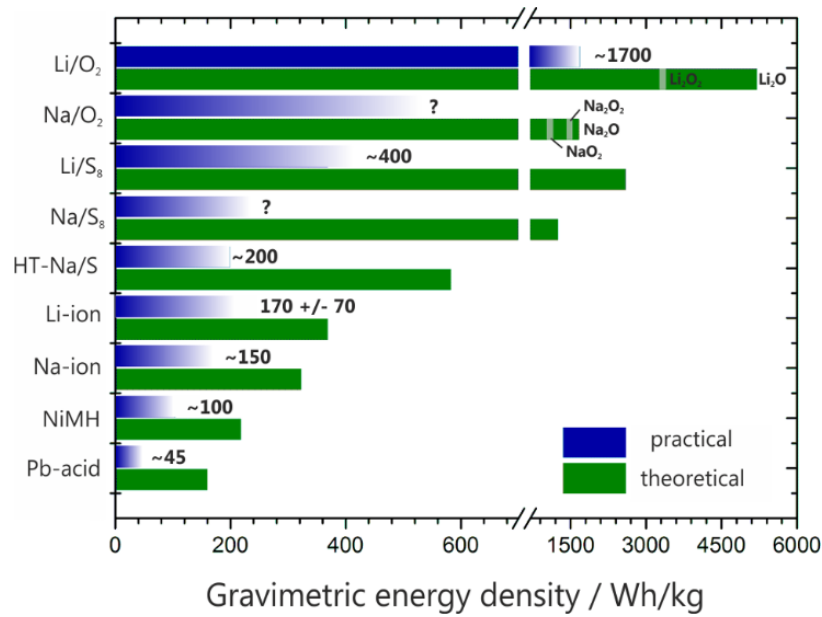


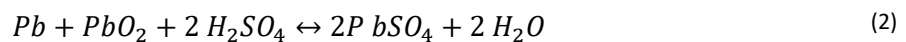
Figure 4.2 Comparison of different battery technologies according to their theoretic performances and already obtained practical results

Secondary batteries, also called accumulators, are batteries that can be discharged and recharged multiple times. Their initial cost is greatly exceeding that of primary batteries, but it can be divided between the multiple cycles of the cell. This makes them considerably more economic – less money and raw materials are wasted. They also typically perform better when discharged at high currents than primary batteries do.¹⁰

There is a wide variety of accumulators, some of which are already being used, while the others are still under development. Their performances are compared in **Figure 4.2**.¹¹ This graph certainly only compares them following one parameter, and other important characteristics like cycling stability or safety are not mentioned, but it illustrates the potential of the battery types.

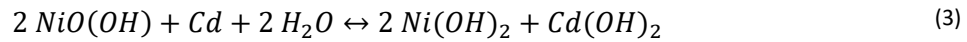
4.1.2.1 Lead-acid

The first rechargeable battery was invented by the French physicist Gaston Planté in 1859 and is still actively used today.¹² Despite it having a low capacity and being not environmentally friendly, it has a high power density, low self-discharge and is cheap, which makes it the perfect choice for automobile starter motors. The cell is using lead and lead oxide with sulfuric acid as electrolyte (**Equation 2**).¹³



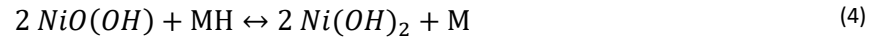
4.1.2.2 Nickel-based batteries

Nickel-cadmium (Ni-Cd) batteries have been invented at the end of the nineteenth century and were already commercially available in the early 1900s.¹⁴ They use nickel oxyhydroxide (NiOOH) as cathode and cadmium as anode (**Equation 3**). They have been the main choice for portable devices for a big part of the twentieth century and are still in use today. They are particularly prized for being very rugged and forgiving, as well as for performing in low-temperature conditions. Although nickel-cadmium batteries are expensive in production, their cost per cycle is one of the best on the market.



However, their specific energy is low compared to newer systems, they develop so-called “memory effects”¹⁵ and, most importantly, the toxicity of the cadmium is a concern.*

Nickel-metal hydride appeared at the end of the twentieth century, as an alternative to nickel-cadmium¹⁰. They use the same cathode material as Ni-Cd and a hydrogen-adsorbing metallic alloy as anode, instead of the toxic cadmium (**Equation 4 and Figure 4.3**¹⁶).



They are used in hybrid electric vehicles since 2001¹⁷ and are appreciated, foremost, for the higher environmental safety than Ni-Cd batteries. They also boast higher specific capacity, a

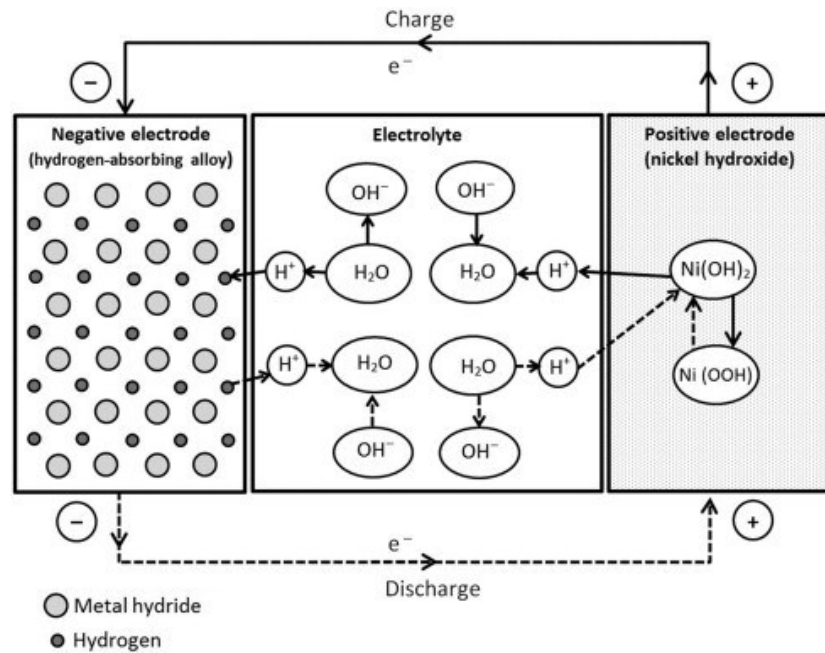


Figure 4.3 Illustration of the working principle of a nickel-metal hydride battery

*So much so, that Ni-Cd cells have been banned from power tools in European countries¹⁵⁷

weaker memory effect and are cheaper than the lithium-ion batteries. One big drawback though is the considerable self-discharge phenomenon.

Other nickel-based batteries include nickel-iron, nickel-zinc or nickel-hydrogen.¹⁸

4.1.2.3 Lithium-Ion (Li-Ion)

Lithium metal is the crème de la crème amongst possible battery materials. It is the most electronegative and the lightest among the metals, providing, therefore, the highest specific energy. It gaining attention by the battery community was therefore just a question of time.

The first Li-ion battery has been commercialized by Sony Co. in 1991, being the result of years of competitive research (**Table 4.1**).

There are two distinguished methods for building Li-ion cells. The first one utilizes pure metallic lithium, while the second uses lithium alloys or lithium-containing inorganic compounds (e.g. lithium cobalt oxide or lithium iron phosphate, cf **Figure 4.4**²⁰). This second approach is generally preferred for the safety it offers since it avoids lithium dendrite formation.²¹

Table 4.1 List of lithium metal battery systems¹⁹

System	Voltage (V)	Specific energy (Wh·kg ⁻¹)	Energy density (Wh·L ⁻¹)	System	Company
Li/TiS ₂	2,1	130	280	1978	Exxon
LiAl/TiS ₂				1979	Hitachi
Li/LiAlCl ₄ -SO ₂ /C	3,2	63	208	1981-1985	Duracell
Li/V ₂ O ₅	1,5	10	40	1989	Toshiba
Li/NbSe ₃	2,0	95	250	1983-1986	Bell Lab
LiAl/Polyaniline	3,0		180	1987	Bridgestone
LiAl/Polypyrrole	3,0		180	1989	Kanebo
Li/Al/Polyacene	3,0			1991	Kanebo/Seiko
Li/MoS ₂	1,8	52	140	1987	MoLi
Li/CDMO(Li _x MnO ₂)	3,0			1989	Sanyo
Li/Li _{0.3} MnO ₂	3,0	50	140	1989	Tadiran
Li/VO _x	3,2	200	300	1990	HydroQuebec

The electrolyte, which is usually a solution of lithium salt in a solvent mixture, typically carbonates, is not stable at the operating potential of the anode during charging. It, therefore,

undergoes an irreversible chemical decomposition, forming a solid electrolyte interface (SEI) at the anode. This interface is lithium-ion conductive and is a protection for the anode.

Since there is a large variety of materials used in Li-ion batteries, a general description of the charge and discharge processes can be formulated. As it was stated above, the cathode* consists of a lithium compound and the anode – of an intercalation material, generally graphitic carbon**. Immediately after construction, the cell is in a discharged state. During charge, the lithium ions (Li^+) leave the cathode and penetrate the anode, forming Li_xC_6 intercalation complexes. Reciprocally, during discharge, they travel back. The particular case of cobalt oxide is given for illustration (Equation 5).



Li-ion batteries are the state of the art nowadays. They have the highest energy density amongst all commercial batteries, a good cycling stability and a competitive pricing. The only drawbacks are the still existing safety issues and the reduced performance at high or low temperatures.²¹

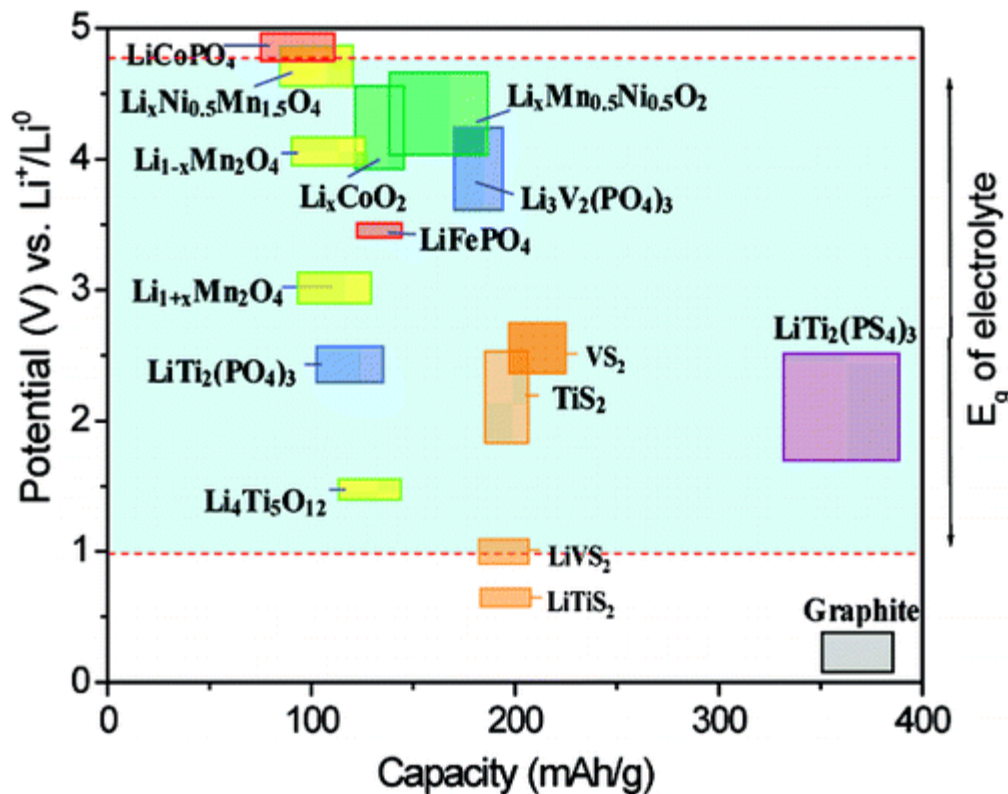


Figure 4.4 Selection of electrode materials based on the thermodynamic stability of the electrolyte

* The cathode and anode of a battery being inversed between charge and discharge, one defines the electrode from which the electrons flow through the external circuit during discharge as “anode”. The other electrode is, respectively, “cathode”.

** Although silicon is lately intensively researched on, since it could offer considerably higher capacities¹⁵⁸

4.1.2.4 Lithium-Sulphur

Although these batteries also use lithium ions, the electrochemical reactions are different from the intercalation reactions of Li-ion batteries, which warrants them a different category. Li-S batteries have a theoretical specific capacity which is six times higher than that of the presently dominating Li-ion cells. Despite them being known, and even patented since 1962,²² multiple issues hinder their commercial usage. Today, commercial prototypes already exist and Li-S cells are used in, for example, unmanned aerial vehicles²³, where they offer a great benefit thanks to their reduced weight. It has been predicted that they will be introduced to the general market after the year 2025 (**Figure 4.5**).^{21,24}

4.1.2.5 Lithium-Air

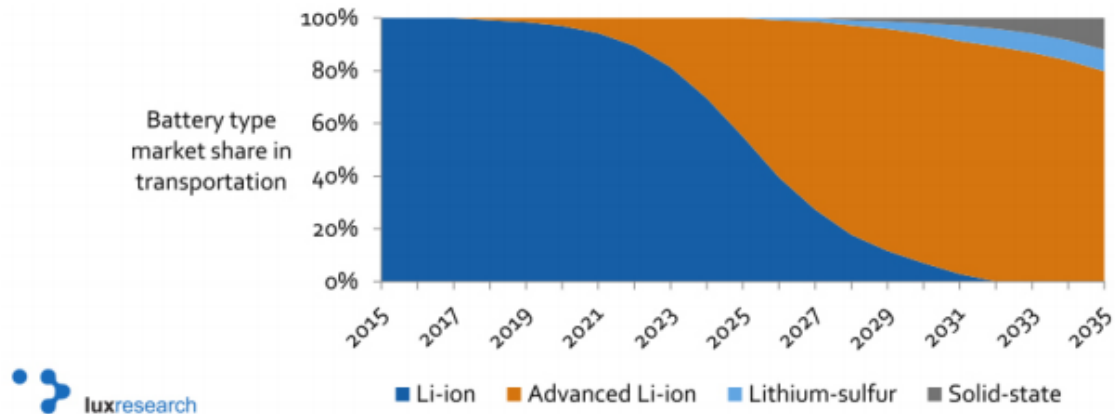


Figure 4.5 Market shares by type of battery within the transportation sector

Lithium-air systems are nowadays regarded as the holy grail amongst batteries by many researchers. First, lithium is, as mentioned earlier, the metal with the highest specific capacity (3842 mAh.g⁻¹). Second, the participation of ambient air in the electrochemical reaction would reduce the mass and the volume of the final cell and therefore augment its specific energy and energy density. A theoretical specific energy of 3,582 Wh.kg⁻¹ has been mentioned.²⁵

Nonetheless, there are still several challenges to be overcome before one can seriously consider their commercialisation and use. All cell components need intensive research and, above all, the safety issue has to be addressed*.²⁶

* as it is for all high energy density batteries

4.2 LITHIUM-SULPHUR CELL

Lithium-sulphur batteries are the topic of the present work. In this part, their working principle will be thoroughly explained in this chapter. Afterwards, the main problems and the possible solutions will be discussed.

4.2.1 Mechanism

A lithium-sulphur cell typically consists of a Li^0 -containing anode*, a sulphur cathode, a separator and an electrolyte. Since sulphur is insulating, it is generally encapsulated in a conducting matrix. These cell components will be discussed more thoroughly in paragraph 4.2.3

The functioning of Li-S batteries is based on the reaction between lithium and sulphur (S_8). Unlike Li-ion batteries, Li-S are in their charged state immediately after construction (**Figure 4.6A**). During discharge, the electrons travel from the lithium metal anode towards the cathode through an external circuit, powering the attached device. The formed Li^+ ions are drawn towards the cathode, where they will react with the sulphur **Figure 4.6B, Equation 6**). Its average voltage is 2,15 V with respect to Li^+/Li^0 .



$$C_T = \frac{x \times N_A \times Q_e}{M} \quad (7)^{**}$$

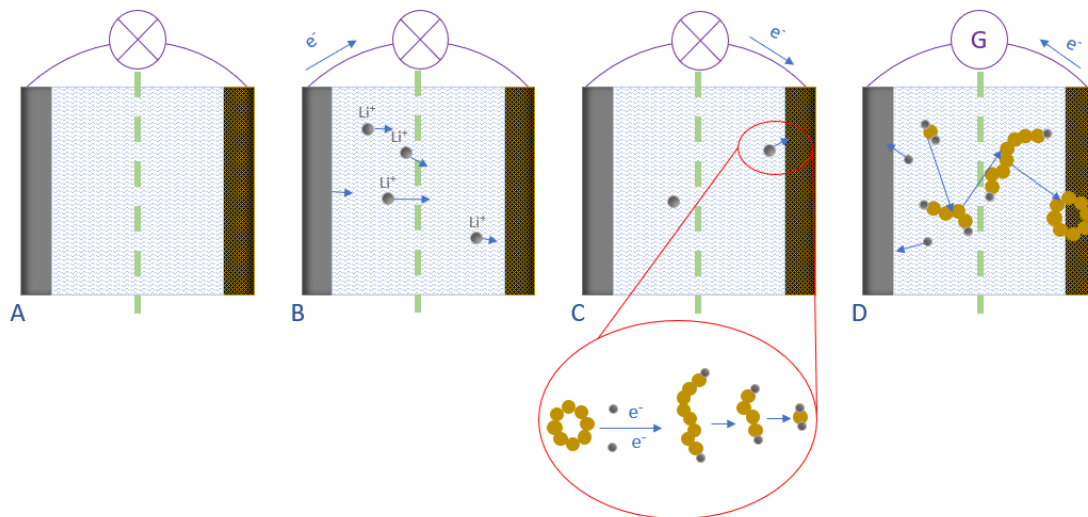


Figure 4.6 Functioning principle of the Li-S battery; (A) open circuit, (B) beginning of discharge, (C) sulphur is reduced inside the cathode and the soluble lithium polysulphides migrate into the electrolyte, (D) recharge

* Generally metallic lithium, although research is done to replace it by a safer material.

** Here x is the number of electrons provided by one molecule, N_A – the Avogadro number, Q_e – the charge of one electron, expressed in Coulomb and M – the molar mass. Upon calculation, one obtains a theoretical capacity of 6020 C.g^{-1} , which can be converted into the commonly used value of 1672 mAh.g^{-1}

Sixteen electrons can be converted per sulphur molecule, which in turns leads to the high theoretical capacity of such a cell (**Equation 7**).

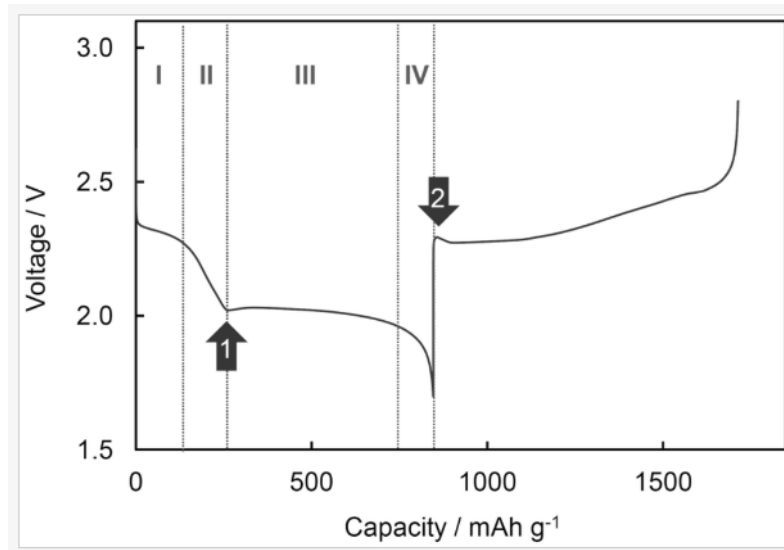


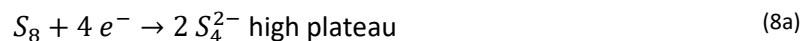
Figure 4.7 Typical discharge curve of a Li-S battery

The discharge reaction starts at about 2.4 V – a plateau can be seen on the discharge curve (zone I in **Figure 4.7**²⁷). This is when long-chain polysulfides (LiPS) are formed: the S_8 ring opens up to form S_8^{2-} , which are combined with two Li^+ ions, to give Li_2S_8 ²⁸. They are then reduced to polysulfides of medium length, which is reflected by the zone II on the discharge curve (**Figure 4.7**). A second plateau can be observed at approximately 2 V and corresponds to the reduction to short polysulfides: Li_2S_2 and Li_2S (III in **Figure 4.7**).

The points 1 and 2 in **Figure 4.7** indicated by the red arrows, correspond to the point where the viscosity inside the cell is at its highest and, respectively, to the reduced polarization due to the solid-liquid interface.

Multiple attempts have been made to describe the mechanism of the reactions. This task is quite difficult since there is a multitude of species which cannot be isolated.

The most simplified model is the scheme comprising two reactions (**Equation 8**). It was obtained based solely on the Nernst equation* and the discharge plateaux²⁹.



* $E = E^0 + \frac{RT}{z_e F} \ln Q_r$, where E is the reduction potential, E^0 – the standard reduction potential, R – the universal gas constant, T – the temperature of the system, z_e – the number of transferred electrons, F – the Faraday constant and Q_r – the reaction quotient

Further calculations and experiments permitted to look deeper into it, bringing up the formation of S_6^{2-} via a disproportionation reaction. The reaction, through which it is formed, exists in two versions (**Equations 9&10**).



Another entity which was repeatedly encountered by different groups' work is the radical S_3^- . It is generally believed to be formed by the dissociation of S_6^{2-} ^{27,30}.

If all the sulphur reacted, at the end of the discharge the cathode would consist purely of Li_2S , the final product of the reaction. This is not happening for a simple reason: all the polysulfides besides Li_2S_2 and Li_2S are soluble in the electrolyte* and leave the cathode during the discharge process. A part of them reaches the anode and gets reduced directly at its surface, and another – remains in the electrolyte. This phenomenon is called “polysulfide shuttle”.

In the end, the cell is then charged and the reaction reversed (**Figure 4.6D**).

4.2.2 Problems to Be Solved

Despite the lithium-sulphur technology being known about for almost a century and its very attractive properties, there still are almost no such cells on the market. Several factors are responsible for this.

4.2.2.1 Insulating Nature of Sulphur

As already mentioned, a battery functions in the following way: electrons move from anode to cathode via an external circuit and are accepted by the oxidant at the cathode, which is turned into ion and proceeds to react immediately inside the cell. Therefore, in order for the reaction to happen, the electrons need to first reach the active material, which they cannot do if there is an insulator in the way. To overcome this problem, an electrically conducting material is added to the sulphur, usually graphitic carbon. Then, there are two requirements to keep in mind. First, a conducting matrix is needed – the amount of the additive has to be such that the percolation threshold is reached³¹. Second, each sulphur molecule has to have access to this conducting material in order to be reduced. One may, of course, decide to assemble sulphur and conductive additive in such a way, that there is a large excess of the latter, but this approach would generate

* elemental sulphur is also insoluble, but it cannot be called a lithium polysulfide

another problem: since the conductive additive is not actually involved in the electrochemical reaction, the energy density of the cell will be diminished.

4.2.2.2 Volume Variation throughout the Cycling

The density of elemental sulphur is of approximately 2 g.cm^{-3} .^{*} Lithium sulphide (Li_2S) has a density of $1,66 \text{ g.cm}^{-3}$. This leads to a strong expansion when the sulphur is converted to lithium sulphide³². During multiple charge and discharge cycles, the expansion and contraction of active material damages the architecture of the cathode. First, there may be a breach of electric contact, causing the loss of active material for further reactions. Second, parts of cathode may be entirely delaminated off the current collector. Both these events reduce the cell's performance and cycling stability. The attempts to resolve this issue include the targeted synthesis of adapted conducting carbons and the careful choice of the binder material.

On the other side, since the lithium ions travel towards the cathode during discharge, an important volume loss is noticed at the anode^{**}. This further sees to the destabilisation of the cell.

4.2.2.3 Dendrite Growth at the Anode Surface

Right after the cell construction, the lithium metal anode has a smooth surface. The repetitive stripping and plating of lithium throughout the cycling process leads to the modification of the anode: tree-like structures, called dendrites, form at its surface. Amongst possible causes the unstable solid-electrolyte interface³³, impurities at the electrode surface³⁴, current density or stack pressure³⁵ are cited. This phenomenon leads to serious safety issues since the dendrites are capable of piercing the separator and provoking a short-circuit when reaching the cathode surface. Besides, they cause the further cracking of the SEI, which exposes fresh lithium to the electrolyte³⁶. Images obtained by scanning electron microscopy (SEM) visualize this problem quite nicely (**Figure 4.8**³⁷). The parts pointed at by the white arrow (**Figure 4.8d-f**) are electrically insulated from the electrode and qualified as "dead".³⁷

4.2.2.4 Polysulphide shuttle

Crystalline elemental sulphur is insoluble in the electrolytes used for lithium-sulphur batteries. The same goes for the short amorphous³⁸ $\text{Li}_2\text{S}_2/\text{Li}_2\text{S}$, which are the final products of the

^{*} the most common allotrope of sulphur, α -octasulphur, has a density of $2,07 \text{ g.cm}^{-3}$

^{**} the extent of it is delimited by the amount of sulphur available

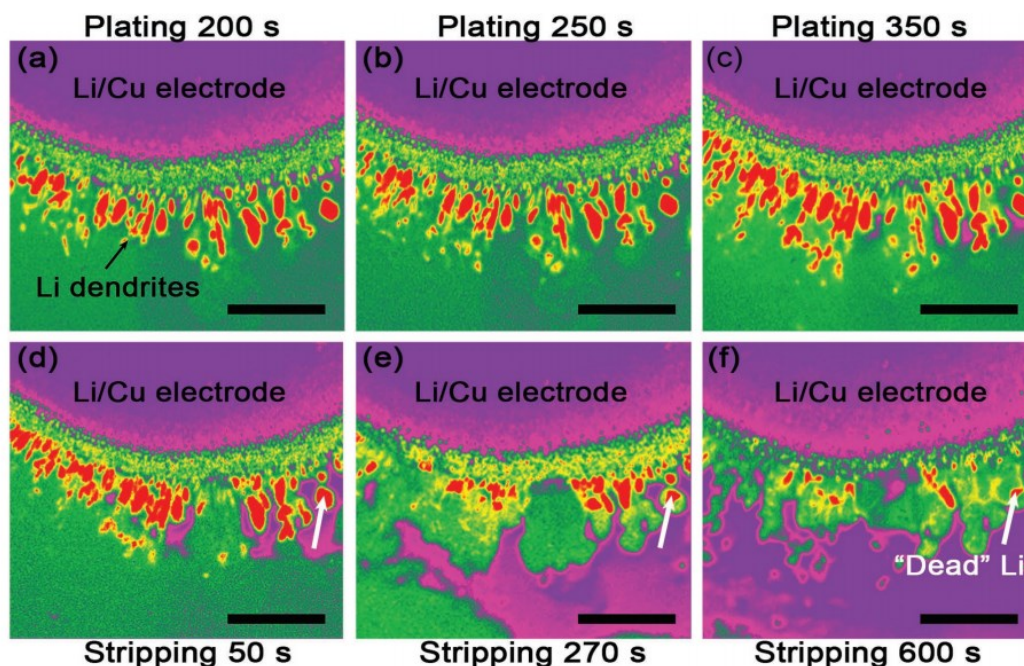


Figure 4.8 SEM images for an in-situ plating (a-c) and stripping (d-f) experiment of lithium in a standard electrolyte for Li-S batteries. The colours are added in function of the contrasts in greyscale. Scale bar: 20 μm .

reaction. All the other reaction intermediates, grouped under the name of lithium polysulphides, are, however, easily soluble.³⁹ During discharge, the following happens. Sulphur reacts to form S_8^{2-} , which is dissolved in the electrolyte and opens the access to the active material underneath for further reaction; this is beneficial for the total performance. Then, there are two concurring processes that can take place. On one side, there are the further reduction reactions, which happen as long as the electrons from the cathode can reach the polysulphide and add up to the cell capacity. They cap in the formation of lithium sulphide. On the other side, there is the diffusion of the soluble polysulphides into the electrolyte. There, since the electrical contact is lost and there is no source of “new” electrons, they can undergo dissociation or recombination reactions. In the end, these polysulphides can reach the anode and then the whole electrochemical reaction (electron and ion exchange) will take place at its surface. Yet worse is the fact that insoluble lithium sulphide can be formed, which passivates the anode, hinders further reactions and enhances the previously discussed dendrite formation. Another negative consequence of the polysulphide shuttle is the loss of active material: if with every cycle a part of the sulphur is reduced at the anode and another part remains dissolved in the electrolyte, there will be less sulphur available for future cycles. Finally, there is the issue of the high reactivity of the polysulphides – the aggressive medium can, for example, damage the metal contacts.

4.2.3 Battery components

The problems listed in the previous part are addressed by a careful orchestration of the cell components.

4.2.3.1 Cell casing

The literature on this topic is very scarce⁴⁰. The choice of cell configuration rather belongs to the domain of common knowledge, acquired by each research group independently. Nevertheless, it can dramatically influence the performance of the battery. In this part, the three most common possibilities will be shortly discussed.

First of all, there is the Swagelok® cell or other geometries of the kind. The cell components are sandwiched between two piston-like electrodes in a sealed, air-proof environment. This is the easiest configuration since no particular equipment is needed besides the cell itself, which is reusable. The main drawback is the limited control over the pressure with which the cell is closed – it is done by hand and may vary from cell to cell. Besides, the Swagelok® build needs an increased amount of electrolyte, which leads to an increased material loss via the polysulphide shuttle and is detrimental to the energy density. In the end, due to their size and weight, such cells are purely used in research laboratories.

Then, there is the coin cell – the design that became the standard for research. It requires little material, which is optimal for laboratory conditions and the necessary equipment is space-efficient and affordable. The cells are closed by a crimping machine, which makes the results reproducible. They exist in several sizes and thicknesses. Even though they can be found in stores, the coin cells are relatively unpopular and are only used when small size is the decisive factor.

Finally, there is the pouch cell. It is light, flexible and lends itself to be stacked into packs. Still, the equipment necessary is pricier than that for previous cells and, most importantly, pouch cells use up a considerable amount of material. It is the design which comes into play when the aim is to check if the cell is mature enough for an introduction to the industry.

Other cell designs include cylindrical or prismatic cells, but they are seldom a choice when constructing Li-S batteries.

The main problem linked with the cell design lies in the fact that a cell with a very good performance in one geometry will not obligatorily function well in another one.⁴¹

4.2.3.2 Cathode

The cathode is the most studied Li-S cell constituent: according to a recent review, 64% of the articles focus on it.⁴² A generic cathode in a Li-S cell consists of a current collector, encapsulating and conducting material, binder and sulphur.

The current collector channels the electrons and, often also provides mechanic stability to the cathode material. It is generally out of aluminium^{43–47}, although other materials like nickel^{48,49} or carbon in different forms^{50,51} can also be encountered.

As it has been discussed earlier, the sulphur being electrically insulating, a conductive material is necessary for such a cell. On the other side, there is the polysulphide shuttle that needs to be kept under control. These two challenges are often addressed by one solution – an adapted encapsulation material. In the same time, it assures a routing of electrons to the sulphur and sees to trapping the polysulphides within the cathode. Attempts have even been done to use this same material as a current collector by introducing rigid foams.^{48,50}

First of all, this cathode material has to be electrically conducting. It requires a considerable specific area, which would maximize the contact with the sulphur, but also large pores so that it can store more of it. It also has to have a structure that would hinder the diffusion of polysulphides into the wide. On the other hand, the electrolyte has to be able to access the sulphur in order for a reaction to happen altogether. In the end, it would be appreciated if it were light-weight– mass plays a vital role in the specific energy of the cell. Carbon is unanimously considered to be the best material according to these criteria. The specific surface area of a single graphene sheet is as high as $2630 \text{ m}^2.\text{g}^{-1}$ ⁵² and carbon materials with surface areas of over $2000 \text{ m}^2.\text{g}^{-1}$ are widely available⁵³. Carbons called “graphitic”, which means they have a predominate sp^2 hybridization, are electrically conducting. Carbon structures of complicated architectures (porous carbons with pores of different sizes, fibres, onion-like structures, etc.) can be synthesised and tailored for the specific needs. Even though there are other conducting materials, like metals or conducting polymers, the first are generally heavier than carbons and the latter – less chemically stable.

There is a panoply of studies about carbon materials for Li-S cathode. One of the probably most cited materials is the CMK-3⁴⁶. It is a mesoporous carbon synthesised using the commercial silica SBA-15 as template and it consists of hexagonally ordered carbon rods separated by voids, where the sulphur can be infiltrated (**Figure 4.9**).

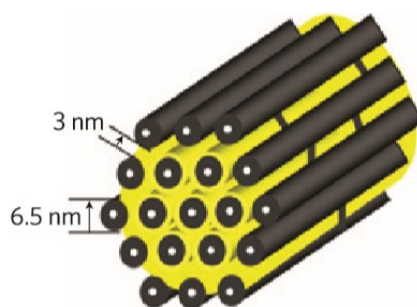


Figure 4.9 Schematic representation of sulphur-infiltrated CMK-3 carbon, copied from ⁴⁶

There is one more approach used to reduce the polysulphide shuttle: an “adsorbent” is introduced into the cathode, either as functionalization of the carbon material ⁵⁴ or as additive ⁵⁵. Since the lithium polysulphides are polar molecules, and carbon is not, it alone can only retain them by prolonging their path towards the exterior of the cathode. Therefore, one introduces molecules that could adsorb the lithium polysulphide to better retain it inside the cathode.

Although the most important component of the cathode is the sulphur itself, there is limited research dealing directly with it. One of the approaches that have been taken into consideration is, for example, the modification of the allotropic form. As it has been said earlier, sulphur is an element which has a multitude of allotropes, the most prevalent being S_8 . But, by breaking up the ring and introducing it into confined spaces (micropores) where it cannot reform, one can obtain batteries with cathodes containing S_{2-4} instead of S_8 .⁵⁶

Finally, there is the binder – a material that ensures the adhesion of the carbon-sulphur composite to the current collector and that adds to the system’s elasticity – an important factor during the cyclic expansion and contraction of the active material. The most commonly used binder is the polyvinylidene fluoride (PVDF) ^{57–60}, borrowed from the lithium-ion technology. Another binder material used for Li-S batteries is carboxymethyl cellulose (CMC) ⁶¹, whose solvent (water/ethanol) is considerably less toxic than the N-Methyl-2-Pyrrolidone (NMP) necessary for the PVDF.

4.2.3.3 Separator

The main function of the separator is that of an electric insulator between the two electrodes, which excludes the possibility of a short-cut. For lithium-sulphur batteries, there is another task to fulfil – the already mentioned polysulphide retention. The separator is the second cordon in this story: it retains the LiPS on the anode side of the cell. Despite these facts, the separator gets little attention from the researchers – to an extent at which it is often not even mentioned which exact material is used in the constructed cell.^{62,63}

A separator has to be chemically, thermally and electrically stable, it has to be easily penetrated by the electrolyte and it is desired for it to be light and thin. The most commonly used separators are porous polyolefin films, such as Celgard®.⁶⁴

The research mostly focuses on two directions: ion-conductive membranes and all-solid-state cells. There are several studies that use lithiated Nafion™ membranes.^{65,66} They rely on the fact that the H^+ ions in the $-SO_3H$ group can be replaced by Li^+ ions. Then, during the cell cycling, the free lithium ions can bounce through the foil, pushing one ion at a time to the next position. The same principle is used for ceramic materials.⁶⁷ The all-solid-state cell replaces the separator and electrolyte by a solid interlayer, usually containing lithium sulphide^{68,69}. The benefits of such a configuration are obvious: the polysulphide shuttle is entirely eliminated. The difficulties are also easy to deduct: in the conditions of lack of solvent, the reaction is harder to be initiated, and the sulphur in the cathode has to be dispersed on the conducting material in a very thin layer. Besides, the chosen material has to have a very good ionic conductivity and the whole system has to remain safe, which is harder to achieve when using a brittle, glassy material.

4.2.3.4 Electrolyte

The electrolyte is the medium in which the ionic exchange takes place in an electrochemical cell and thus is of the utmost importance in cell design.

In the majority of cases, the electrolyte used for battery construction is liquid. For lithium-based batteries, it is usually a lithium-ion containing solution. There are several conditions that have to be met by a potential electrolyte. First of all, the electrolyte solvent has to be stable in the voltage window characteristic for the electrochemical couple which constitutes the battery. Second, a good electrolyte/electrode contact is necessary for a smooth reaction. Third, it has to have good ionic conductivity and low viscosity to facilitate ionic transport. Fourth, it should not react with the other cell components and with the products of the electrochemical reactions.

For the special case of Li-S batteries, a certain solubility of the reaction products which are the lithium polysulphides in the electrolyte is also desired.

Polysulphides are an extremely reactive species: this impedes the use of common battery electrolyte solvents such as carbonates, esters or phosphates⁷⁰. The best results are shown by ethers, such as dimethoxyethane (DME)⁷¹ or tetraethylene glycol dimethyl ether (TEGDME)⁷². A cyclic ether, 1,3-dioxolane (DOL), which is also frequently used in Li-ion batteries, confers the electrolyte a lower viscosity and undergoes ring-opening-polymerization at the anode, forming a protective layer⁷³. A certain amount of attention is accorded to sulphones, such as tetramethylene

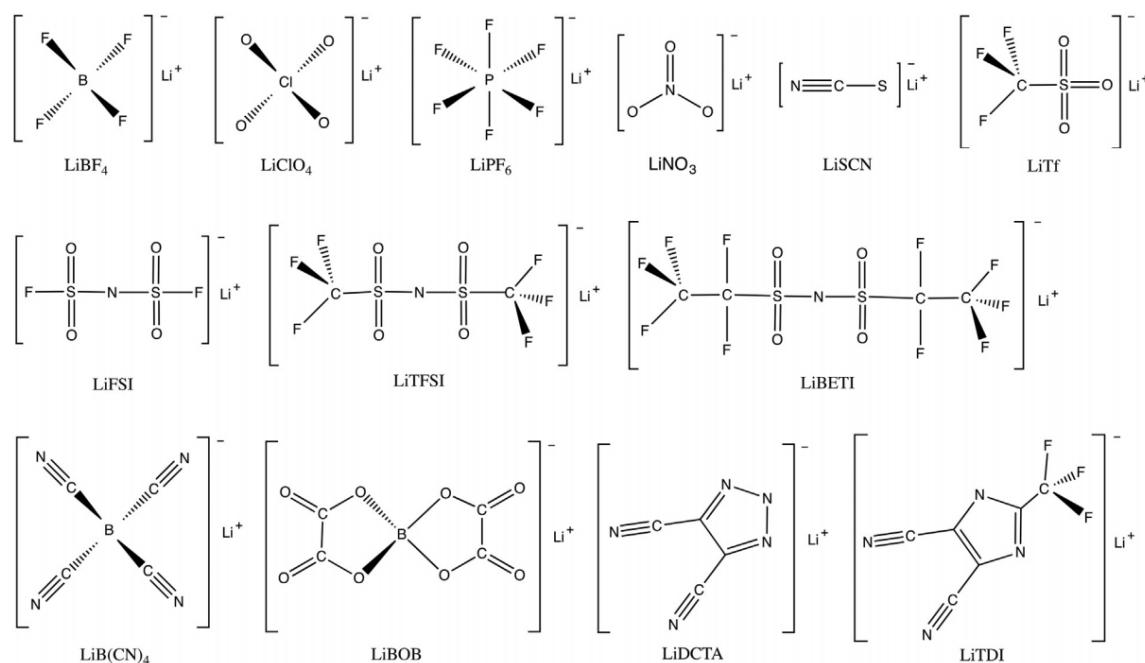


Figure 4.10 List of possible lithium salts for Li-S batteries

sulphone (TMS) or ethyl methyl sulphone (EMS)⁷⁴. They are appreciated for their high dielectric constant, low cost and safety⁷⁵. Another approach relies on using bad polysulphide solvents⁷⁶, which would solve the problem of LiPS shuttle.

The role of the salt in the electrolyte is to promote ion transportation. It has to be well soluble in the electrolyte solvent, have a high degree of dissociation and, at the same time, be chemically and electrochemically stable within the considered system. A list of salts that have already been tested or might be potentially used for Li-S cells (**Figure 4.10**⁷⁷).

The first salt to be tried was expectedly LiPF_6 ^{78,79} – the salt conventionally used for Li-ion batteries. This is, however, not the optimal choice: the carbonate solvent used to dissolve lithium fluorophosphate reacts with the polysulphides and so does the salt itself (**Equation 11**). The same also holds true for other conventional lithium salts such as LiBF_4 or lithium bisoxalatoborate (LiBOB).



Lithium bis(trifluoromethanesulfonyl)imide (LiTFSI) is chosen almost unanimously⁷⁷. It is known to corrode the Al current collectors⁸⁰, but this happens at the voltage of 2,8 V vs. Li and can be avoided in Li-S systems.

Another possible constituent of the liquid electrolyte is the additive. There is a vast number of additives used in Li-ion batteries⁸¹, but not in Li-S. The most known one is the LiNO_3 : it participates in creating a passivating layer at the anode and, thus, provides protection for it.⁸²

Besides liquid electrolytes and all-solid-cells, there are the ionic liquids (ILs)^{83–86}, which are lately getting increased attention. They are liquids entirely consisting of ions, whose solvent properties arise from interactions between cations and anions. ILs are non-volatile, non-flammable, they possess a wide electrochemical window and are ionically conductive. They can also be custom-made to have the exact properties needed for the considered system: some sources talk about 10^{12} possible ILs.⁷⁷

4.2.3.1 Anode

The lithium anode is, presently, only starting to get into the focus of attention – only two per cent of the total research articles are dedicated to this topic.⁴² Most of the researchers are contented with using lithium metal foil. This approach has advantages: it is very easy in production and the lithium is present in large excess, which assures complete reaction of the sulphur. It also has several disadvantages, the most important of them being the safety issue posed by the presence of pure metallic lithium. Other disadvantages include the dendrite growth, the formation of a passivation layer and the reaction with the electrolyte, leading to the depletion of the latter and to gas formation.

The passivation layer is an ambiguous story. On one side, it can increase the internal resistance of the cell⁸⁷, which reduces its performance. It can also crackle during the charge, worsening the SEI formation and dendrite growth phenomena. On the other side, this same layer is known to protect the anode from the highly reactive polysulphides and thereby reduce its degradation⁸⁸.

On the contrary, the dendrite growth is definitely a negative phenomenon. The attempts to reduce it include the adaptation of the electrolyte components to form protective SEI films [90], the physical protection of the anode prior to the cell construction,⁹⁰ the complete isolation of the anode from the corrosive polysulphides through the use of the already mentioned solid electrolytes or the modification of the anode structure (**Figure 4.11**).⁹¹

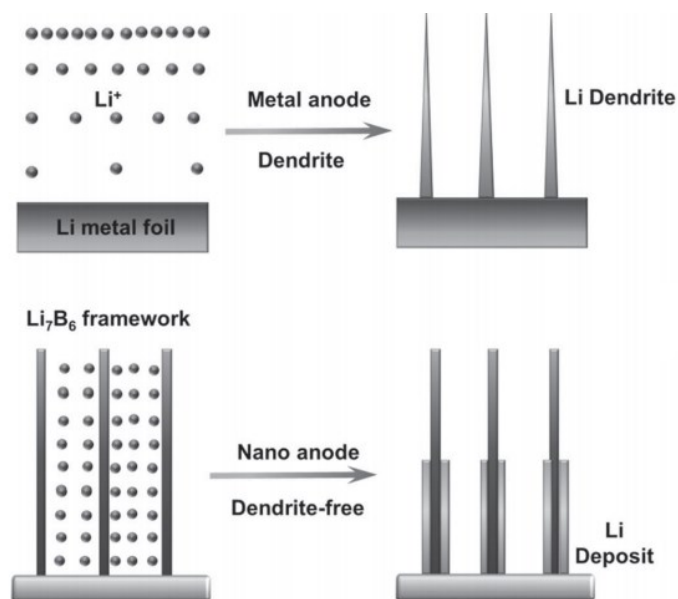


Figure 4.11 Nanostructured anode containing free and alloyed Li metal compared to standard Li-foil ⁹¹

An entirely different approach consists in eliminating metallic lithium from the cell altogether. It is not new: this is the exact principle used in Li-ion technology. It can be done in two ways. The first consists in using a Li_2S cathode ⁹² and an anode which would be the host for the lithium*. The second approach relies on taking a conventional sulphur cathode, but a prelithiated anode instead of the metallic lithium.^{93,94} These methods are promising, but they still need maturing before they could be a serious alternative to metallic lithium.

* usually out of conducting carbon, in conformity with the Li-ion technology, although silicon also gets considerable attention

4.3 IN-SITU ANALYSIS OF LITHIUM-SULPHUR BATTERIES

As it has already been elaborated on, Li-S technology is extremely complex and, despite the high potential which justifies the amount of effort put into it, it still has problems that need solving. This can, of course, be handled by trying out different configurations and components and hoping to find the right one, but it is very time-consuming and there is no guarantee that the solution will be found. This is why it is important to understand the exact processes taking place in a functioning cell.

4.3.1 Methods

There is a variety of methods to choose from, depending on the aspect to be analysed. The analysis can be done *operando*^{*}, *in-situ*^{**} and *ex-situ*^{***}, which is decided in function of the method, the component to be analysed and the aim of this analysis.

The electrochemical behaviour of the cell is observed via cyclic voltammetry (CV) and galvanostatic charge-discharge testing and internal resistance aspects are identified via electrochemical impedance spectroscopy (EIS). The crystalline elements^{****} are identified by X-ray diffraction (XRD) and the dendrite growth at the anode is observed by scanning electron microscopy (SEM). The formation and evolution of LiPS in the electrolyte can be followed by numerous methods, such as ultraviolet-visible (UV-Vis), high-performance liquid chromatography (HPLC) or Raman spectroscopy. Near edge X-ray absorption fine structure (NEXAFS), also called X-ray absorption near-edge structure spectroscopy (XANES) is a powerful tool, which can penetrate both the solid electrode and the liquid electrolyte in the same measurement and identify sulphur and sulphur-containing species. More information for some of these methods will be discussed in this chapter.

4.3.1.1 XRD

The wavelength of the X-rays is comparable to the distances present in the crystalline lattices. Monochromatic radiation directed upon the sample comes into interference with it and generates a modified diffracted ray, according to the Bragg's Law.

* during the functioning of the cell

** inside the cell

*** outside of the cell

**** such as elemental sulphur or lithium sulphide

Both sulphur and lithium sulphide are crystalline and they can, therefore, be observed via XRD.^{38,95,96} By this method, one can elucidate at which depth of discharge (DOD) the Li_2S is created and, respectively, at which state of charge (SoC) it is converted back to sulphur. It also allows seeing where exactly in the cell the transformations take place and, for example, follow the redispersion of sulphur through the cathode over the cycles.

4.3.1.2 SEM

The sample is bombarded by an electron beam in a raster scan pattern, producing information about its topography and composition. The result obtained is an image whose magnification can be of up to 500'000 times.

SEM is mostly used to observe the cell components before construction and post-mortem, but it can also be applied *in-situ*, like in the case of an all-solid-state cell.⁹⁷

4.3.1.3 UV-Vis

UV-Vis spectroscopy is an analysis method used for materials that absorb light in the visible or ultra-violet spectrum.

Since lithium polysulfides are of bright yellow-orange colour, they are perfectly suitable for this method of analysis. In function of the chain length, the metallic ions and the solvent, different spectra are obtained, that can then be compared amongst themselves and with reference samples (**Figure 4.12**).⁹⁸ There are several research papers that use this principle to identify the entities created at different DODs and to deduce what electrochemical processes take place.^{98–100}

4.3.1.4 HPLC

The dissolved sample is pumped at high pressure through the stationary phase of the column. Since each molecule is individual in its interactions with the mobile and solid phases, the retention time allows its sure identification.

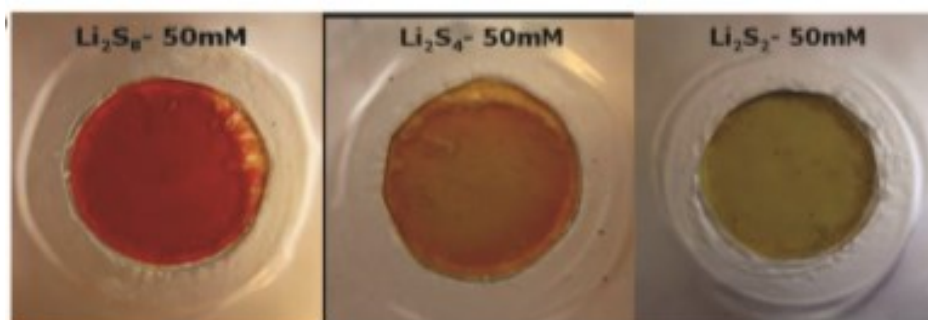


Figure 4.12 Lithium polysulfides prepared with different stoichiometric proportions of reactants

Each polysulphide molecule has its molecular mass and, although they are difficult to differentiate, this task is not impossible and has been achieved on several occasions.^{27,101,102}

4.3.1.5 NEXAFS

There is a variety of analytical methods that rely on the absorption of radiation by the sample, and NEXAFS is one of them. When X-ray absorption spectroscopy is conducted, the incoming photon interacts with the core electrons of the atom. Such a core electron is excited and, if the absorbed energy is equal to or higher than its binding energy, it is promoted to an unoccupied higher state and leaves a hole behind. This hole is immediately filled by an electron from a higher energy level, accompanied by the emission of a photon. The energy can also be transferred to a third electron, which is then ejected through the Auger effect. In condensed matter, the emitted photon or electron will then scatter from neighbouring atoms. The results of all the scattering events are then recorded and interpreted. NEXAFS is element-specific, and it is also sensitive to the electronic structure of the species, its oxidation number, coordination environment and structure geometry, which makes it a very powerful tool.¹⁰³ However, the interpretation of the results is extremely complex and is presently mostly relying on the comparison of the obtained spectra to standards, which is the fingerprint identification.

4.3.2 Raman Spectroscopy

Since an important part of this work is concentrated on the *in-situ, operando* analysis of the Li-S battery, it is reasonable that the theory behind Raman spectroscopy is explained in a more in-depth manner.

4.3.2.1 Theory behind Raman Spectroscopy

A molecule with N atoms is classically modelled as a set of N mathematical points with mass, interconnected by massless springs. In the equilibrium state, the lengths of the atomic bonds and the angles between them have set values. Nonetheless, these atoms are not immobile, neither in respect to the environment, nor in respect to each other. The N atoms of the molecule have $3N$ degrees of freedom, including translation, rotation and vibration.

In the case of spectroscopic analysis, one is only interested in the internal degrees of freedom (vibrational), which are in the number of $3N-6$ for a nonlinear molecule and $3N-5$ for a linear molecule (the rotation of the molecule around its axis does not include the movement of the mass points).

There are two analytical methods that can obtain information about the molecule's structure based on its vibrational transitions: infrared and Raman spectroscopies. Although the theory behind Raman is more complex, there are several parallels between them, which makes starting by an explanation of the infrared spectroscopy legitimate (**Figure 4.13**).

Infrared spectroscopy functions in the following way: a range of infrared and/or near-infrared frequencies are passed through the material. Only the energy of the frequencies corresponding to the natural vibrational frequencies in the molecules can be absorbed. Besides the coincidence of the frequencies, a molecule will only absorb infrared radiation if the energy transfer and the resulting molecular vibration will cause a change in the dipole moment of the molecule. IR absorption is, therefore, a one-photon event: the photon reaches the molecule and is absorbed by it.¹⁰⁴ In the result of these manipulations, one will obtain a graph giving the intensity of the transmitted light in function of the frequency. The resulting spectra are characteristic of different functional groups and molecules. One can therefore either identify the molecule if its fingerprint is known or deduce its appearance from the different functional groups present. It has to be noted that reflection absorption spectroscopy can also be applied, but it is less common and generally needed for samples present in a very low quantity.

In 1923, the Austrian physicist Adolf Smekal predicted the fact that photons could be inelastically scattered by molecules.¹⁰⁵ Some years later, this phenomenon was observed by Sir C.V. Raman and his student K.S. Krishnan – and was judged worth a Nobel Prize.

At any given moment, a molecule has a particular vibrational energy, which can be modified through its interaction with its neighbours. At room temperature, most molecules exist in a non-excited, ground state, also known as zero-point energy. Some molecules can also be in higher vibrational energy states.* The number of molecules occupying a particular energy state can be calculated using the Boltzmann distribution (**Equation 12**)**.

$$p_i = \frac{1}{Q} e^{-\varepsilon_i/kT} \quad (12a)$$

$$I = I_0 \frac{8\pi N \alpha^2}{\lambda^4 R^2} (1 + \cos^2 \theta) \quad (12b)$$

When photons meet molecules, they are absorbed and reemitted. If there has been no energy transfer between the two, the scattering is called elastic - it has been studied by Lord

* It is important to make the difference between vibrational and electronic energy levels of polyatomic molecules. Vibrational transitions take place between different vibrational levels, but within the same electronic state.

** where p_i is the probability of state i , ε_i – its energy, k – the Boltzmann constant, T – the system's temperature and Q -the canonical partition function

Rayleigh and carries his name (**Equation 12b**). He has calculated its intensity to be dependent of the number of scatterers N , their polarizability α , the photon wavelength λ and the distance to the observer R .

In the opposing case and if a nuclear motion is involved, the scattering is inelastic. The photon interacts with the group of atoms or molecule and its oscillating electric field pushes it for a short period of time up to a virtual quantum state - a distortion of the electron distribution. Then it is emitted, but it carries more or less energy than it did initially. This is the Raman effect. If the photon has lost energy during this interaction, it is called Stokes scattering and if it has gained energy from the molecule – it is respectively anti-Stokes. In both cases, the difference between the incident and the emitted photon energies is equal to the difference between energies of the ground and the first excited states (**Figure 4.13**).¹⁰⁶

If the molecule was initially in the ground state, it cannot give any energy away – the inelastic scattering can only be Stokes. Since, as it has been mentioned earlier, the majority of molecules are in the ground state at room temperature, the anti-Stokes scattering is considerably weaker than the Stokes.

Raman scattering only occurs if the molecule has anisotropic polarizability: the molecular polarizability has to be different between the initial and the final states. Contrarily, the molecule is IR-active if there is a change in the permanent dipole moment. This is why Raman and IR spectroscopies are said to be complementary and are often viewed as a set.

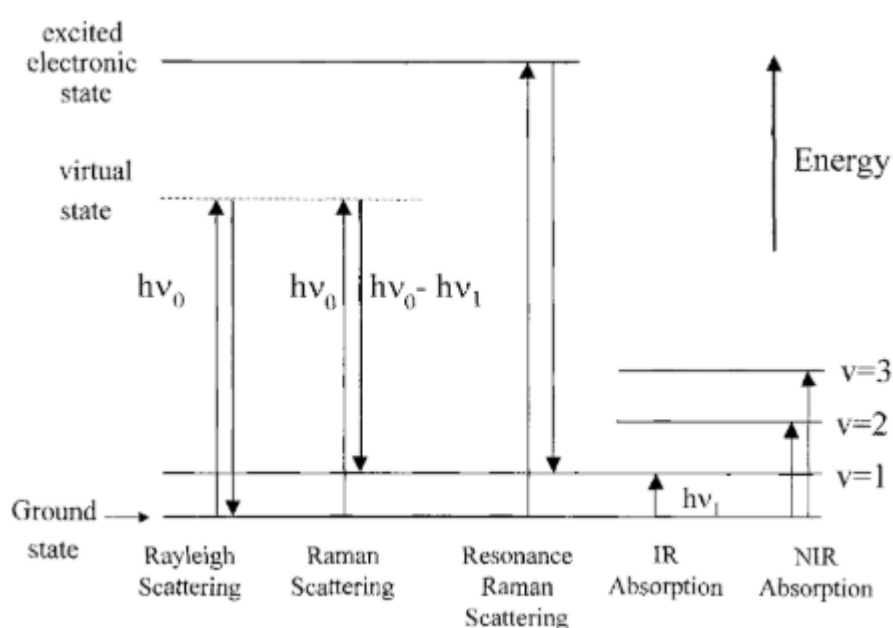


Figure 4.13 Spectroscopic transitions underlying several types of vibrational spectroscopy¹⁰⁶

To go from theory to praxis, Raman spectroscopy runs as follows: the sample is illuminated with a monochromatic ray, usually laser, with a wavelength between near-infrared and near-ultraviolet. The photons of this ray interact with the molecules in the sample and a part of them return carrying less or more energy than initially. This difference in energy then gives us information about the vibrational modes in the sample and, ultimately, about its nature. Raman spectroscopy is a powerful analytical method which, nonetheless, faced several problems which had to be addressed before it could be practically used.

4.3.2.2 Developments in the domain of Raman spectroscopy - problems and solutions

The first and possibly main issue consisted of the very low probability with which Raman scattering occurs. Only about 0,001% of the incident photons will undergo inelastic scattering, so the weak spontaneous Raman signal has to be separated from the largely predominant Rayleigh scattering. In his experimental setup, Sir C.V. Raman used crossed polarizing photographic filters to obtain monochromatic light from sunlight and to afterwards filter these photons and only “keep” the inelastically scattered ones. Such a double monochromator setup is bulky and inefficient: besides the Rayleigh line, there also is the stray light that needs to be attenuated in order to not distort the spectrum. The introduction of laser rejection filters revolutionized the Raman instrumentation and allowed to considerably reduce its size and complexity.¹⁰⁴ These are differentiated into edge filters, which only let the Stokes or the anti-Stokes signals through and notch filters, which blind the laser line and transmit both Stokes and anti-Stokes signals (**Figure 4.14**).¹⁰⁷

As seen in **Figure 4.14**, the edge filter has the benefit of cutting the signal closer to the laser line, enabling the measuring of the even small Raman shifts. It is only in the situation when one is

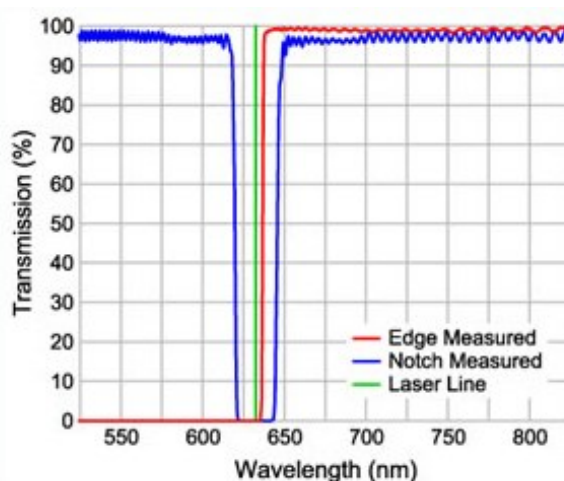


Figure 4.14 Filter comparison for Raman instrumentation, illustrating the advantages and disadvantages of each possibility

interested in very low frequencies (under 100 cm^{-1}) that more complicated instrumentation, such as a triple spectrograph, is needed.

Better results can also be obtained if, instead of solely counting on the spontaneously occurring Raman scattering one was to amplify the effect by stimulating it. One can illuminate the sample with a very strong laser pulse, which will generate Stokes waves that, in turn, will interact with the incident beam and induce a third-order polarization.¹⁰⁸ One can also shine a second laser beam at Stokes frequency concomitantly with the first laser¹⁰⁹, giving rise to a multitude of coherent Raman techniques.¹¹⁰

A second problem faced when acquiring Raman spectra is the fluorescence. Just like it is the case for Raman scattering, the molecule or group of atoms will absorb a photon and then reemit it, remaining in a different vibrational state than it was in at the beginning. The major difference though is in the fact that, in the case of fluorescence, the absorption of the photon will bring it up to a real, higher electronic energy level and not to a virtual energy level. This process is much more efficient than Raman scattering, which makes it so troublesome. In effect, the fluorescence intensity is several orders of magnitude higher than it is the case for the Raman signal and even fluorescence coming from trace amounts of impurities will be sufficient to completely suppress the Raman information in the spectrum.

Several techniques have been developed to solve this issue. First, fluorescence only concurs with Stokes scattering, whereas this problem is non-existent for the anti-Stokes. Therefore, one can augment the part of anti-Stokes lines by either just raising the sample's temperature or by turning to the stimulated coherent anti-Stokes Raman spectroscopy (CARS). Second, one can use lasers with higher wavelengths as the excitation source, since, contrarily to Raman, fluorescence is anchored to specific wavelengths. Typically, the near-infrared excitation at 785 nm or the Fourier-transform Raman system based on 1064 nm is used. Third, one may try to minimize the fluorescence, especially if it arises from impurities, by chemical or photochemical bleaching.¹¹¹ Surface-enhanced Raman spectroscopy (SERS) relies on the fluorescence suppression in the presence of metal nanoparticles. Other methods take advantage of the lifetime differences between Raman and fluorescence signals, peak widths, or resonance phenomena.¹¹²

Another important component of the Raman instrumentation is the laser itself. At the dawn of the technology, light generated by a gas discharge lamp was filtered to give the monochromatic ray that would be shone upon the sample. The first laser* was built only thirty years later and it

* Laser is in fact the acronym of "Light Amplification by Stimulated Emission of Radiation" but has made its way into a common noun.

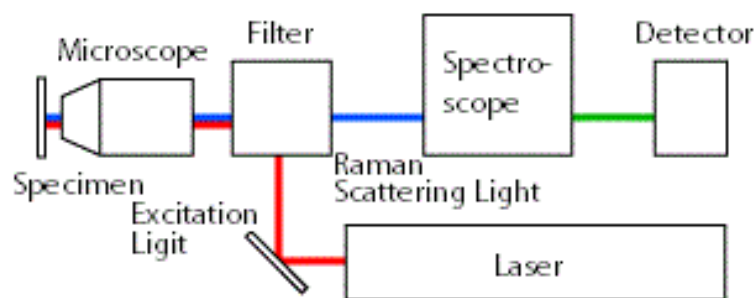


Figure 4.15 Schematic representation of a Raman microscope

significantly boosted the use of Raman spectroscopy. Nowadays, a variety of lasers between ultraviolet (under 360 nm) and infrared (up to 1064 nm) is available. The principles according to which the right wavelength for a given problem is selected will be discussed later.

The technology also benefited from the development of Raman microscopy and the usage of optic fibres. The Raman microscope is constructed by combining a Raman spectrometer with a standard optical microscope (**Figure 4.15**¹¹³) and it allows for the measurement with resolutions under 1 μm . One can also add up a spatial filter, giving birth to confocal Raman microscopy, which permits measuring not only at precise XY coordinates but also along the Z-axis. This instrumentation has enormous potential in analysing heterogeneous samples. When taking it to the maximum, one comes to the Raman spectral mapping, which consists in analysing small areas (pixels) of a macroscopic sample independently in order to obtain the localized chemical compositions.

The optic probe is indispensable in the cases when the sample cannot be brought close to the instrument, as inside a chemical reactor or a living organism. For example, one can pass an optical fibre through a biopsy needle, which would provide guidance during brain surgery (**Figure 4.16**¹¹⁴).

4.3.2.3 Choice of Analysis Conditions

A large variety of instruments and configurations exist nowadays for Raman spectroscopy. On one side, this demonstrates better than anything else its usefulness and popularity, on the other – one needs to take all these aspects into account in order to have the optimal conditions for the measurement at hand.

The first and most obvious is the choice of the laser, and there are several criteria to take into consideration here. The Raman scattering intensity is inversely proportional to the wavelength at a power of four, therefore, if it is possible, lasers of smaller wavelengths should be chosen. Another reason to choose lasers with shorter wavelengths is the sample degradation: the material

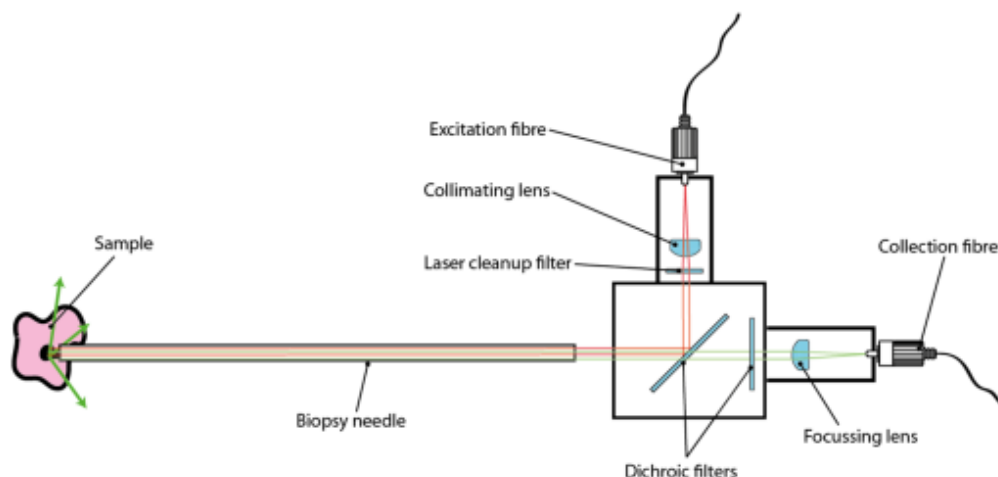


Figure 4.16 Schematic representation of the setup for optical biopsy via Raman spectroscopy

can absorb the light, heat up and burn. However, if there are fluorescence issues, one should opt for a near-infrared wavelength.

Next comes the filter. It has been already discussed previously, so it will only be shortly reiterated. If one may be interested in both Stokes and anti-Stokes spectra, a notch filter is the obvious choice. In the opposite case, one should prefer the edge filter since it allows to see the lines closer to the origin. In the case when the lines under 100 cm^{-1} are of interest, one should take a triple spectrograph.

One also gets to decide between incoherent and coherent spectroscopy (CRS). The first is the classical spontaneous Raman spectroscopy, whereas the second is the stimulated one. The spontaneous Raman gives a linear result – the spectra of all the molecules present in the sample as a function of their concentration. Respectively, the result for the coherent signal is non-linear: one amplifies the signal of one given molecule. This method is appreciated in the case when the sample only consists of one molecule and eventual impurities or when one is only interested in the specific one molecule and its distribution in space and time.

Other criteria are mostly interesting from the cost point of view. The spectral range denotes which wavenumber region will be covered. Many organic molecules have their fingerprint lines between 400 and 1800 cm^{-1} , which would be insufficient for the analysis of polysulphides for example – their lines are mostly present between 150 and 500 cm^{-1} . The spectral resolution describes how well defined the individual lines will be. Most Raman spectrographs employ charge-coupled device (CCD) detectors. In the case of very low scattering or low concentrations, one might opt instead for back-thinned CCD to enhance the sensitivity.

4.3.2.4 Theoretical calculation of Raman spectra

A molecule is a group of bound atoms interacting amongst themselves. The results of spectroscopic measurements are none other than the response of its electron cloud to applied electromagnetic perturbations. One can, therefore, approach this problem from two sides. On one hand, one can perform the analysis and interpret the results, and on the other – take the characteristics of the molecule as a base and calculate the properties of the molecule.

At the beginning of the last century, experimental results suggested that electrons behave in a way similar to the light waves. In 1926, E. Schrödinger introduced the wave function describing the electron motion (**Equation 13**), where \hat{H} is the total non-relativistic Hamiltonian operator, Ψ is the eigenfunction and E is the energy of the system.

$$\hat{H}|\Psi\rangle = E|\Psi\rangle \quad (13)$$

He proceeded to apply it to the hydrogen atom, which gained him precious information and confirmed the equation's correctness. Although it can be theoretically applied to any atomic system which is a molecule, its complexity becomes very quickly overwhelming with an increasing number of electrons. This is why, in order to calculate the properties of molecules, one needs simplifying approximations and vast computing power.

Several theories allowing for calculations of properties of different orders have been developed over time.¹¹⁵ The simplest of them is the Hartree-Fock method, which consists in replacing a multiple-electron wave function by a system of single-electron functions. One can then solve it by applying the self-consistent field theory, which reduces the electron-electron interactions to an average potential created by the other electrons¹⁰⁷. Even though this approximation is extremely simplified, it is included in most of the quantum chemistry computer programs.

The usual proceeding is the following: a presumption is made concerning the molecular structure and, based on it, the theoretical spectra are calculated. They are then compared with the experimental data and, if they coincide, the presumption is validated.

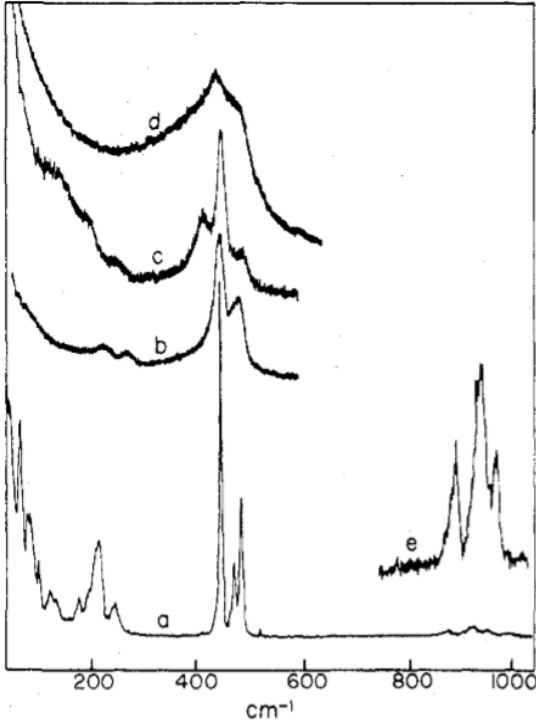
4.3.2.5 Overview of Literature handling Lithium Polysulphide Analysis by Raman Spectroscopy

Raman spectroscopy is particularly suitable for the analysis of homo-nuclear non-polar bonds, so it is, evidently, a method of first choice for sulphur and polysulphide chains. Attempts to analyse them ex-situ, in solid salts and solutions, as well as in-situ, when created inside of Li-S

cells have been undertaken numerous times. There are, nonetheless, a couple of major problems which make this analysis difficult. There exist a large number of polysulphides, and all of them have their fingerprint lines in the region between 150 and 550 cm^{-1} . Besides, a polysulphide solution is generally a mixture of several entities in equilibrium. Finally, the exact wavenumbers will depend on the solvent used, and, in the case of a solid salt, on the cation present. These issues make the identification complicated and unsure. In order to provide an overview of previous work in the topic, I compounded several publications which set out to analyse and identify polysulphide salts in solid and dissolved state in **Table 4.2**.

Table 4.2 Literature concentrating on the analysis of polysulphide chains

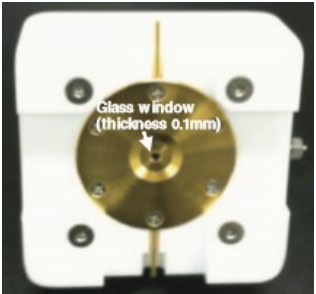
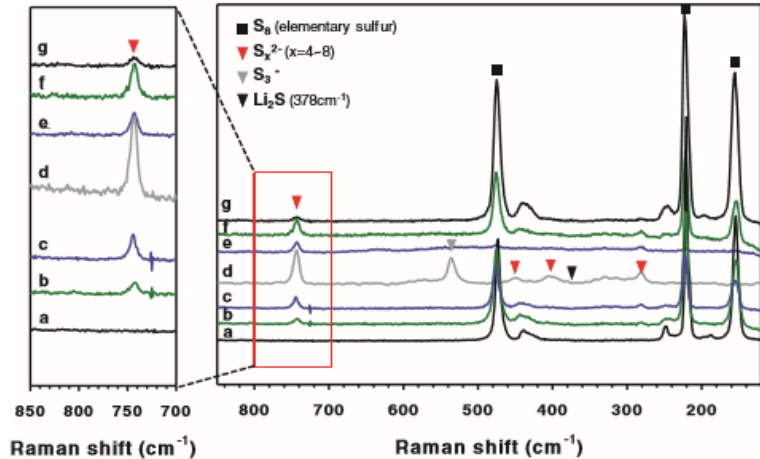
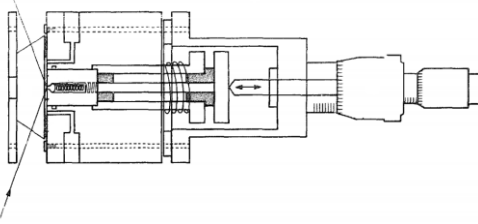
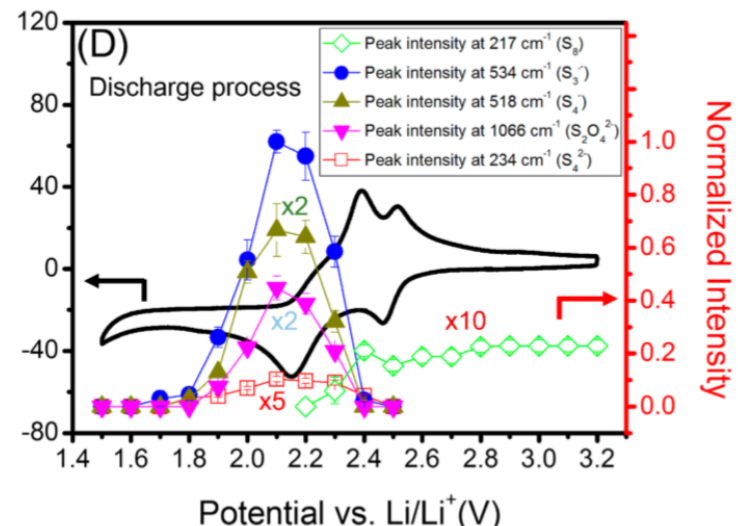
Publication	Analyte	Results (expressed in cm-1)				
Chivers et al. ¹¹⁶	S ₃ ⁻	534				
Daly et al. ¹¹⁷	Rhombic sulphur in different solvents	bands attributed to S ₄ ²⁻				
		ethylenediamine		n-propylamine	monomethylamine	
		195		193		
		245		242		
		396		397	399	
		434		438	437	
		502		505	502	
	Na ₂ S ₄ – solid and dissolved	bands attributed to S ₄ ²⁻				
		solid	water	ethylene-diamine	n-propylamine	mono-methylamine
		123	115			
		209	191	196	195	
		278	245	240	242	
		424	414	400	393	398
		448	448	433	442	433
		481	497	503	502	503
Dubois et al. ¹¹⁸		lithium polysulphides in liquid ammonia solution; nS + 2Li + NH ₃ → Li ₂ Sn + NH ₃	Li ₂ S ₄ (at RT)	identification of S ₆ ²⁻ S ₄ ²⁻ and assumption about the		
	188		existence of S ₅ ²⁻ in solution;			
	236		observation of the temperature-dependent			
	430		disproportionation to S ₃ ⁻ and calculation of the			
	472		equilibrium constant of disproportionation			
	490					
	535 – S ₃ ⁻					

Janz et al. ¹¹⁹	Analysis of Na ₂ S ₂ , Na ₂ S ₃ , Na ₂ S ₄ , Na ₂ S ₅ by Raman and IR spectroscopy	polycrystalline salts at 25°C			
		Na ₂ S ₂	Na ₂ S ₃	Na ₂ S ₄	Na ₂ S ₅ (stable α lattice)
		64	238	222	103
		130	458	267	135
		451	476	446	214
				476	266
				487	391
					444
					488
	Comparison of the spectra in polycrystalline, glassy, molten and aqueous states	spectra for N ₂ S ₄			Legend a: polycrystalline b: glassy c: aqueous d: molten e: overtone region for the polycrystalline material with expanded coordinate
					

To avoid overcharging, the focus of this table is set on the S₄²⁻ ion. The first observation is related to the results for the same entity in different solvents ^{117,118}. The lines are shifted when compared amongst themselves and, in the case of certain systems (e.g. Na₂S₄ dissolved in monomethylamine), are straight-out absent. This is a logic state of things since a solvated molecule interacts with its solvent: there are additional forces exercised on it, which will modify its response. Still, this circumstance obviously complicates the analysis. The next observation regards the different results obtained by different working groups ^{117,119} for the same sample. Finally, even the same molecule analysed by the same operator and in the same conditions will show different results in function of its internal structure. ¹¹⁹

Despite the slightly disappointing results, there is one piece of information which is verified and agreed upon by the scientific community: the S₃⁻ radical possesses a Raman line at 535 cm⁻¹.

Table 4.3 Raman analysis of Lithium-sulphur batteries

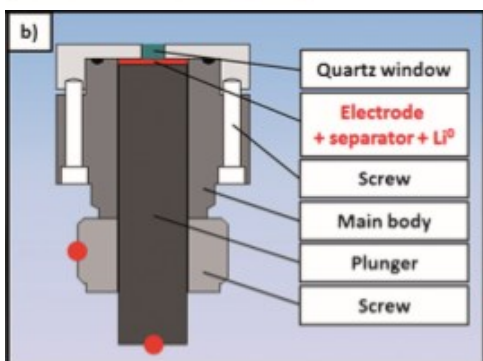
Publication and description	Cell composition and configuration	Results	
<p>Yeon et al.¹²⁰</p> <p>ex-situ analysis of electrodes after cell cycling and disassembly</p>	<p>cathode: sulphur + super P (conducting carbon additive) + PVDF on Al current collector</p> <p>electrolyte: 1M LiTFSI solution in TEGDME, DOL or TEGDME/DOL mixture</p> 		<p>Legend</p> <p>a: pristine cathode</p> <p>b: discharged to 2,28 V</p> <p>c: discharged to 2,1 V</p> <p>d: fully discharged (1,5 V)</p> <p>e: recharged to 2,34 V</p> <p>f: charged to 2,4 V</p> <p>g: fully charged (2,8 V)</p>
<p>Wu et al.¹²¹</p> <p>in-situ, in-operando analysis</p> <p>potential kept constant for 15 min at each 100 mV step to ensure analysis at the electrochemical equilibrium</p>	<p>cathode: sulphur + super P (conducting carbon additive) + PVDF on Al current collector</p> <p>electrolyte: 1M LiTFSI solution in TEGDME/DOL mixture</p> <p>cell configuration described in¹²²</p> 	<p>Results for the discharge process</p> 	

Hannauer et al.
123

in-situ, in-
operando analysis

interpretation
supported by
density functional
theory (DFT)
computational
chemistry

cathode: sulphur + super P (conducting
carbon additive) + PTFE on Al current
collector
electrolyte: 1M LiTFSI solution in
TEGDME/DOL mixture

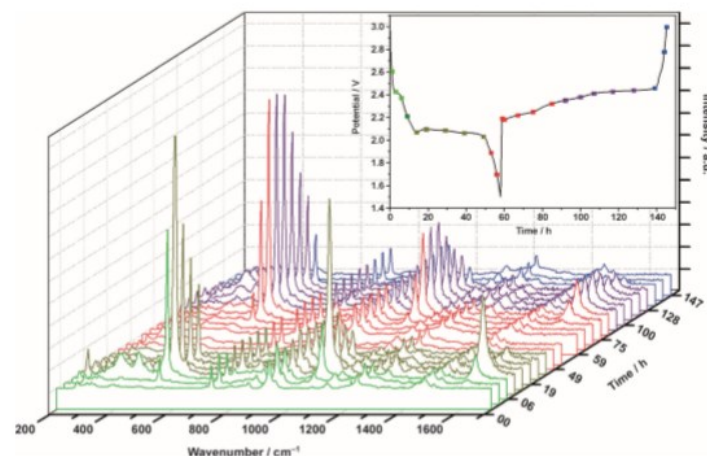


a: cell picture

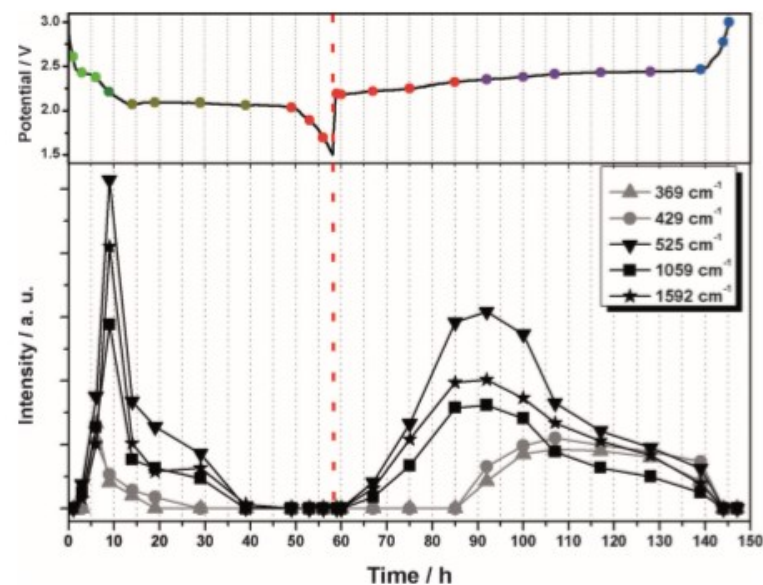
b: schematic representation

the measurement was made possible by
a hole in the Li anode and the use of a
glass fibre separator

Time and DOD-resolved spectra



Intensities of selected peaks in function of time and DOD



Peak attribution

Polysulphides identified
based on calculated and
literature values

Wavenumbers (cm⁻¹)

S22-: 420


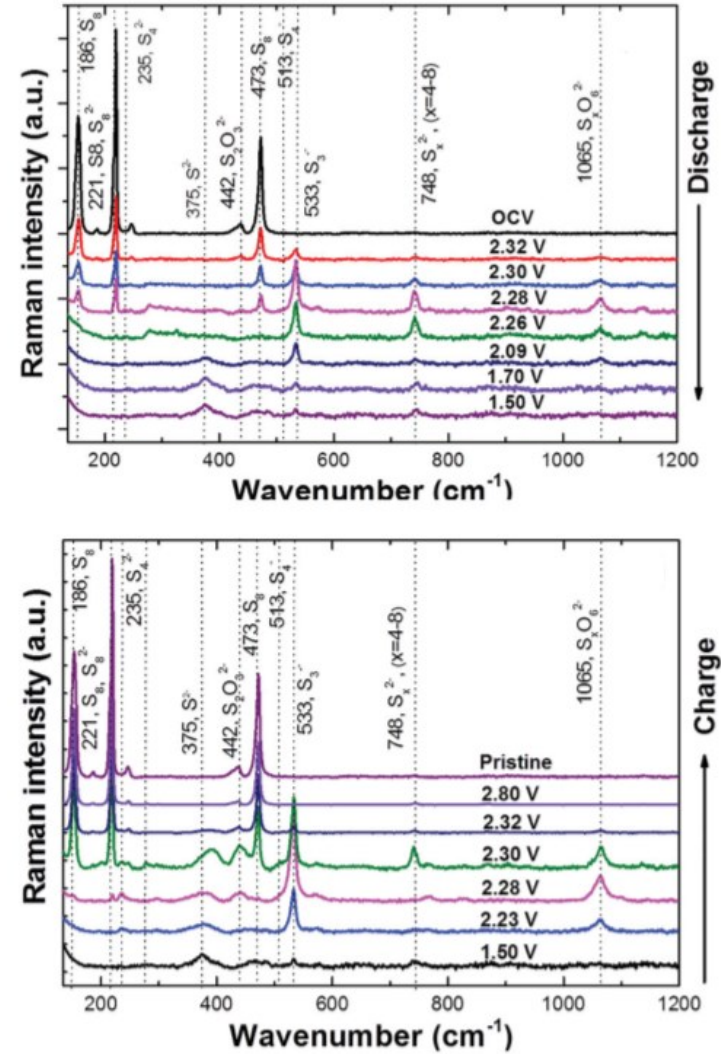
S3-: 220, 229, 495, 504,
525, 1059, 1592

S42-: 369, 442

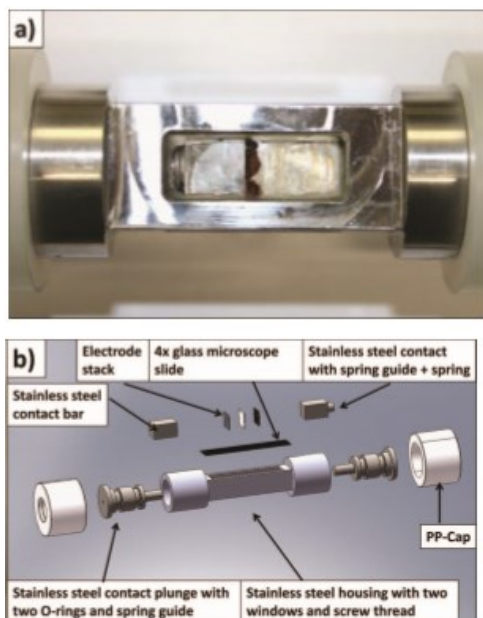
S62-: 453

S82-: 459

S62- or S82-: 315, 369, 390,
429

<p>Vinayan et al. ¹²⁴</p> <p>in-situ, in-operando analysis</p>	<p>cathode: sulphur in nitrogen-rich carbon host matrix ¹²⁵ + PVDF on Al current collector</p> <p>electrolyte: 1 M LiTFSI and 0,2M LiNO₃ solution in DOL, DME and ionic liquid (N -methyl N -butyl pyrrolidinium bis(trifluoromethanesulfonyl)imide (Pyr14TFSI) mixture, at the volume ratio 1:1:2</p> <p>ECC-Opto-Std test cell ¹²⁶</p> 	<p>Raman spectra obtained at different DOD and the entities corresponding to the peaks</p> 
<p>Hagen et al. ¹²⁷</p> <p>in-situ, in-operando analysis</p>	<p>cathode: binder-free carbon nanotube electrode ¹²⁸</p> <p>electrolyte: 0.7M LiTFSI and 0,25M LiNO₃ in DME/DOL mixture</p>	<p>Raman spectra obtained at different DOD and the entities corresponding to the peaks</p>

vibrational frequencies of different polysulphides calculated (DFT) in vacuum and THF solvent



a: cell picture

b: schematic representation

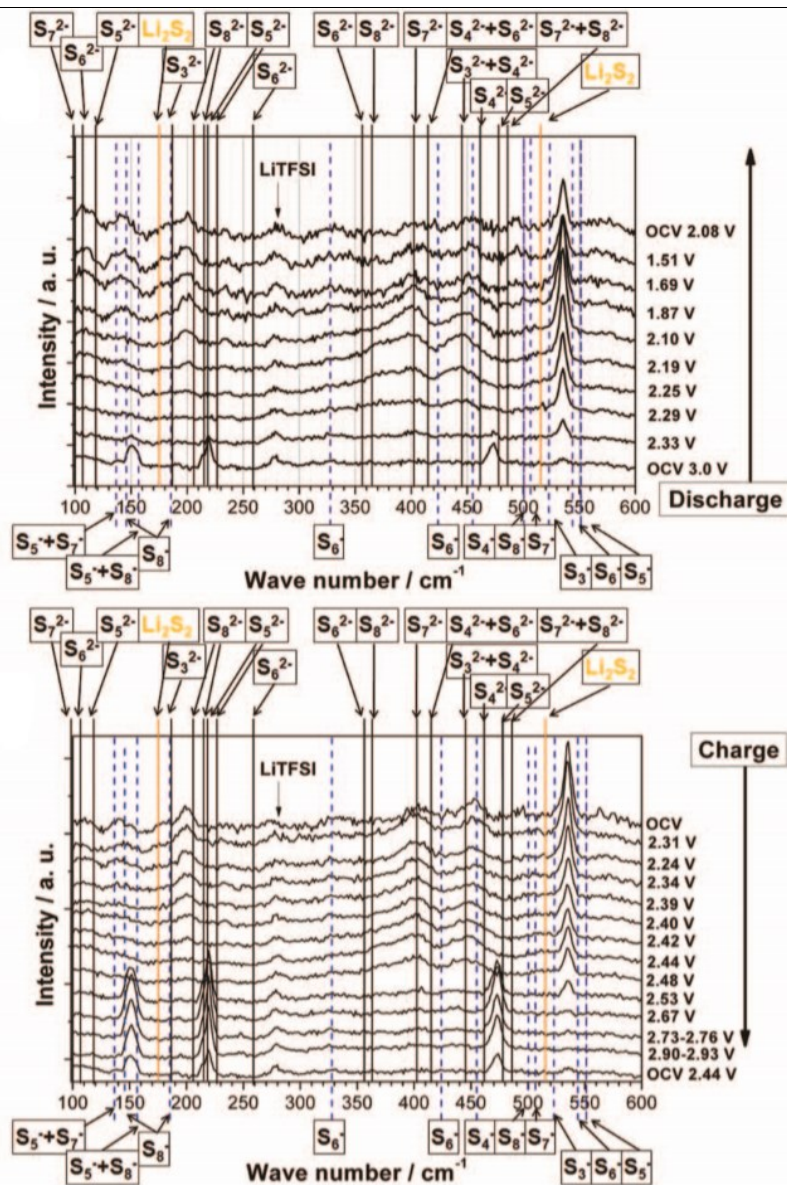


Table 4.3 groups the publications analysing the Li-S cells throughout cycling by Raman spectroscopy. Firstly, the analysed system is described – the electrolyte, for instance, has a considerable influence on the entities formed and their stability. Second, the cell configuration is depicted, since it influences both the processes taking place inside the cell and their “visibility” for the Raman spectrometer. Finally, the obtained results and the attribution of the observed Raman lines to different molecules are given. The polysulphides are identified based on values given in the publications listed in **Table 4.2**^{116–119} and on own calculations^{123,127}. The problem with the first approach has been discussed previously – there is little agreement as to which lines correspond to which molecules. From this point of view, the calculated spectra should be more reliable, but more data is needed before they could be unanimously used as fingerprint spectra.

5 EXPERIMENTAL PART

5.1 MATERIALS

Table 5.1 List of Used Materials with their Purity

Cell components	Substance or materials	Supplier
Cathode	Carbon black (CB) – Super C65	TIMCAL
	Sulphur (S ₈), >99,5%	Sigma Aldrich
	Poly(vinylidene fluoride) PVDF M _w ~ 534,000	Sigma Aldrich
	Guar gum	Sigma Aldrich
	Aluminium foil 15 µm, >99,3 %	MTI Corporation
	Carbon-coated aluminium foil 18 µm; Al foil – 16 µm, >99,9%	MTI Corporation
	Ultra-thin aluminium foil (2 / 4,5 µm), 99,0%	GoodFellow
	Lithium sulphide (Li ₂ S), 99,98%	Sigma Aldrich
Anode	Lithium chips, 99,9%	MTI Corporation
Separator	FS2190	Freudenberg
	C2325	Celgard
	C2320	
	C2340	
	H1612	
	H2512	
	PES B	Synthesized in the institute by the group of Dr. Meier-Haack
	PES C	
	BW532	
	BW708	
	BW716	
	Lithium hydroxide monohydrate (LiOH), ≥98,0%	
	1,2-Dimethoxyethane (DME), 99,5%	Sigma Aldrich
Electrolyte	1,3-Dioxolane (DOL), 99,8%	Sigma Aldrich
	Bis(trifluoromethane)sulfonimide lithium salt (LiTFSI), 99,95%	Sigma Aldrich
	Lithium nitrate (LiNO ₃), 99,99%	Sigma Aldrich
	Lithium perchlorate (LiClO ₄), 99,99%	Sigma Aldrich
	Resorcinol, ≥99,0%	Sigma Aldrich
	Formaldehyde solution in water/methanol, 37%	Sigma Aldrich

They were used as received, besides the electrolyte salts, which have been additionally dried.

5.2 CELL COMPONENT FABRICATION AND CELL ASSEMBLY

The exact methods of preparation and fabrication for the studied cells will be given immediately before the corresponding analysis results and interpretation. Here, the standard methods are presented.

5.2.1 Cathode

The cathode of the lithium-sulphur cell consists of sulphur encapsulated inside a conducting carbon matrix and applied on a current collector (**Figure 5.1**).

Sulphur (S_8) powder is mixed with the carbon material* in a ratio of 2 to 1. They are introduced into a milling beaker (stainless steel) and the stainless-steel milling balls are added. Their number is calculated in the following way: the powder mass is multiplied by 20. Half of this mass is completed by 4 mm diameter balls and the other half – by 5 mm. These numbers remain approximative to the mass of a single milling ball. The powder is then treated in a vibrational ball mill (MM400 from Retsch GmbH) at a frequency of 15 Hz r twice for one hour, with a thirty-minute break. The reason for it is to avoid overheating and consequential damage to the material. The mixture is then introduced into a test tube sealed with a septum and filled with argon and heated for 5 hours at 155°C, to assure the melt-infusion of the sulphur into the structures of the carbon. It is then mixed with conducting carbon black (CB) in a proportion 82% of sulphur-in-carbon to 10% of CB. The mixture is milled again in the same conditions as previously for thirty minutes. Then an amount of binder representing 8% of the total mass is added along with the solvent to

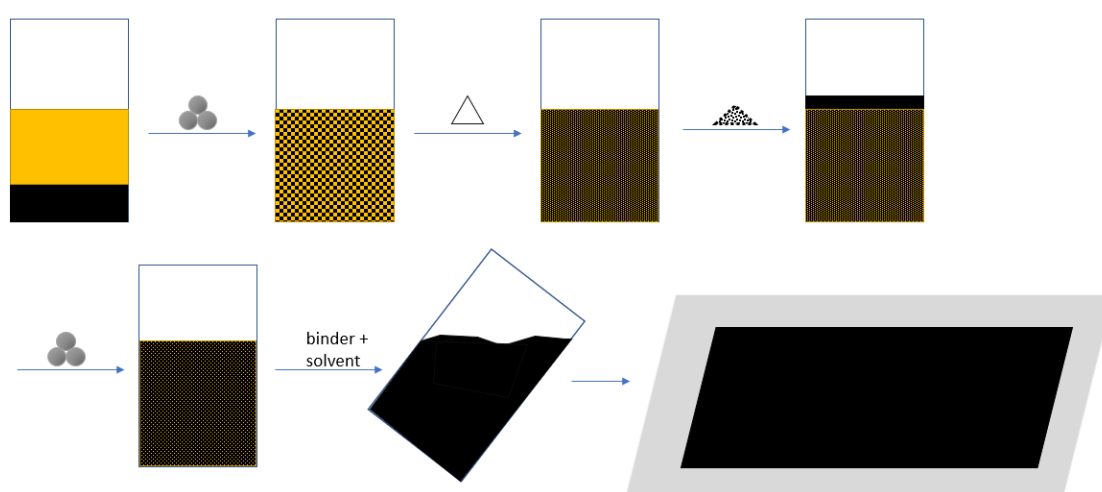


Figure 5.1 Schematic representation of the steps involved in the cathode preparation

* carbon black in the case of the standard cell, used for Raman investigations and as reference with which all the modified cells are compared

create a slurry of the consistency of honey. It is applied on the current collector using a doctor blade and dried in air and then at 95°C immediately prior to the cell assembly.

5.2.2 Electrolyte

The electrolyte components being the most susceptible to absorb atmospheric water, they are always stored in an argon-filled glovebox. The two solvents, DME and DOL, are mixed in a 50/50 by volume ratio. The standard electrolyte is composed of 1M LiTFSI and 0,25M LiNO₃.

5.2.3 Electrochemical Cells

In a standard cell, the anode and separator are used as received. The particular case of separator modification will be discussed later. The lithium chips are stored in a dark glass jar in the argon-filled glovebox. The separators are dried at 90°C, then stored in the glovebox until solicited.

The cell casing of 1.96 cm diameter was purchased at MTI Corporation and includes the top and bottom parts, the spacer and the spring. The cathode is cut into round electrodes of a 1.4 cm diameter, the separator diameter is of 1.95 cm, to exclude the risk of a short-circuit, and the diameter of the lithium anode is of 1.9 cm, to ensure complete overlapping with the cathode even in the case of its dislocation. The cathode is positioned into the bottom case of the cell and centred. Then, the non-woven polypropylene (PP) separator (Freudenberg) is placed on top of it and 70 µL of electrolyte is added. The second separator (Celgard) is positioned, followed by the lithium disc.

The spacer is placed on top of the lithium anode in a way that their borders coincide, to avoid indentations into the soft foil. Then, the spring is placed on top and the cell is closed with the top cover. It is then sealed in a cell crimping machine. A PP sealing gasket ensures the cell's airtightness (Figure 5.2).

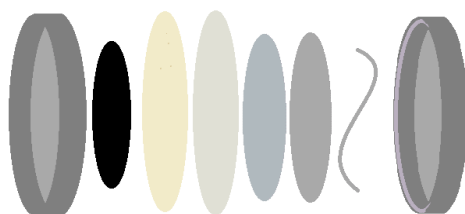


Figure 5.2 Exploded view of a coin cell, picturing its solid components

5.3 RAMAN SPECTROSCOPY

As I came to learn while working on this thesis, one of the most important parts in the in-situ, in-operando analysis, is the experimental setup. The influence of cell geometry has already been discussed in chapter 4.2.3, and it is even more decisive when one has to alter it in order to observe the behaviour of the system.

5.3.1 Cell for In-Situ, In-Operando Measurements

Since the cell components are sensible to water, the electrochemical cell has to be sealed from atmospheric air at all times. At the same time, Raman spectroscopy relies on the waves from the visible spectrum, so a translucent medium is essential. The first cell to be tested was a Swagelok[®] three-electrode cell, where a quartz window was fixed at the base of the third electrode (left in **Figure 5.3**). The optic probe could then be introduced and fixed in front of the electrochemical cell.

The next modification consisted of completely removing the slot for the third electrode, which would allow the access of the Raman microscope to the cell (right in **Figure 5.3**). This, in turn, would make the measurement more exact and would permit the analysis at different points between the two electrodes. The third cell configuration is based on the coin cell. A hole is made in the cell case and a 15 μm thick Kapton[®] window is glued to it with a UHU 2-component epoxy glue. A symmetric hole is made in the electrode. This cell is the closest to the cell for NEXAFS analysis performed by the project partner and allows for the best comparison of the results obtained by both methods. Its drawback is that, since there is no electrode in the analysed spot, one has to entirely rely on the diffusion processes.

The third cell configuration is based on the coin cell (**Figure 5.4**). A hole is made in the cell case and a 15 μm thick Kapton[®] window is glued to it with a UHU 2-component epoxy glue. A symmetric hole is made in the electrode. This cell is the closest to the cell for NEXAFS analysis performed by the project partner and allows for the best comparison of the results obtained by

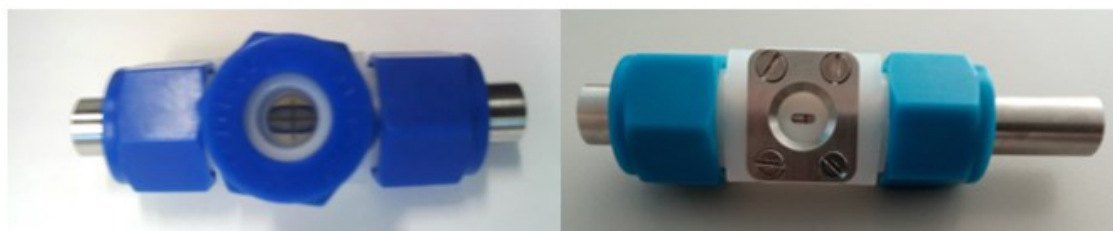


Figure 5.3 Modified three-electrode Swagelok[®] cell for in-situ analysis; left: optic probe, right: Raman microscope

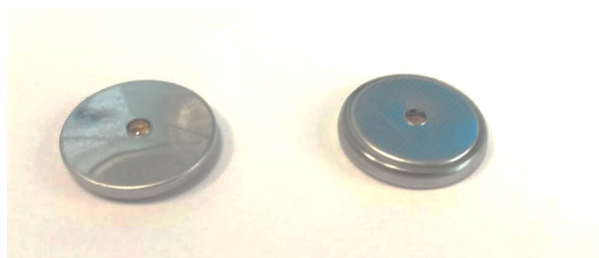


Figure 5.4 Coin cell modified for in-situ measurements; left: on cathode side, right: on anode side

both methods. Its drawback is that, since there is no electrode in the analysed spot, one has to entirely rely on the diffusion processes. The choice of the in-situ, in-operando cell will be discussed in a more detailed way in chapter 6.2 **Error! Reference source not found..**

5.3.2 Analysis Setup

Since the electrochemical cell is concomitantly analysed by galvanostatic charge-discharge and by Raman spectroscopy, it had to be immobilized under the microscope and electrically connected. This is quite straight-forward for the Swagelok® cell: it is fixed on a horizontal support and the plugs are introduced into the plungers. In the case of the optic probe, even the horizontal support is not necessary.

For the coin cell, the best possibility would be to have the cell in the coin cell testing board, but, unfortunately, the measuring distance of the microscope does not permit it. This is why, in a first layout, the cables were fixed as shown in the left picture of **Figure 5.5**.

Since the contact was not optimal, which had negative effects on the cell's electrochemical performance, it was later replaced by the in-house built device seen in the right picture of **Figure 5.5**

The analysis was performed using a RAMAN Image System WITec alpha300R instrument (RAMAN microscope) and an objective with a magnification of 20x. A green laser with a wavelength of 532 nm and a power output of 5 mW served as the excitation source. The working distance was individual for each cell, but typically between 1 and 3 mm.

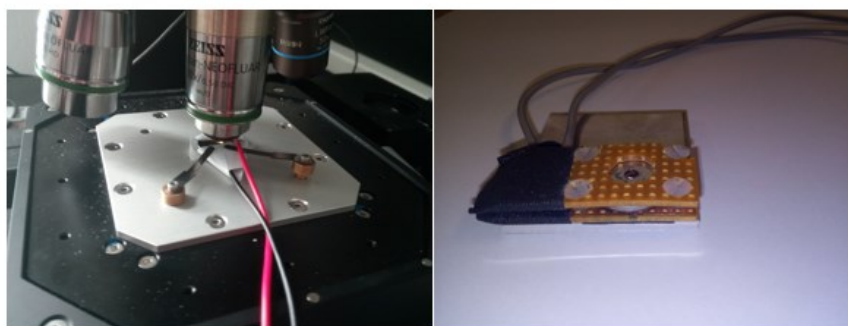


Figure 5.5 Setup for cell analysis; left: initial setup, right: enhanced setup

5.4 MATERIAL AND PERFORMANCE ANALYSIS

5.4.1 Scanning Electron Microscopy (SEM)

Scanning electron microscopy is a powerful tool for the visualisation of structures of sizes inferior to the wavelength of visible light, their topography, chemical composition and crystallinity. The electrons, carrying a specific kinetic energy, are decelerated by the analysed sample upon encounter. The energy is dissipated and a variety of signals is produced, such as secondary electrons (SE), backscattered electrons (BSE), photons, heat or others ¹²⁹.

As far as SEM is concerned, only the secondary and backscattered electrons are of interest (Figure 5.6¹³⁰). The BSE are electrons whose trajectory is deviated after their elastic collision with the atom. The intensity of the generated signal depends on the size of the atom, which provides information about the sample composition. The SE originate from inelastic interactions of the incident electron with the sample. They are electrons from the sample that are ejected by the beam electrons. Such an electron then moves towards the surface of the sample and excites it – this is why they are particularly helpful for topography analysis. This is also the signal that was of particular interest in this work.

SEM pictures were recorded on a Zeiss Ultra Plus, with a 3-kV acceleration voltage. The samples were glued to the sample carrier and coated with a 3.5 nm platinum layer, for

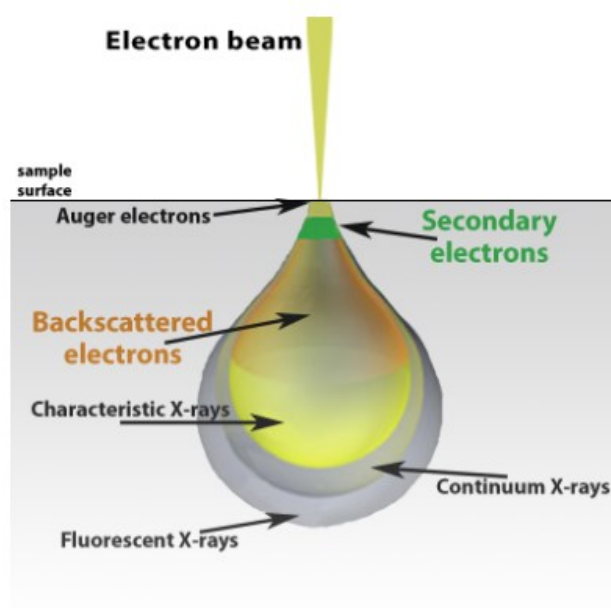


Figure 5.6 Different possible electron beam interactions

conductivity and to avoid charging effect. This step was omitted in the case of intrinsically conducting samples, such as graphitic carbon.

5.4.2 Thermogravimetric Analysis (TGA)

This method was used for the confirmation of the sulphur content in the cathode after the preparation.

The sample is heated in a controlled way and in a controlled atmosphere and the mass of the sample is registered in function of the temperature. In this way, one can obtain information about absorption and adsorption phenomena to which the material has been subject to, as well as follow the thermal decomposition of the molecule. Depending on the atmosphere, one can also observe the reactions of the sample with the ambient gas.

The instrument used in this work was a TGA Q5000 from TA-Instruments. The sample was heated within the temperature range between 25 and 800 °C at a heating rate of 10 K/min and under a constant stream of nitrogen gas.

5.4.3 Gas Sorption Analysis

The gas sorption is a widely used tool for the identification of specific surface areas^{131,132}, as well as of porosities of solids. It is particularly important to know when one is interested in interfacial processes.

Solid materials tend to adsorb gas molecules. According to the Langmuir adsorption model, the adsorbate is an ideal gas whose partial pressure and volume are related. It binds to the surface of the adsorbent so that there can only be one molecule per site and there are no interactions between neighbouring gas molecules. Their interaction with the solid is, on the contrary, viewed as a chemical bond*. The scientific community today mostly makes appeal to the Brunauer–Emmett–Teller (BET) theory, which operates with multiple gas molecule layers.

The gas principally used for the analysis is the nitrogen, but a variety of other gases can also be used, such as helium, argon, n-butane or carbon dioxide.

The measurements were carried out using the Autosorb-1 of Quantachrome, USA. The material was weighted**, introduced into the sample cell and degassed for 3h at 80°C in vacuum.

* which it is not

** the mass of the material to analyse is chosen depending on the expected specific surface area

The specific surface was then measured using nitrogen and the analysis was performed at liquid nitrogen temperature (77 K).

5.4.4 Electrical Conductivity

As has been previously discussed, one of the main requirements for the encapsulating material is it to be electrically conductive. Electric conductivity describes the capacity of the material to conduct electric current between two points and is defined as the voltage necessary to get a certain amount of current to flow. Its value depends on the number of mobile electrons available and the density of the atoms. In turn, the number of “free” electrons is given by the number of electrons near or above the Fermi level.

The powder conductivities were measured on an in-house built device and on a custom-made software, developed with TestpointTM. The functioning principle is the following: the powder is placed between two electrodes and the resistance values are measured between them. Since the system geometry is known, one has all the data needed for the calculation of the conductivity.

The powder to be analysed was introduced into a PMMA cylinder with a cavity diameter of 5 mm and pressed together with a piston with a gold electrode situated at its tip. The resistivity was measured by a DMM 2001 multimeter of Keithley Instruments. The pressure was varied between 0 and 1 MPa – higher pressures were avoided in order to not damage the material’s porous structure.

5.4.5 Contact Angle Measurement

The interface between two substances with different physical properties is a special region where a number of tension forces are at work. A whole domain in physics and chemistry focus on interfaces. This is of course even more true for the special point in which the solid, liquid and vapour phases meet.

The contact angle Θ_c is the angle formed by the edge of a liquid droplet on a solid support, while surrounded by a gas, as illustrated in **Figure 5.7**.¹³³

The surface or interfacial tensions are represented by σ . These forces and, in occurrence, the contact angle, depend on the properties of the three constituents of the system in equilibrium. The microscopic structure of the solid* and its chemical affinity to the liquid denote how the behaviour of the droplet will be.

* its roughness

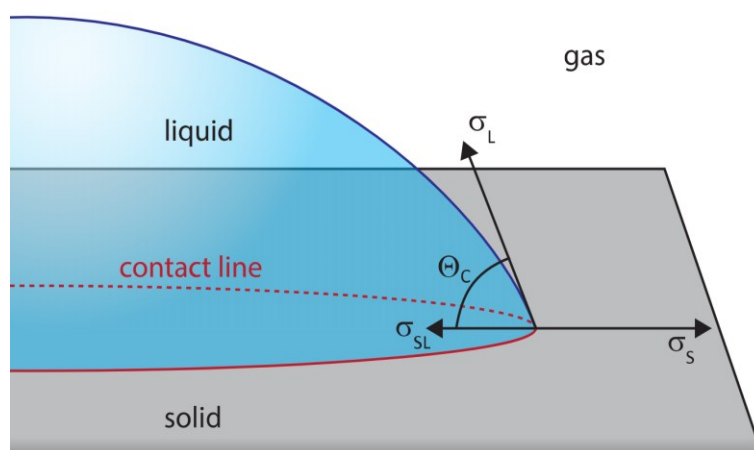


Figure 5.7 Contact angle at solid-liquid-gas interface

Within this work, the measurement was performed on an OCA40 by DataPhysics Instruments GmbH.

5.4.6 Galvanostatic Charge-Discharge

This is the method which is most widely used for the characterisation of electrochemical devices such as batteries and supercapacitors. The operating mode is the following: the battery is cyclically discharged and charged under constant current and the adjusted voltage is measured at regular time intervals. The capacity of the cell is then calculated by multiplying the duration of an individual charge or discharge step by the applied current.

The current to be applied was calculated in function of the amount of active material (sulphur) inside the individual cell and expressed as a C-rate*. In this work, a C-rate of 0,1 C has been used for the discharge and one of 0,2 C – for the charge. Thus, in the case of the full reaction of the active material, a complete cycle had to last for 15 hours. The voltage range was set between 1,6 and 2,8 V or between 1,8 and 2,6 V.

Besides the specific charge and discharge capacities, other information can be acquired from the obtained results. Since electrochemical reactions occur at a constant voltage, the curve will feature a plateau. The shape of the discharge and charge curve, including plateaux and artefacts, carry information about the processes taking place inside the cell at the precise stage. It has been explained in deeper detail in chapter 4.2.1

The measurements were performed on a BST8-MA 8-channel battery cyclers, purchased from the MTI Corporation.

* the rate of charge or discharge as associated with the capacity of the battery: at 1C, an n Ah battery should provide n A for 1 hour

6 RESULTS AND DISCUSSION

6.1 ADJUSTMENT OF STANDARD CELL

When this project started, there already was a strong research group working on the subject of lithium-sulphur batteries. The first standard cell was therefore inherited from the more experienced colleagues and used to determine if the introduced modifications enhance its performance or not. It was also the cell analysed by *in-situ*, in operando Raman spectroscopy.

While conducting this work, new information became available, which brought up the need to make some changes.

6.1.1 Binder and Current Collector

Although the reactants in the Li-S cell are solely the lithium and the sulphur, it consists of a panoply of materials, that have to properly function in unison. The sulphur is embedded in a conducting matrix, usually carbon. This active material cannot be used as a free-stranding film, so it is applied to a current collector, which also enhances the routing of the electrons. A binder ensures its adhesion. Besides, the binder can also aid in keeping the structure of the cathode intact even after multiple charge-discharge cycles, accompanied by expansion and shrinking. To sum it up, the binder hold the active material in place immediately after the cathode preparation and throughout its exploitation, all while being added in a minor amount.

As it has been stated in paragraph 4.2.3, the state-of-the-art binder for Li-S cells is the same as the one used in Li-ion batteries – the PVDF. It is also the binder which was used in our group. The cathodes prepared using PVDF showed a good electrochemical performance, nevertheless, there were two issues which made a revision desirable. Firstly, the solvent necessary when working with PVDF, NMP, is toxic, and should, therefore, be avoided when possible. It also has a



Figure 6.1 Cathode material delaminating from the current collector; scale: 1 cm

high evaporation temperature, requiring energy and time to be removed. The second problem arose on a more technical level: cathodes prepared with PVDF as binder sometimes displayed macroscopic crackling (**Figure 6.1**) and had to be excluded from further study.

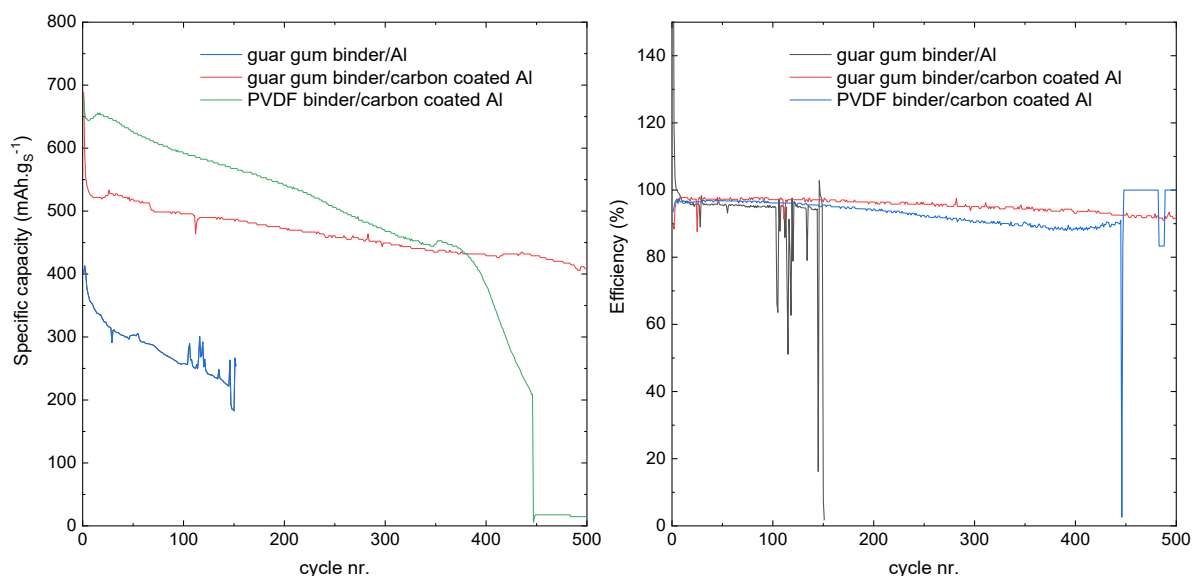


Figure 6.2 Binder and current collector comparison; left: capacities, right: efficiencies. Measurements conducted between 1.8 and 2.6 V, with a current of 0.1C for discharge and 0.2C for charge

This phenomenon was unpredictable and was a serious hindrance to the result reproducibility. For this reason, an alternative, bio-based substance was taken: Guar gum.¹³⁴ First, the preparation method was kept unchanged, with the exception of the binder and solvent. In this way, the cathode was prepared by melt-infusing the sulphur into the carbon matrix, adding the binder and Millipore water and applying the obtained slurry on an aluminium current collector. Very quickly a problem became apparent: carbon is hydrophobic, whilst aluminium is hydrophilic, so the water-based slurry cannot be properly applied. This is why the pure aluminium was replaced by carbon-coated aluminium. The 1 μm thick carbon layer did not considerably add to the cathode's volume or weight, but it ensured better adhesion. The results were then plotted in function of the cycle number.*

The obtained results (**Figure 6.2**) confirms the assumption made after the cathode preparation: guar gum cannot be used on pristine aluminium foil. In the same time, the results obtained for guar gum and PVDF are not so obvious. The specific capacity of the cell prepared with PVDF as a binder is approximately 20% higher when compared to the one prepared with guar gum. On the other side, its decrease is faster and culminates with an abrupt drop. The choice is finally made in the favour of the guar gum, for reasons evoked above.

* It has to be noted that, in this work, the discharge capacity is given unless the opposite is stated. It has been chosen for the simple reason that, in the case of a battery, the most interesting parameter is the amount of energy it can give away.

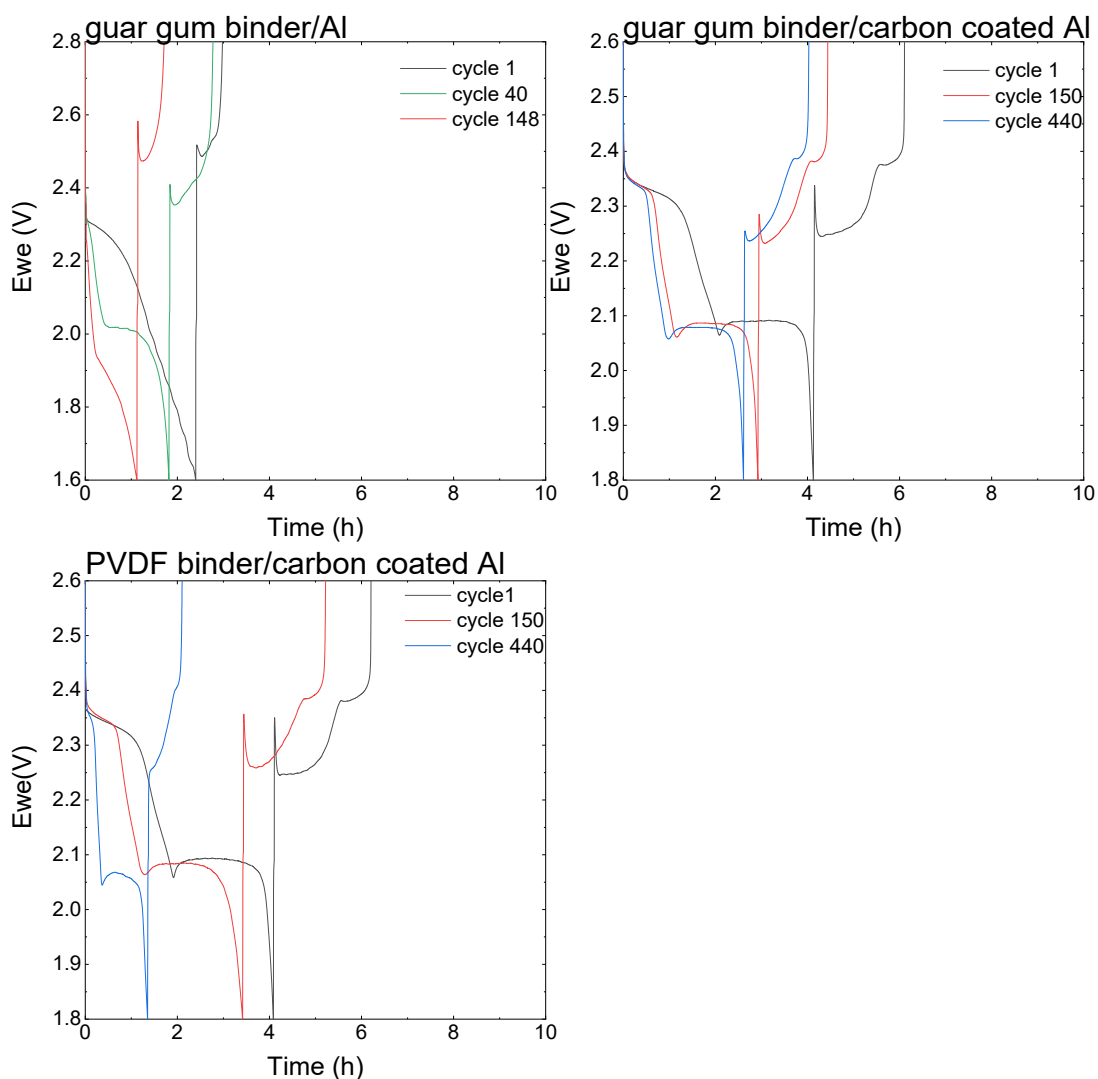


Figure 6.3 Voltage profiles comparison. Measurements conducted with a current of 0.1C for discharge and 0.2C for charge

The voltage profiles of the three cells have also been monitored and compared (**Figure 6.3**). The voltage window has been modified during the study since the discharging down to 1,6 V instead of 1,8 V and the charging to 2,8 V did not add much to the capacity of the cell. The narrowing of the voltage window was therefore considered to benefit the performance of the cell since one would eliminate potential side reactions. Although the compared cells have been cycled in different conditions, the behaviours are still representative and can be compared.

Besides the duration of the individual cycles, which is directly linked with the capacities, one should also note the shapes of the curves. In the case of the cell constructed with uncoated aluminium as current collector, the discharge curves are different amongst themselves and from the commonly seen curve. Using a material which is not adapted to the system largely impedes the running of the reaction – since the binder does not perform correctly, the active material has a weak contact to the current collector, so the current cannot travel properly through the cell.

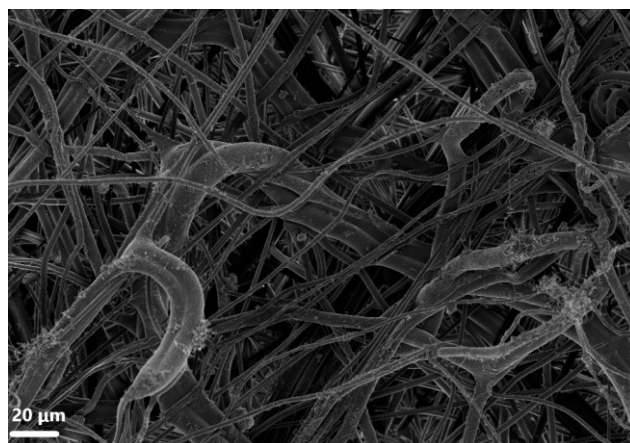


Figure 6.4 SEM image of FS2190.

The profiles of the cells built with guar gum and PVDF as binders are equivalent: the guar gum does not induce the rise of unwanted side reactions and does not alter in any other way the normal running of the electrochemical reactions.

6.1.2 Separator

The main duty of a separator is to prohibit the direct contact between the two electrodes of the battery, thus avoiding a short circuit. Nevertheless, it can take on other roles, such as stopping the soluble lithium polysulphides from spreading throughout the cell, which should extend its cycle life. Therefore, the choice of an adapted separator is important and needs researching upon.

At the beginning of the present work, I was given a separator combination which has been put together and which showed good results. Running ahead, these separators have been kept after the study. Nevertheless, it permitted to check the influence of minor modifications in the foil structure.

The first separator was the Freudenberg FS2190. It is a non-woven polypropylene film, with very high porosity (>90%) and a thickness of 180 μm (**Figure 6.4**)

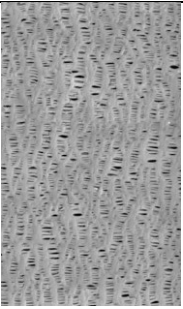
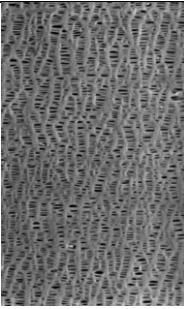
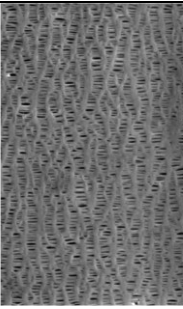
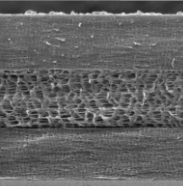
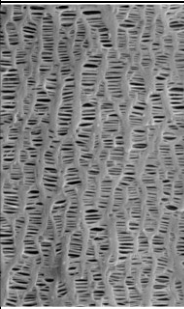
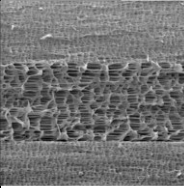
Used alone, it shows a limited performance since it can neither hinder the lithium dendrite growth nor stop the polysulphide shuttle. The polyolefin fibres are, by their intrinsic structure, resistant to solvents and chemicals. This is highly advantageous for a separator since it should maintain its structure in any conditions. On the other hand, though, there are also no interactions which could retain the diffusion of the polysulphides.

The reason for its application lies in the fact that the thick membrane with an appearance reminiscent of cotton acts as a reservoir for the electrolyte, allowing for better and more uniform wetting of the cathode.

The second separator was the Celgard C2325. It is a trilayer polypropylene-polyethylene-polypropylene (PP/PE/PP) film whose porosity is not intrinsic, like in the previous case, but artificially introduced after the foil casting. Besides the C2325 membrane, the manufacturer offers a variety of other products, which I went on to test. A comparative study between C2325, C2320, C2340, H1612 and H2512 was made (**Table 6.1**). The shrinkage, tensile strength and puncture strength parameters are interesting from the point of view of mechanic resistance during cell construction and cycling. The Gurley value represents the air permeability of the membrane and is intimately linked with its porosity and thickness. In the case when both porosity and thickness are unchanged, its variations are explained by the tortuosity of the pores. In order to be able to compare the five membranes, the assumption has to be made that the pores are identical in all the cases and the variations of the Gurley value are only provoked by the porosity and thickness. Since all the membranes are trilayer PP/PE/PP films, we are presented with the following couples:

- C2320/C2325 – same porosity ($\pm 2,5\%$), different thicknesses
- C2340/H1612 – same porosity ($\pm 1,1\%$), different thicknesses
- C2325/H2512 – same thickness, different porosities

Table 6.1 Separator material properties as provided by the supplier

	C2320	C2325	C2340	H1612	H2512
Image				 cross-section: 	 cross-section: 
Thickness (μm)	20	25	38	16	25
Gurley (s)	530	620	780	250	320
Porosity (%)	41	39	45	44	50
TD Shrinkage at 105°C/1h (%)	0	0	0	0	0
MD Shrinkage at 105°C/1h (%)	1,5	2,21	3,26	1,6	4,5
TD Tensile strength (kg.cm^{-2})	143	150	165	160	150
MD Tensile strength (kg.cm^{-2})	2261	1700	1630	2000	1800
Puncture strength (Grams Force)	481	380	500	360	450

In the couple C2320/C2325, the first membrane shows a visibly superior performance, which is counterintuitive (**Figure 6.5**). It is thinner and, if we return to the Gurley value, it is lower for C2320 – its air permeability is higher. Consequently, its polysulphide retention capacity should be overall lower.

The cell cycling can be roughly divided into three parts. This division is purely imaginary and is only meant to facilitate the analysis. First, the lithium ions are brought by the electrolyte to the cathode. In this case, high ionic conductivity is desired in order to accelerate the reaction. Then, the ions react with the cathodic sulphur, and on this step, it is important to hinder their diffusion away from the cathode. Finally, the cell is recharged and the reactions inversed. Here, the separator permeability is again desired, since it would ensure the return of the diffused

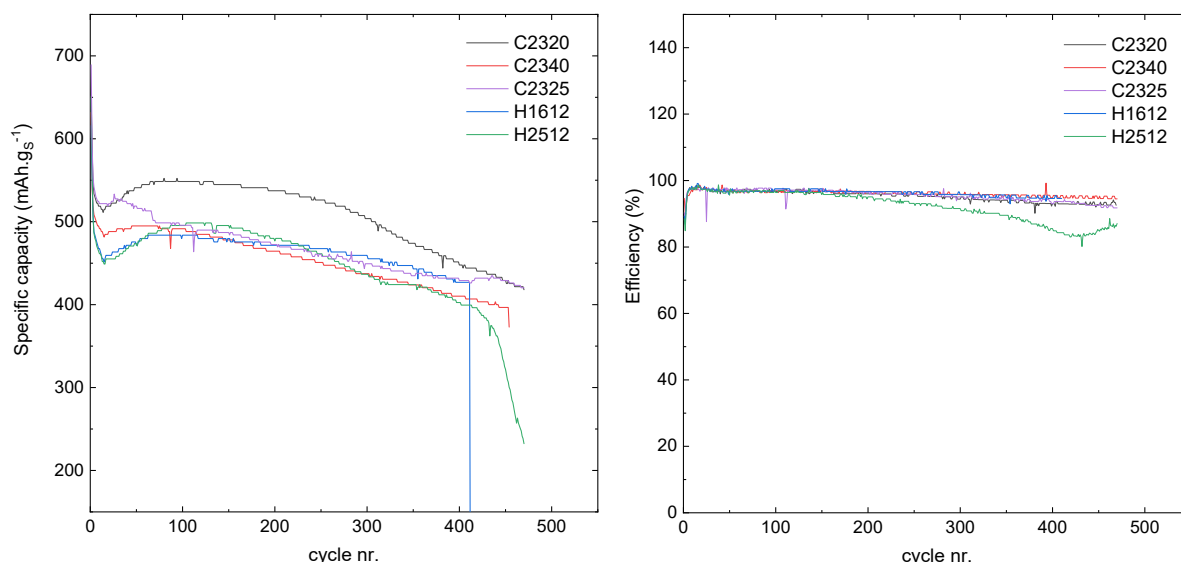


Figure 6.5 Comparison of different Celgard membranes; left: capacities, right: efficiencies. Measurements conducted between 1.8 and 2.6 V, with a current of 0.1C for discharge and 0.2C for charge

polysulphides back to the cathode. In conclusion, in order to obtain a well-functioning cell, one has to maintain the equilibrium between permeability and retention. This assumption is confirmed by the similitude of results in the couples C2340/H1612 and C2325/H2512 (**Figure 6.5**).

Another noteworthy detail is the reproducing drop and subsequent rise of the capacity at the beginning of the cycling. The first cycles, when a high quantity of active material is available, show elevated capacities. Still, fewer than half of the sulphur reacts at the first discharge. Therefore, the local minimum at approximately 15 cycles corresponds to the moment where the easily accessible sulphur has been partly consumed*, whilst the remaining one is still hard to access.

When looking at the efficiencies, they are stable and close to 100% throughout the cycling. Even though the cells lose in performance, they do not consume more electric energy than they can deliver. The only deviation is seen for H2512, but it cannot be explained by the properties of the membrane – most likely, it is a local defect.

* the sulphur remains in the electrolyte in the form of lithium polysulphide, is precipitated in the separator as a result of disproportionation reactions, or is reacted to lithium sulphide at the anode; in any of these cases it does not have a contact with the conducting cathode and, therefore, does not participate in further reactions

6.2 IN-SITU AND IN-OPERANDO ANALYSIS

6.2.1 Analysis of Cell Components and Polysulphide Solutions

A Li-S battery is a complex system with many components. This is why, before the beginning of in-operando Raman experiments, the cell parts have been analysed individually. This way, one can directly eliminate the peaks originating from the separator or electrolyte (**Figure 6.6**).

In the wavenumber domain between 0 and 1000 cm^{-1} : sulphur and lithium polysulphide spectra only show lines at wavenumbers inferior to 600 cm^{-1} . It is interesting to notice that there is no sulphur signal in the case of the cathode, even though the majority of the active material consists of it. This confirms the fact that the material is well homogenized and that the sulphur is encapsulated inside of the carbon pores. The electrolyte and separator possess lines in the same domain as sulphur and have to be taken into account when interpreting the results.

Afterwards, polysulphide solutions in the electrolyte solvents have been prepared for further use as reference. Sulphur and lithium sulphide have been introduced into a 50/50 wt. mixture of DME/DOL and the quantities have been chosen in function of the stoichiometric proportions. Seven solutions have been prepared as follows (**Equation 14-20**).

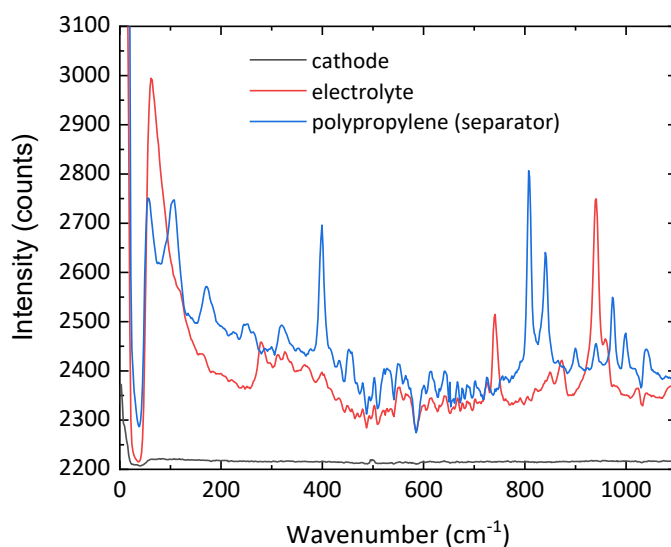
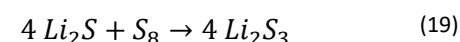
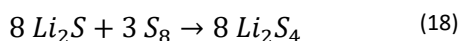
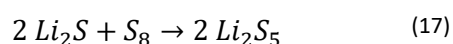
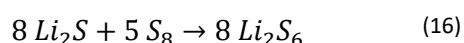
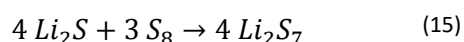
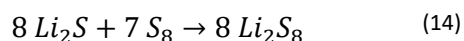


Figure 6.6 Raman spectra of the Li-S cell components measured each by themselves.

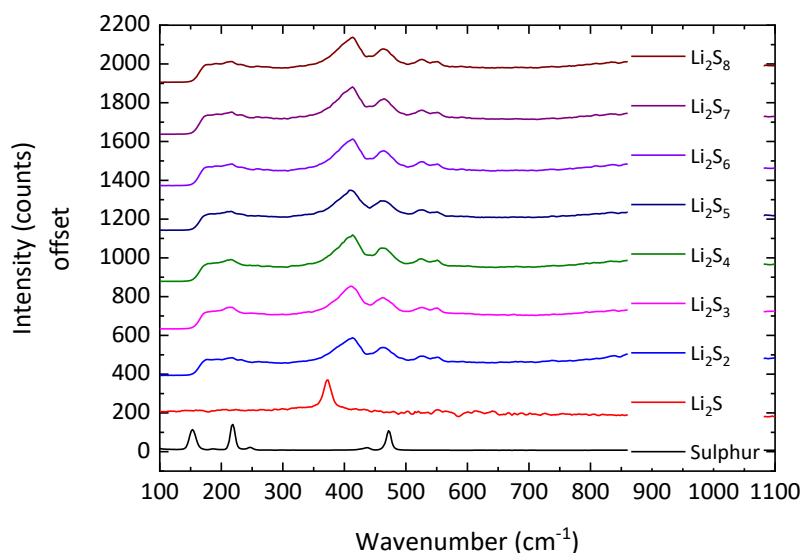


Figure 6.7 Raman spectra of lithium polysulphide solutions prepared with different stoichiometric proportions.

The solutions were then filtered and analysed (**Figure 6.7**).

It is evident that all the solutions have exactly the same Raman lines, which makes it impossible to use them for the identification of the encountered polysulphides. Regardless of the stoichiometry of the prepared solutions, they all consist of the same entities. The legend given in the graph corresponds to the desired, and not the actual salt. Therefore, I relied mostly on the results obtained by Hagen *et al.*¹²⁷

6.2.2 Modified Swagelok® Cell

At the beginning of the present project, the most promising approach for conducting in-situ Raman analysis consisted in modifying a three-electrode Swagelok® cell. The idea consisted of placing an optical window instead of the third electrode, perpendicularly to the cell. The measurement would then be performed as depicted in **Figure 6.8**. A crystal quartz window was chosen for its availability and performance in the studied system.

6.2.2.1 First Swagelok® Cell Modification

As it has already been mentioned, the first cell was made for the analysis via an optic probe. The cell was discharged and recharged as normal, while the Raman spectrum was acquired (**Figure 6.9**).

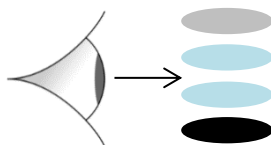


Figure 6.8 Raman analysis using a modified Swagelok® cell; direction of observation

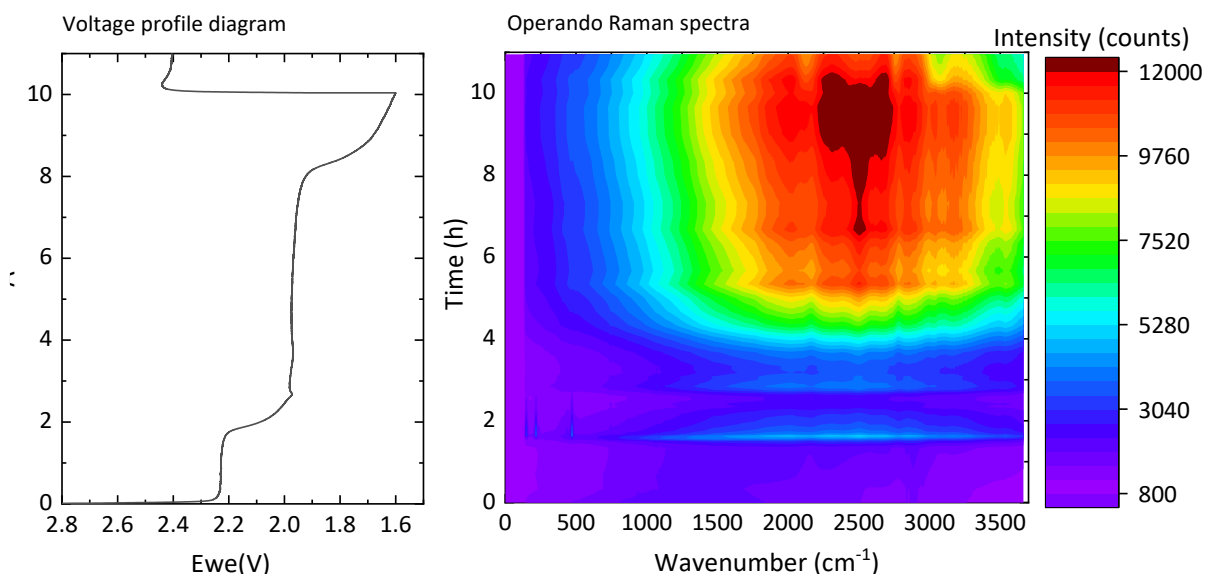


Figure 6.9 In-situ Raman and associated voltage profile: first cell configuration.

There are two major observations that can be done from this map. First of all, this experiment allowed to follow the rise and decay of elemental sulphur (148 , 215 , 438 and 474 cm^{-1}) between roughly 1h30 and 2h30. This domain corresponds to the transition between the two discharge plateaux and has been enlarged in **Figure 6.10** for better recognition. The solubility of sulphur in electrolyte solvents has been tested and proved to be null or neglectable – after one day of stirring and subsequent filtering, no sulphur was identified in the solvent via Raman spectroscopy. Therefore, the observed sulphur was a reaction product and not merely dissolved material. It has been formed as a result of dissociation reactions and either underwent further reactions or diffused away from the analysed spot.

The second observation concerns the very high intensities between 1500 and 3500 cm^{-1} , explained by the concurrent fluorescence phenomenon. Since it is considerably more efficient than Raman scattering, it might hide away valuable results. For better visualisation, the intensities

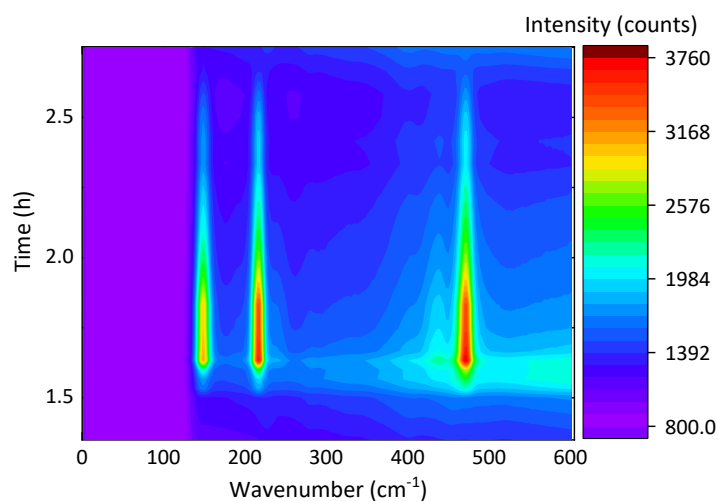


Figure 6.10 Sulphur lines manifestation.

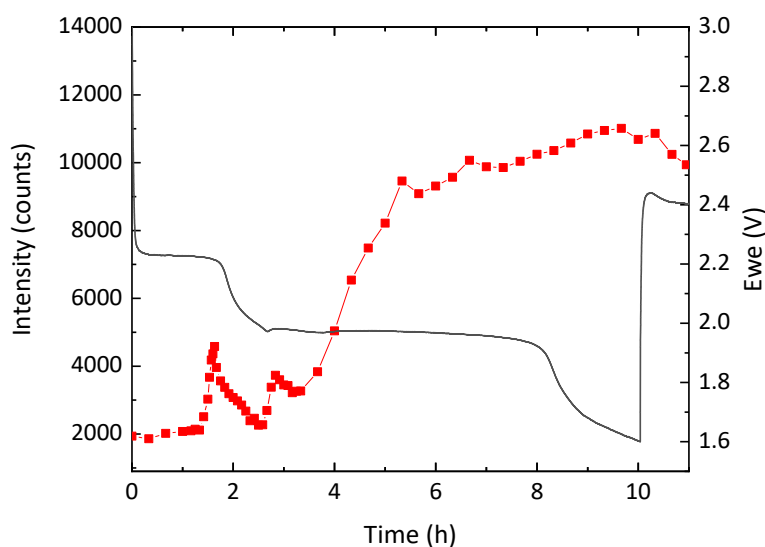


Figure 6.11 Fluorescence phenomenon throughout the cycling.

are taken at a wavenumber where no polysulphide-specific peak is present. They are plotted against the voltage profile in **Figure 6.11**

Fluorescence is generally caused by impurities, but it is not the case here: the cell is sealed and, since the initial spectra show a low background, no impurities have been introduced during the assembling. It is also not caused by the degradation of the analysed material by the laser heat – the baseline drops again when the cell starts to be recharged. The assumption is therefore made that microscopic particles of carbon can be detached from the cathode and transported through the highly porous FS2190 membrane. This assumption has been checked and is discussed later.

There also is a local maximum shortly before the transition between the two discharge plateaux. It is linked with the appearance of the elemental sulphur.

This experiment allowed to confirm that an in-situ Raman analysis of a functioning lithium sulphur cell is possible and thus provided a first proof-of-principle. Consequently, I shifted the interest towards the possibility to have more control over the setup by adjusting the cell architecture.

6.2.2.2 Second Swagelok® Cell Modification

The cell was now adapted for the analysis via Raman microscope. This allows to measure in a defined focus point and to analyse in different regions of the cell (e.g. close to the cathode or the anode) during its cycling. Besides, measures have been taken to dampen the fluorescence: the FS2190 and C2325 separators have been switched in their position in the cell structure. In this way, the film-like, less porous membrane is halting the carbon particle transport. As can be seen

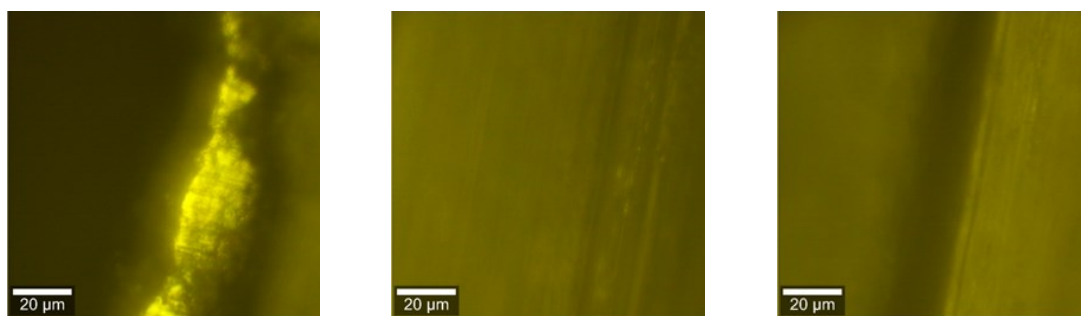


Figure 6.12 Cell images obtained by optic microscopy; left to right: anode, separator layers, cathode.

in **Figure 6.13**, even though there still are regions where the baseline is higher, the overall picture is considerably better. Another modification consisted in keeping the sizes of all components equal, instead of having the separators be larger than the electrodes. This slightly augmented the risk of contact between electrodes and consequent of a short-circuit, but facilitated the choice of the point to measure, since one could now easily find the anode and calculate the position relatively to it.

The difference between the two separator films and between separators and metallic pistons is hard to make out with the naked eye (**Figure 6.12**). For this reason, the possibility to clearly see the lithium anode is very valuable. Knowing the separator thicknesses, one can calculate the position of the cathode and choose where exactly the analysis will be performed, which was the main reason for opting for Raman microscope measurement instead of the Raman probe. This said I decided to conduct the measurements in the centre of the two electrodes (**Figure 6.13**).

Like in the previous case, the polysulphide signals appear mostly during the transition between the two discharge plateaux. Unlike previously, here also other molecules besides sulphur are visible. Several chosen spectra are plotted in **Figure 6.14** for better visibility and interpretation.

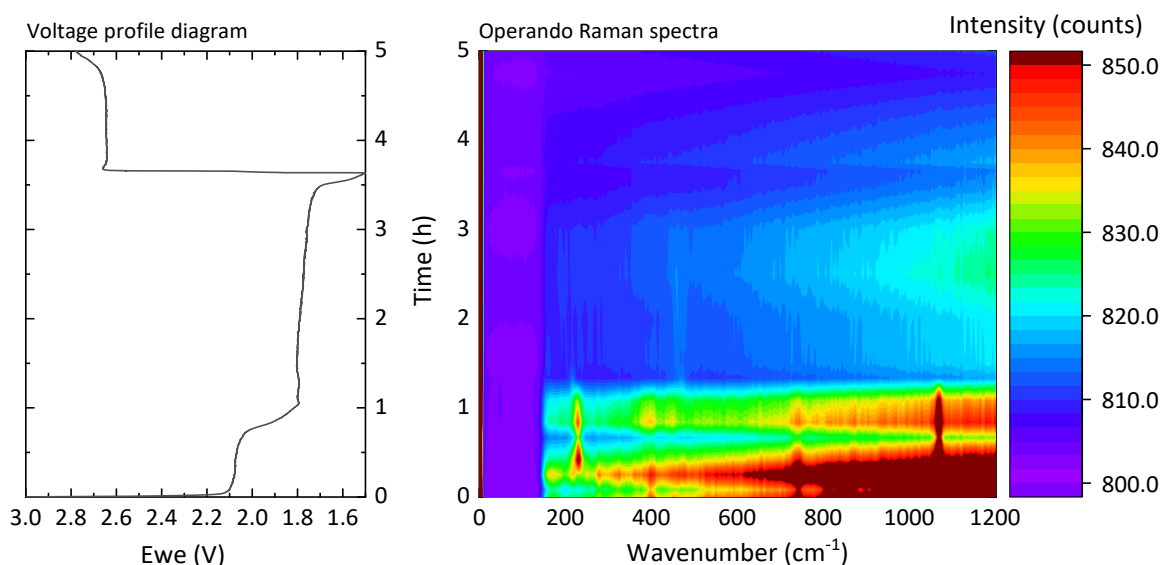


Figure 6.13 In-situ Raman and associated voltage profile: second cell configuration.

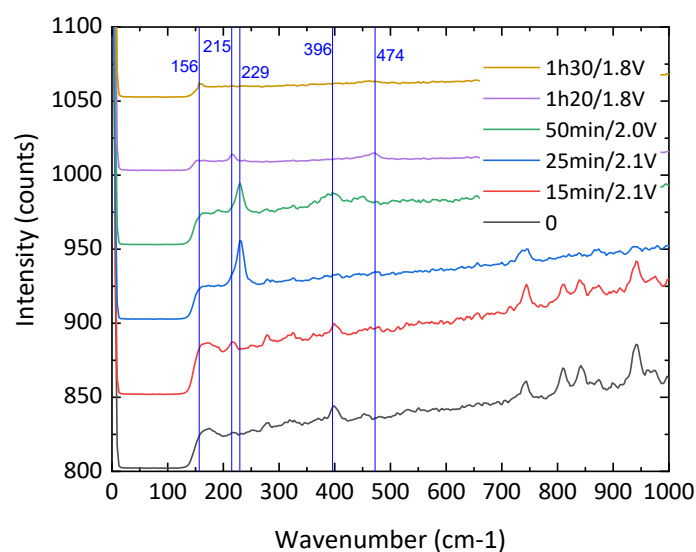


Figure 6.14 Spectra from first discharge plateau and transition region.

The elemental sulphur makes a short appearance 1h20 into the discharge. Besides it, there are other molecules which can be seen. Alas, the result is overall unsatisfactory – the signals are scarce and weak for a battery which is known to have solvated polysulphides inside its electrolyte at nearly any cycling step. This is due to the edge effects – the molecules of interest remain inside the cell, where the laser beam has no access. The cell configuration only allows measuring at the edge of the cell.

In order to handle the presented problem, it was decided to entirely replace the separator material. The choice is made in the favour of cellulose. This material has a very high affinity with the polysulphides, so the assumption was made that the polysulphides would travel to the edge

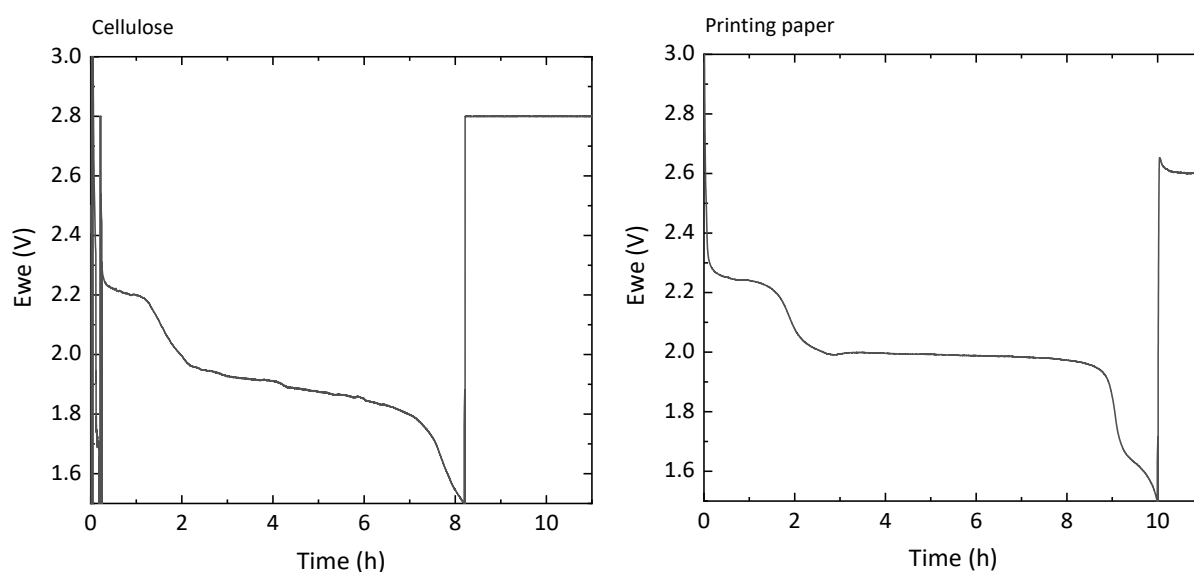


Figure 6.15 Polysulphide absorbent separator; left: cellulose, right: printing paper.

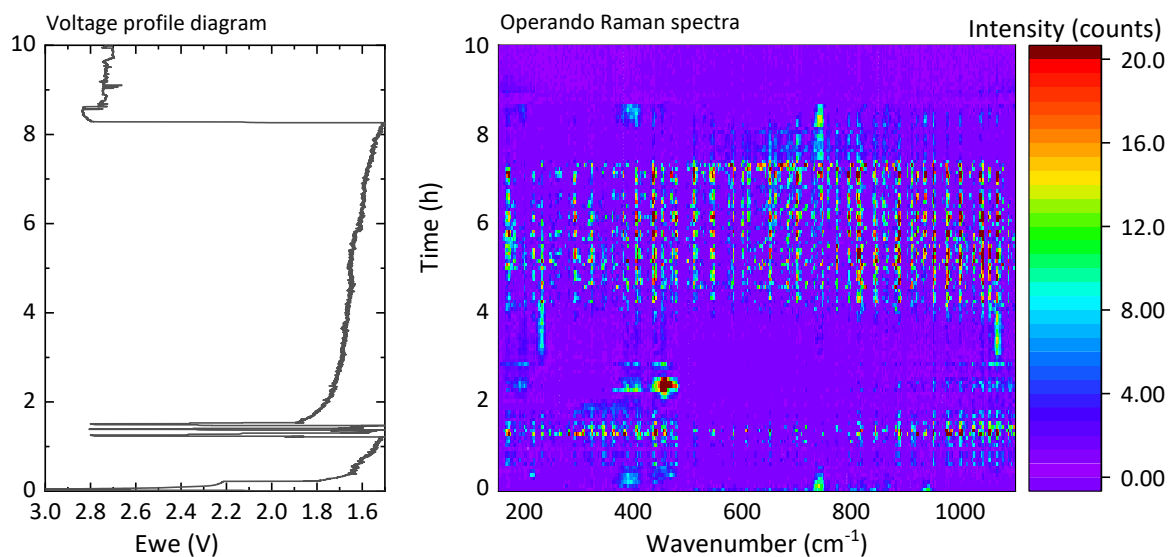


Figure 6.16 In-situ Raman and associated voltage profile: second cell configuration using printing paper as separator.

of the cell, where they would be accessible for the analysis, instead of remaining concentrated inside the cell.

First, the cellulose membrane manufactured by Nippon Kodoshi was considered. The second possibility was the use of printing paper. The later was more robust, but it had the disadvantage of being chemically bleached and of possibly containing additives such as chalk or white clay. Both materials have been tested for their performance in an electrochemical cell (**Figure 6.15**).

The cellulose separator shows a very fast first discharge and subsequent charge before displaying a recognizable voltage profile. The cell constructed with printing paper had an appropriate discharge voltage profile. Both cells only functioned for the one discharge – the recharging did not occur. Based on the results, printing paper was selected for further experiments (**Figure 6.16**).

Despite the prior test, the electrochemical curve is quite unsatisfactory. Nevertheless, the cell still underwent the discharge process, even though the voltage profile is different from that of the standard cell. The results are kept for further analysis.

The colourmap indicates the presence of a variety of molecules, but it is not adapted for a more in-depth interpretation. In particular, the low signal to noise ratio makes it necessary to check not only the height but also the shape of the peaks. For this reason, the intensities of the peaks characteristic for lithium polysulphides are presented in relationship with the discharge curve (**Figure 6.17**).

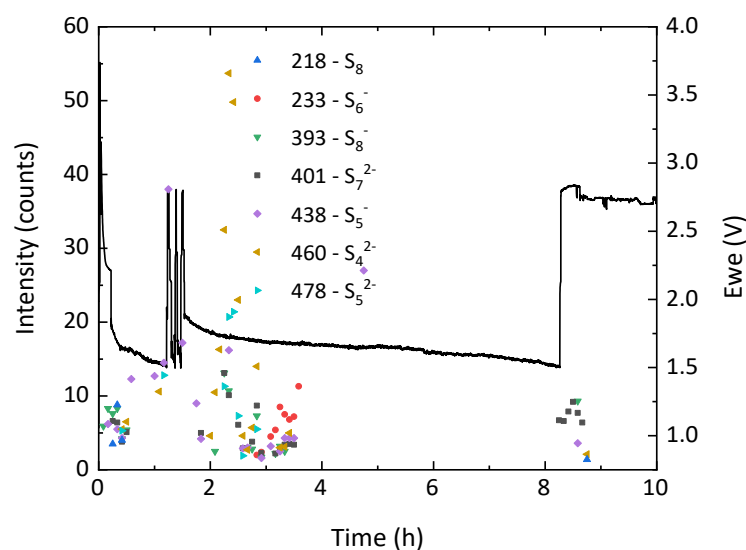


Figure 6.17 Peak intensities at different wavenumbers (in cm^{-1}) in relation to the electrochemical discharge curve.

As it has been extensively explained in 4.3.2, when it comes to the vast number of polysulphides, the peak interpretation presents serious complications. The theoretically calculated values being the most trustworthy, have been taken as basis in this work. All the peaks* are identified with the help of the calculations made by Hagen *et al.*¹²⁷. The polysulphide molecules corresponding to the peaks are given in the legend. First of all, it has to be noted, that elemental sulphur appears at the beginning of the first discharge curve, right after the transition between the two plateaux. Even in the case of “incorrect” cycling behaviour, the formation of sulphur at a well-defined DOD, from the dissociation reaction, is highly reproducible. Secondly, the employment of cellulose separator has proved reasonable: indeed, a larger variety of polysulphide molecules is visible, and that over a longer time period. On another hand, their appearance is quite chaotic and no further conclusions can be drawn from the present picture.

The modified Swagelok® system has offered valuable information but has come to the limit of its capacity. An entirely new system has to be constructed to allow for reproducible and flexible testing.

* besides the elemental sulphur which has an easily measurable spectrum and S_3^- - in this case the work of Chivers *et al* is judged trustworthy



Figure 6.18 Raman analysis on the cathode (left) and anode (right) sides using a modified coin cell.

6.2.3 Modified Coin Cell*

There were three reasons why an entirely new system was opted for. Firstly, the results obtained using the modified three-electrode cell were unsatisfactory. Secondly, one of the aims of the project was to analyse the cell by both Raman and NEXAFS spectroscopy. It would, therefore, be desirable to perform both analyses on the same system, which would make a direct comparison of the results more sensible; the coin cell geometry allows it. Finally, the coin cell is the state-of-the-art cell configuration for battery research. Having the possibility to analyse the data without having to extrapolate for a different system is extremely valuable. The analysis was done through an opening (**Figure 6.18**).

6.2.3.1 Test of the Electrochemical Performance of the Modified Cell

Before the beginning of the in-situ analyses, the electrochemical performance of the modified cell was tested (**Figure 6.19**).

There are several minor differences between the cells. The most noticeable one is the behaviour at charge: when the cell is modified, the overpotential effect at the beginning of the

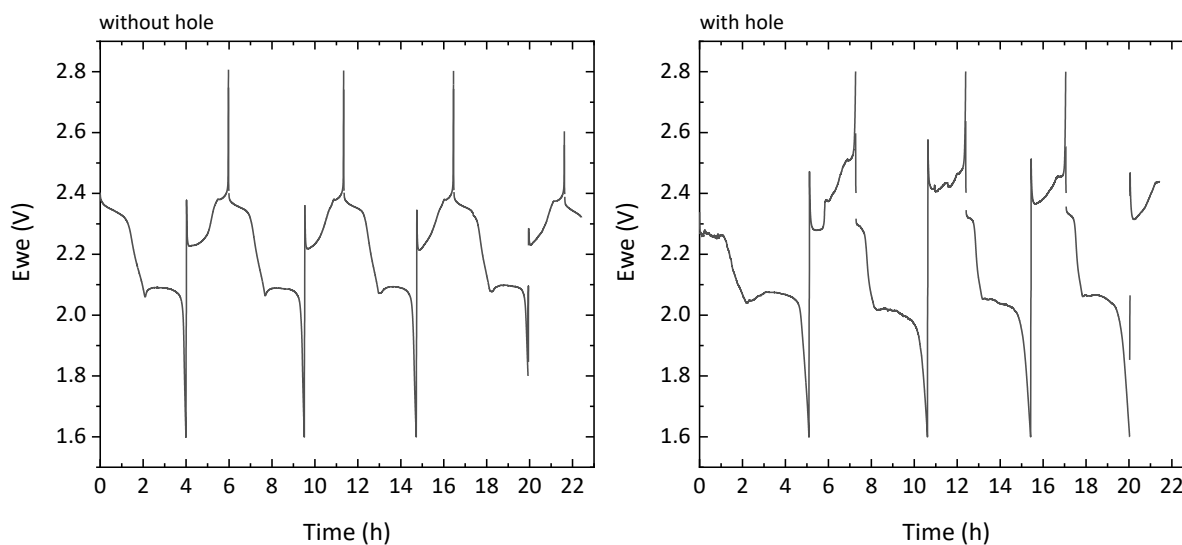


Figure 6.19 Comparison of the voltage profiles between a cell with and without hole.

* Some of the data presented in this chapter has been submitted for publishing

charge is more prominent. Besides, the curve's shape is more irregular. In addition, the first discharge plateau is shorter in the case of the Raman cell – the long-chained polysulphides are converted quicker. The voltage at which the reactions engendering the second plateau occur is slightly lower in the case of the cell with hole, particularly starting with the second discharge. Finally, the voltage drop at the beginning of the second discharge plateau is considerably less pronounced in the case of the modified cell. This drop is explained by a maximum in the viscosity of the electrolyte at this stage in the discharge, caused by a large number of polysulphides of medium length, which impedes the ion transport and, therefore, the reaction is slowed down. One can deduce that the modified geometry of the cell helps to overcome this issue.

Despite these distinctions, the overall voltage profiles of the two cells are very alike, also from the capacity point of view. The results obtained with the modified cell can be transferred to the standard cell with a high level of assurance.

6.2.3.1 Raman analysis: results and interpretation

The measurement was performed both at the cathode (**Figure 6.20**) and anode sides (**Figure 6.21**). In the case of the anode side measurement, the spacer and spring have been placed over to the cathode, in order to diminish the measuring distance. For the cathode measurement, the C2325 and FS2190 separators were switched places for two reasons. First, it has been pointed out above that the C2325 foil can limit the diffusion of carbon particles through the cell and therefore quench the fluorescence phenomenon. Second, it has been done for better visibility, since the non-woven structure of FS2190 hinders the passage of the signal. The hole diameter was reduced from 5mm (made with a paper hole punch) to 2 mm (made with a belt puncher). The baseline of

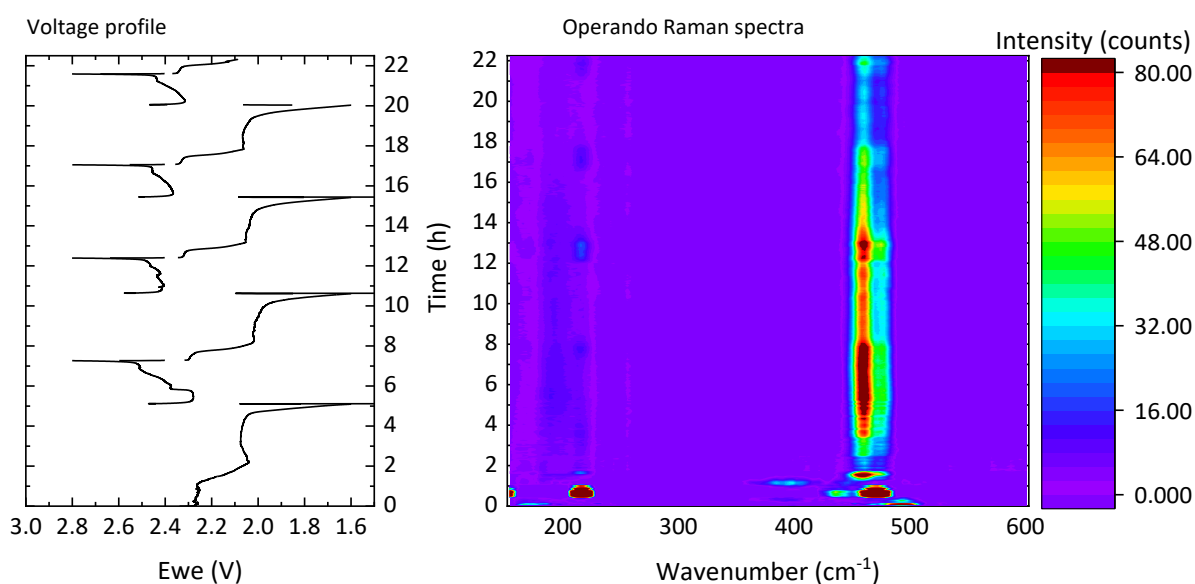


Figure 6.20 In-situ Raman and associated voltage profile: cathode side.

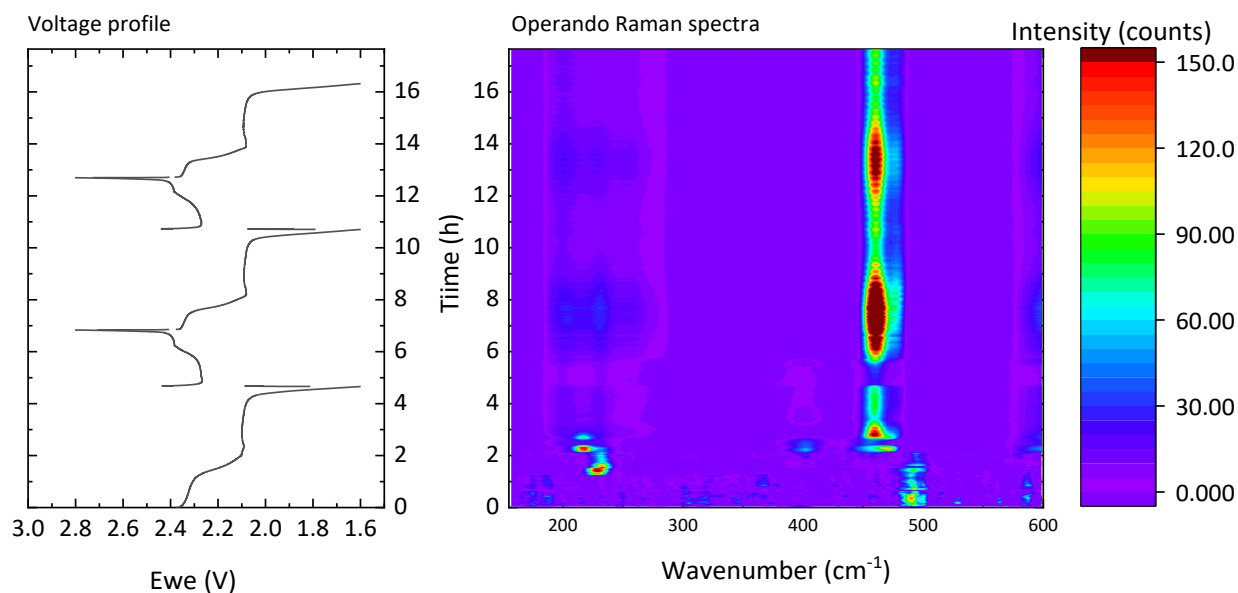


Figure 6.21 In-situ Raman and associated voltage profile: anode side.

the curve taking different values throughout the experiment, it has been subtracted prior to the plotting. The corresponding voltage profiles allow following the evolution of the spectra in function of the DOD.

One of the parameters to take into account when measuring by Raman spectroscopy is the intensity of the incident laser beam. On one hand, the higher it is, the better the definition of the resulting spectra will be. On the other hand, the light can be absorbed, resulting in heat and damage to the material. This is exactly what happened to the separator in the very beginning of the analysis – therefore the appearance of the peak at 492 cm^{-1} , particularly predominant on the anode side (**Figure 6.21**). Nevertheless, once the reaction between the lithium and sulphur started and the soluble polysulphides dissolved in the electrolyte, its total volume rose, displacing the focus point of the laser away from the separator. Further analysis was not hindered by degradation processes.

Before starting with the interpretation of the results, one has to lift the confusion around the Raman line at approximately 475 cm^{-1} . In effect, the elemental sulphur possesses a peak at 472 cm^{-1} , but there also is another molecule which scatters at 478 cm^{-1} . As the two peaks are so close to each other, they can easily be confounded or even merge together to show one apparent peak. For this reason, elemental sulphur is identified by its peak at 218 cm^{-1} . Since the ratio between the peaks at 218 and 472 cm^{-1} for S_8 is equal to one, one can subtract the intensity at 218 cm^{-1} from the intensity of the peak at 475 cm^{-1} . In this way, the result will only correspond to the other species.

As it has already been observed in the case of the previous cells, there is an intense peak characteristic of sulphur at the beginning of the discharge. It appears during the first plateau on the cathode side and at the beginning of the second plateau on the anode side. This deviation can be explained by the time necessary for the molecules to overcome the distance.

The colourmaps are very useful and demonstrative for when one needs a general picture of the processes taking place in the cell, but they are not detailed enough. For this reason, the intensities of the main peaks are recorded and plotted in relationship with the voltage profile (Figure 6.22).

Although, in theory, there is a vast variety of possible polysulphide molecules which can be formed as a result of the electrochemical reactions, in praxis, there are only a few vibrational frequencies present. Out of them, the most distinct and stable are the peaks at 460 and 478 cm^{-1} . They appear on both sides of the cell and keep high intensities throughout the experiment. It is noteworthy that these peaks are absent from the spectra of the polysulphide solutions, prepared in the same solvent. They are also not present in the cell at the very beginning of the analysis after the equilibration reactions happening in the constructed but yet unused cell. One can, therefore, conclude that the electrochemical reaction defines which reactions are going to be favoured and which molecules will be formed.

The reactions occurring in a functioning cell have been shortly given in paragraph 4.2.1 but will be discussed in more detail here.

The peak characteristic of S_8 from the beginning of the discharge is closely followed by a comparable S_4^{2-} peak. The sulphur reformed as a result of recombination reactions is thus likely reduced to the S_4^{2-} - the entity predominant in the cell which is, in turn, reacted further. Afterwards, the peak evolutions are smooth and follow the electrochemical curve.

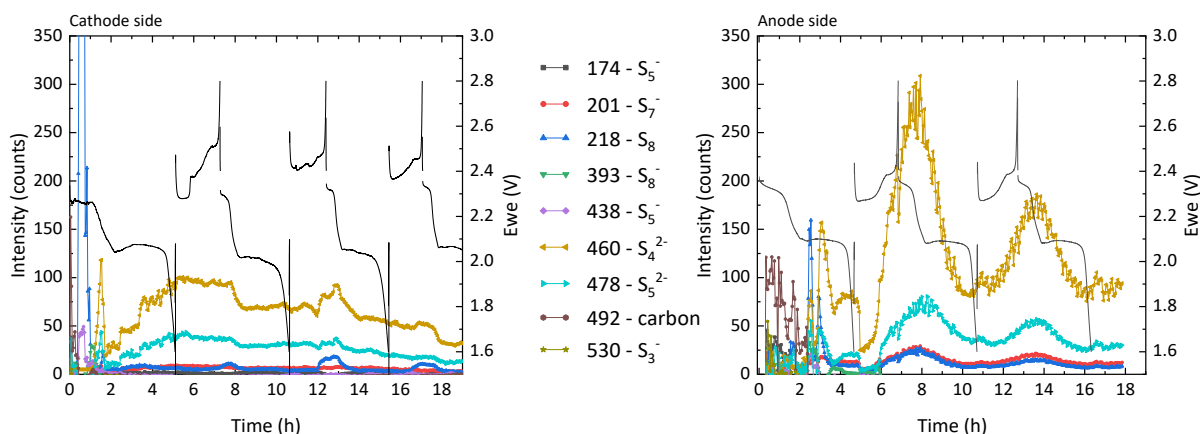
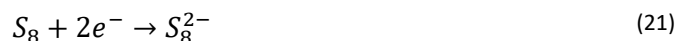


Figure 6.22 Peak intensities at different wavenumbers (in cm^{-1}) in relation with the electrochemical discharge curve; left: on the cathode side, right: on the anode side

It is generally accepted that, as a first step in the discharge, the sulphur ring opens up upon accepting two electrons (**Equation 21**).



Afterwards, the process becomes more complicated: the chain composed of eight atoms can break in any place. Besides, the reaction products can also recombine to give new molecules. There are two main paths which are agreed upon by the scientific community. It is either the series of disproportionation and dissociation reactions as brought in the **Equations 22&23**, or another two-electron reduction as in the **Equation 24**.



The polysulphides then proceed to be reduced all the way to lithium monosulphide and disulphide. Since they are formed at an electrode and, due to their insolubility, cannot diffuse through the electrolyte, they cannot be visualised by Raman spectroscopy in our measurement setup. Their formation is deduced indirectly, by the diminishing of the signals characteristic of other polysulphides, their precursors. More adapted analytical methods, such as XRD^{95,135} or XANES¹³⁵, allowed to visualise their formation.

The peak at 460 cm⁻¹ being identified as S₄²⁻, its presence in large amounts is in good agreement with the literature¹⁰⁰. This picture is considered to be typical for the systems using the DOL/DME solvents for the electrolytes. In the case of other systems, for example, TEGME/DOL electrolyte, the disproportionation-dissociation reactions are predominant, giving rise to intense lines characteristic of S₃²⁻^{120,121,123}. In the case of the present system the duration and intensity of the S₃²⁻ peak are insignificant.

Although the nature of the polysulphides on both cell sides remains pretty much the same, the overall evolution is quite different. When saying “polysulphides”, the S₄²⁻/S₅²⁻ mixture will be meant hereunder. On the cathode side, after the short surge at the beginning of discharge discussed earlier, their amount steadily increases until the end of discharge. The elemental sulphur is reacted continuously, making new sulphur available for the reaction and releasing new polysulphides into the electrolytes. This observation contradicts the common statement that the second discharge plateau is dominated by the formation of short-chain molecules like the S₂²⁻ and S²⁻. The peak intensity then reaches a plateau or, more precisely, a decreasing curve with a very low slope, that spreads all the way to the end of the charging process: the polysulphides are

reacted back to elemental sulphur, but there are new ones diffusing from the anode side, which keeps the concentration high.* At the end of the charge, there is a drop in the peak intensity, coincident with an S_8 peak. It has to be noted that, despite the said “drop”, the concentration of polysulphides at the cathode side remains high – a large number of polysulphides do not return back into the cathode. The following discharges do not exhibit any variations in the polysulphide amount: while new ones are formed inside the cathode, the already existing ones diffuse away towards the anode, following the concentration gradient, and out of the focus point of the Raman microscope. This results in an apparent plateau. During the charges there are peaks of both the polysulphides and elemental sulphur – the polysulphides return from the anode and are oxidized.

On the anode side, the image is, less convoluted. After the initial peak, representing the entities formed directly after the cell construction, there is a short plateau followed by a drop at the end of the discharge: all the polysulphides present have been reduced to lithium monosulphide at the surface of the anode. The intensity then strongly increases throughout the charge: those monosulphides are reacted back to soluble polysulphides. During the subsequent discharge, the concentration of dissolved polysulphides visible at the anode decreases steadily, and there is only a small local peak when the cell is fully discharged: they are reacted to S_2^{2-} and S^{2-} faster than new ones are diffused from the cathode. The overall amplitude is decreased for the ulterior cycle – part of the monosulphide did not react back, remaining as a passivating layer at the surface of the cathode.

6.2.3.1 Comparison of the Results Obtained by Raman and NEXAFS Spectroscopy

Cells of identical construction** have been analysed on both (anode and cathode) sides by the two spectroscopic methods. The results have then been put into relationship (**Figure 6.23** and **Figure 6.***** For practical reasons, the total amounts of polysulphides have been taken. In the case of Raman spectroscopy, the intensities of the peaks characteristic to lithium polysulphides**** have been summed, which gives a rough estimate, but a still interpretable picture. The NEXAFS measurements, data treatment and interpretation have been performed by Ms Claudia Zech, PhD student of Dr Burkhardt Beckhoff at Physikalisch-Technische Bundesanstalt Institut Berlin. In the

* As soon as the molecule reacts to an insoluble entity, it drops out of the solution, leaving a lesser concentration at the cathode side. Therefore, the concentration is higher at the anode side – a concentration gradient is engendered. It is dealt with through simple diffusion.

** the only difference consisted in the window at the cell casing – Kapton© in the case of Raman spectroscopy and highly oriented pyrolytic graphite (HOPG) for NEXAFS spectroscopy; the choices have been done in function of the penetration properties of the used rays

*** the x-scales of the two plots are chosen in a way to show the same number of cycles

**** these do not include elemental sulphur

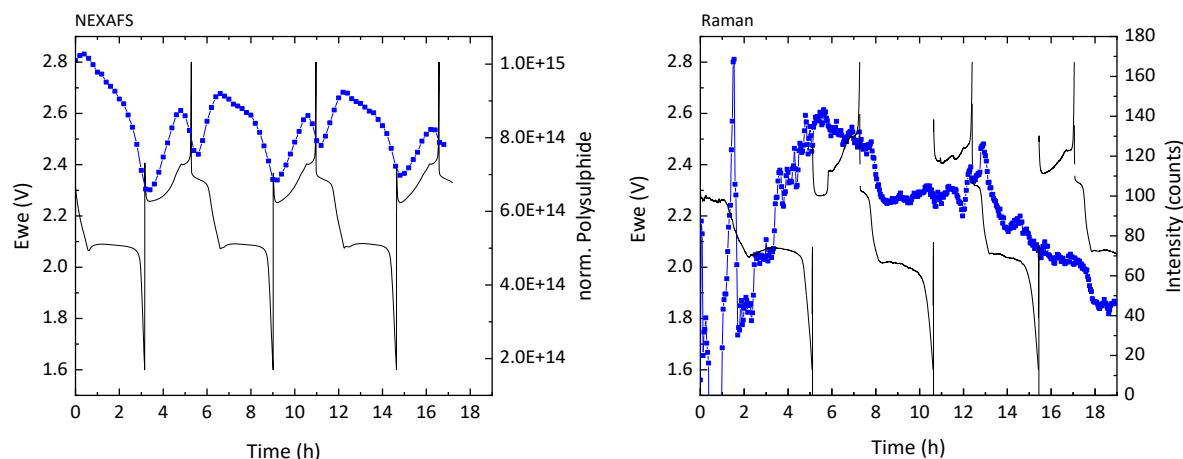


Figure 6.23 Total polysulphide amount at the cathode side, obtained by left: NEXAFS and right: Raman

case of the NEXAFS experiments, the first discharge plateau is missing on both cell sides. This is due to the waiting time between cell construction and analysis, where self-discharge processes took place.*

First, it has to be noted that even though the cell components and construction were kept identical, minor differences between individual cells are still possible. Second, the Raman and NEXAFS instruments are different from various points of view, including the penetration depth and spot size. The focus point of the Raman microscope is of an area of $1 \mu\text{m}^2$ and the penetration depth has been measured to be around $2 \mu\text{m}$ in the case of the used system (electrolyte-soaked separator). For NEXAFS, those values are rather of 1 mm^2 and up to $30 \mu\text{m}$ respectively – the obtained result is, therefore, the sum over this whole volume. On one hand, this difference is responsible for the non-coincidence of the polysulphide distribution picture, but on the other, it allows for a more ample analysis of the results.

Since the polysulphides are soluble in the electrolyte, there are two processes taking place in a functioning Li-S cell: the electrochemical reaction and the diffusion of the entities through the electrolyte, according to the concentration gradient. Taking into account the differences in the analysed volume, the Raman spectroscopy will rather give information about the polysulphides in the immediate vicinity of the hole, while the NEXAFS result carries on the total amount of polysulphides in the electrolyte. When combining the two, one can observe the polysulphide formation and their spreading through the cell. After the construction of the cell, there is an intense polysulphide peak seen by Raman, which immediately disappears, and a high amount of polysulphides seen by NEXAFS, followed by a slow decay until the end of the discharge. The first conclusion to be drawn consists, therefore, is the fact that, in a resting cell, the diffusion mostly

* Since the NEXAFS measurement is performed in conditions of high vacuum, several hours may pass between the moment where the sample is mounted and where it can be analysed

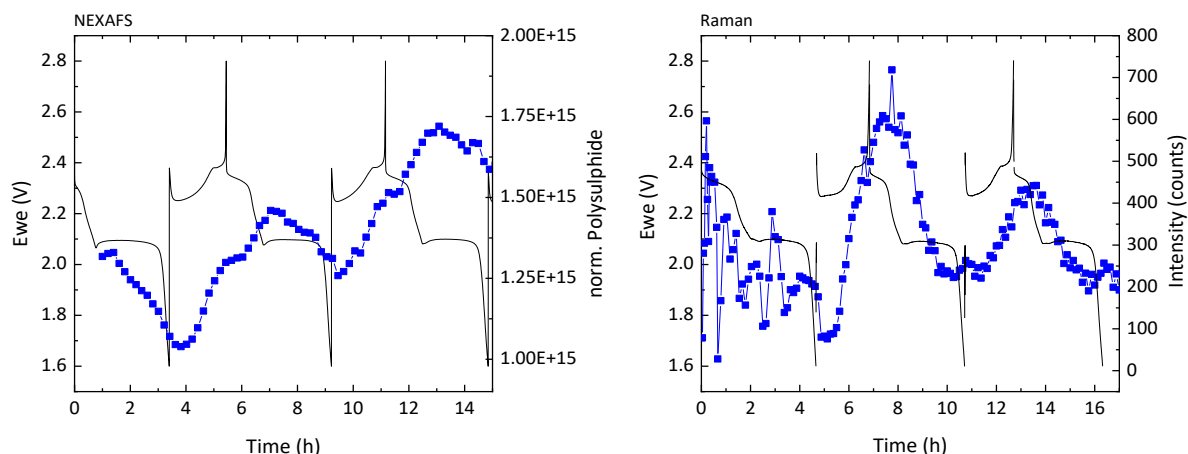


Figure 5.24 Total polysulphide amount at the anode side, obtained by left: NEXAFS and right: Raman

takes place horizontally. Although the concentration at the anode side is considerably lower, the separator hinders the transport of the bulky ions. The polysulphides travel towards the anode only when there is a current generated by the active discharging of the cell: in this case, it joins to the gradient, which becomes sufficient for their conveying.

When following the first discharge of the cell by both analysis methods, one notices that amount of polysulphides formed at the cathode constantly increases: the sulphur reacts and dissolves in the electrolyte, making more sulphur available for further reactions. On a larger scale though, seen on the NEXAFS graph, the total amount of polysulphides in the cell steadily decreases: the reaction to insoluble Li_2S at the anode is faster than the formation of new polysulphides. Still, even at the end of the discharge, there is still a large amount left in the cell – the drop only represents approximately 40% of the maximum. The charging process demonstrates a slow decay by Raman spectroscopy and an increase by NEXAFS, with a local maximum shortly before the cell is fully charged. The insoluble salts at the anode react back to soluble polysulphides, which greatly increases their total concentration in the cell. But, as soon as they actually reach the cathode, they are reacted back to elemental sulphur and disappear for the Raman beam.

The spectra obtained on the anode side are more similar. At the beginning of the discharge, there already is a certain amount of polysulphides in the cell. It decreases through the discharge, because of the reaction to insoluble salts, and reaches a minimum at the end of the discharge. It then increases during the charging process: the insoluble Li_2S_2 and Li_2S react back to soluble polysulphide and reaches a local maximum, particularly well visible in the case of NEXAFS spectroscopy. The increase continues over the first discharge plateau of the consequent discharge – new polysulphides come from the cathode and the totality is still not reduced. The reduction to Li_2S_2 and Li_2S follows as the discharging process progresses. The total polysulphide amount seen on the anode side of the cell steadily increases through the cycles: a large amount of the

polysulphides does not make it back to the cathode, which is partly responsible for the capacity loss. This evolution is not noticeable by Raman spectroscopy, immediately next to the anode: the lost polysulphides stay on the anode side of the separator, but far away from it to not react to insoluble salts.

All in all, this is not the first work performing Raman spectroscopy on a functioning Li-S cell – several previous publications have been listed in chapter 3.3.2. Nevertheless, the obtained results and their interpretations differ. It has been noted that one of the greatest difficulties consists in the identification of the observed molecules, which is conducted in an unsatisfactory way in most of the available literature^{120,121,124}. In effect, it was done based on experimental values, not reproducible between different publications. Solely one group has taken the task differently and has calculated the theoretical values¹²⁷, which have also been used in this work. Still, the said publication was mostly focused on demonstrating the possibility of such an analysis. This work has, therefore, put the previous results to use when observing the processes taking place in a functioning cell with the aid of a well-adapted cell.

6.3 RESORCINOL-FORMALDEHYDE BASED CARBON MATERIALS

One of the aims of this work was to put the insights gained in the *in-situ* study to use and develop a carbon material which would enhance the overall properties of the cell and, at the same time, be easy and cost-effective to produce in industrial quantities. There already exist numerous materials that have been studied and developed, but, astonishingly, carbon aerogels did not get the attention they deserve.*

Gels are a class of materials whose main constituent is liquid, but which demonstrate a solid-like behaviour due to a three-dimensional framework within the fluid. The framework consists of interconnected molecules, and the junctions can be of different natures, both physical and chemical.

R.W.Pekala was the first to report the so-called organic aerogels¹³⁶, made up through a polycondensation reaction between resorcinol (1,3-dihydroxy benzene) and formaldehyde in alkaline medium (**Figure 6.24**).

The most interesting properties of these gels include high porosities and surface areas. Besides, they can be tailor-made to fit specific needs, by modifying the synthesis or processing

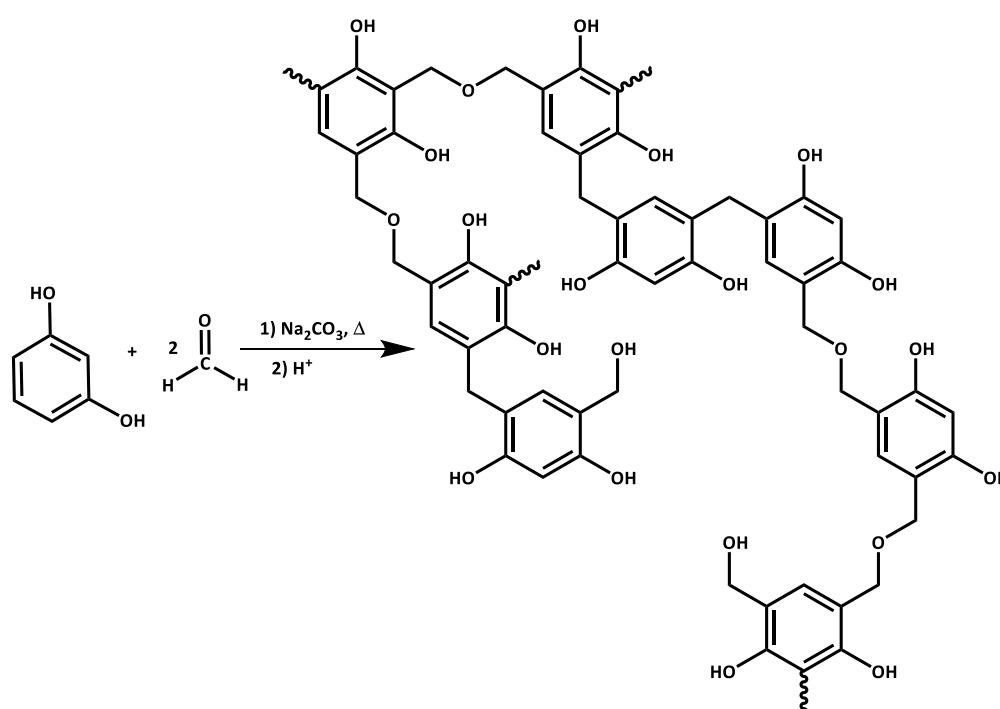


Figure 6.24 Exemplary reaction equation and potential structure of a resorcinol-formaldehyde resin

* Preliminary works on the subject have been performed by Dr Ivan Raguzin and Neelakandan M.S. at the Leibniz Institute for Polymer Research, Dresden

conditions. In the present work, the aerogels have been synthesized using one procedure, then the influence of the drying and carbonisation processes has been studied.

The synthesis has been performed following the protocol given in ¹³⁶ and went as follows: 3,19 g of resorcinol, 4,71 g of 37 wt.% formaldehyde solution in water with 10-15% methanol stabilizer and 0,03 g of sodium carbonate have been put together into a 100 mL volumetric flask, which was then filled up with Millipore water. The composition of the solution was then of 0,29 M resorcinol, 0,57 M formaldehyde and 2,89 mM sodium carbonate. The mixture was introduced into glass ampoules, sealed with the aid of an acetylene torch and cured in an oven at 85 °C for seven days. They were then removed from the ampoules and agitated for three days in a 0,125% solution of trifluoroacetic acid in water. This was done for further condensation of hydroxymethyl groups, which formed additional crosslinks between the molecules. The stirring had to be kept slow to not break up the gels. Then, the acid solution in water was replaced by acetone inside the gels.

6.3.1 Processing Conditions

6.3.1.1 Drying of the Gels

The synthesized gel was divided into three parts, that were dried by different methods.

One part was dried by critical point drying with liquified carbon dioxide. During this process, the acetone inside the pores is slowly replaced by the carbon dioxide, while leaving the pores intact. The as-dried gel keeps the integrity of its 3D polymeric framework intact. The procedure was the following: the gel piece was divided into smaller parts, of volumes of around 10 mm³ – this was done to facilitate the exchange in all points of the sample. These crumbs were then placed into the chamber and covered with acetone. The chamber was closed and, after bringing the temperature within to under 10°C, filled with carbon dioxide. The pressure inside the chamber was then approximately 50 bar. The chamber was rinsed with the carbon dioxide ten times, to entirely replace the acetone, then left for two hours to ensure complete removal of the acetone. This is easily feasible since acetone is well miscible with carbon dioxide. In the end, it was heated to 40°C and the gas was released. The as-obtained gel pieces kept their initial shape and appeared translucent when held in front of a light source. The supercritically dried gel is called aerogel. The main drawback of this method is its extreme slowness, at least in laboratory conditions. However, supercritical drying is a staple process in the food industry ¹³⁷ and thus easily scalable. It should also be mentioned that supercritical CO₂ is considered to be one of the greenest solvents available to chemists.¹³⁸

The second part was dried in atmospheric conditions, in a fume hood. The gel was removed from the acetone and dried on a petri dish. The pieces kept their shape, but drastically lost in volume – the escaping acetone broke through the pore walls, causing their collapse. This sample is thus called the xerogel.

The third sample was freeze-dried. For this, the acetone inside it was replaced again by Millipore water and the gel pieces were introduced into liquid nitrogen to entirely and quickly freeze the contained water. They were then placed under vacuum and the water was sublimated. The final product had a volume comparable to that of the material before drying, but the texture changed – the pieces easily disassembled into flake-like sheets. The reason for this is the formation of ice crystals upon the freezing of the water which damaged the gel's structure. Still, because the physical conditions in which the drying was conducted, the shrinking of the material was avoided. This material is the cryogel.

6.3.1.1 Pyrolysis of the gels

The carbonisation of the organic gels transforms them, as indicated by the name, into carbon structures. It is known¹³⁹ that the higher the pyrolysis temperature, the higher the content of graphitic structures in the carbon material will be. On the other side, higher temperatures lead to a drop in the specific surface area. This is why it has been decided to test the performance of the gels carbonised at 750, 1000 and 1250°C (**Figure 6.25**). In the case of the aerogel, the temperature of 900°C has been added to the list. 750°C has been chosen as the lower limit because carbon materials prepared at inferior temperatures risk to not be electrically conductive.

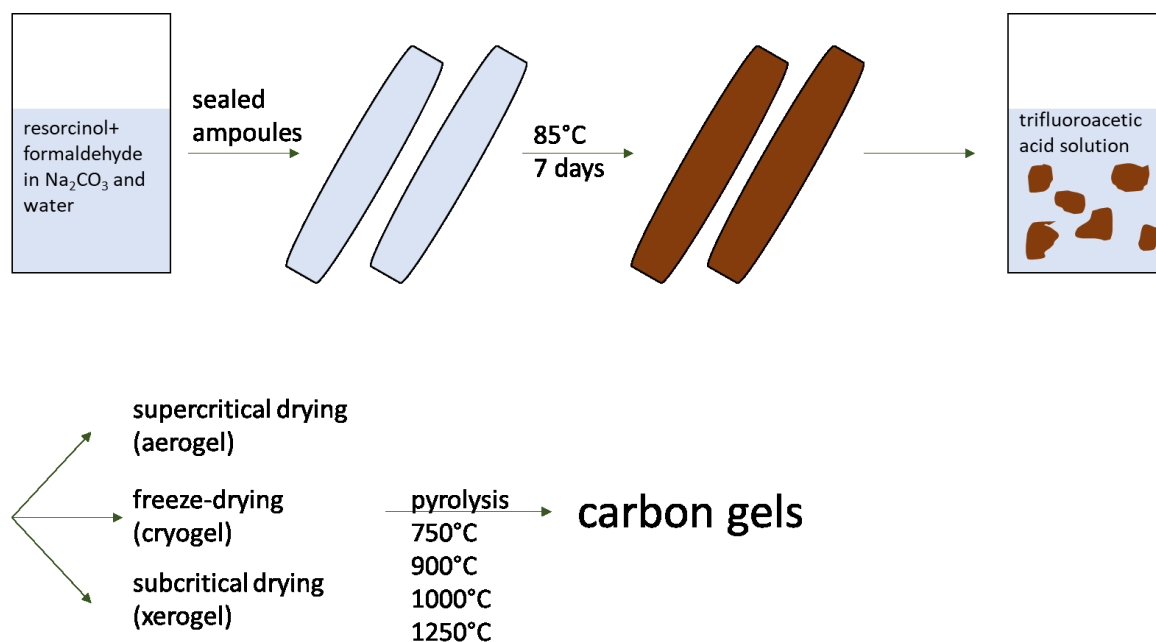


Figure 6.25 Preparation of carbon gels.

The gels have been pyrolyzed under constant nitrogen gas flow. The samples have been introduced into the tube furnace and, after a thorough rinsing with nitrogen, the temperature was raised at a ramp of 4°C/min. Once the desired temperature was reached, it was kept constant for two hours to ensure complete transformation. The furnace was then left to cool down overnight, then the samples were removed.

In the end, the obtained materials have been milled in the ball mill. The milling conditions were adapted to each of the materials so that a fine powder is obtained while keeping the mechanical strain minimal. This was done in order to avoid damaging the material's structure more than necessary. This is why, the milling frequencies have been of 10 Hz in the case of the carbon aerogel, 15 Hz for the cryogel and 20 Hz for the xerogel.

The nomenclature was as follows: the name of the sample included the drying method and the pyrolysis temperature. For example, the carbon obtained from the freeze-dried gel pyrolyzed at 1000°C was named Cryo1000.

6.3.2 Obtained Results

The materials discussed above are investigated and their properties are compared. First of all, their microscopic appearance is pictured by SEM imaging (**Figure 6.26**).

The Aerogel and cryogel were easily separated into small pieces, whereas the hard xerogel had to be milled prior to the analysis. This is why the xerogel particles are smaller.

One can notice the strong difference in textures between the three materials. The aerogel is lightweight and delicate. Even though the porous internal structure cannot be seen, it can easily be guessed. The cryogel consists of thin sheets. The conclusion can be drawn that the water crystals propagated on a preferential plane. The resulting material lost a large number of pores but kept a high surface on the behalf of the reduced thickness of the sheets. Finally, the xerogel is compact and rough. SEM images have also been taken after carbonization and milling (**Figure 6.27**).

The carbon materials show less difference among themselves than the organic gels. The aerogels have slightly lost in volume and in edge softness upon carbonization, which is particularly well visible in the case of the sample pyrolyzed at 1250°C. Removing the oxides and hydrogen groups from the structure influenced the interactions within the gel, causing a drop in the pore volume. The greatest difference between the image before and after carbonization is exhibited by the cryogel. The initially very thin sheets stacked back together. The reason for this remains the same: after pyrolysis, only carbon structures remained instead of the original polymer, whilst the

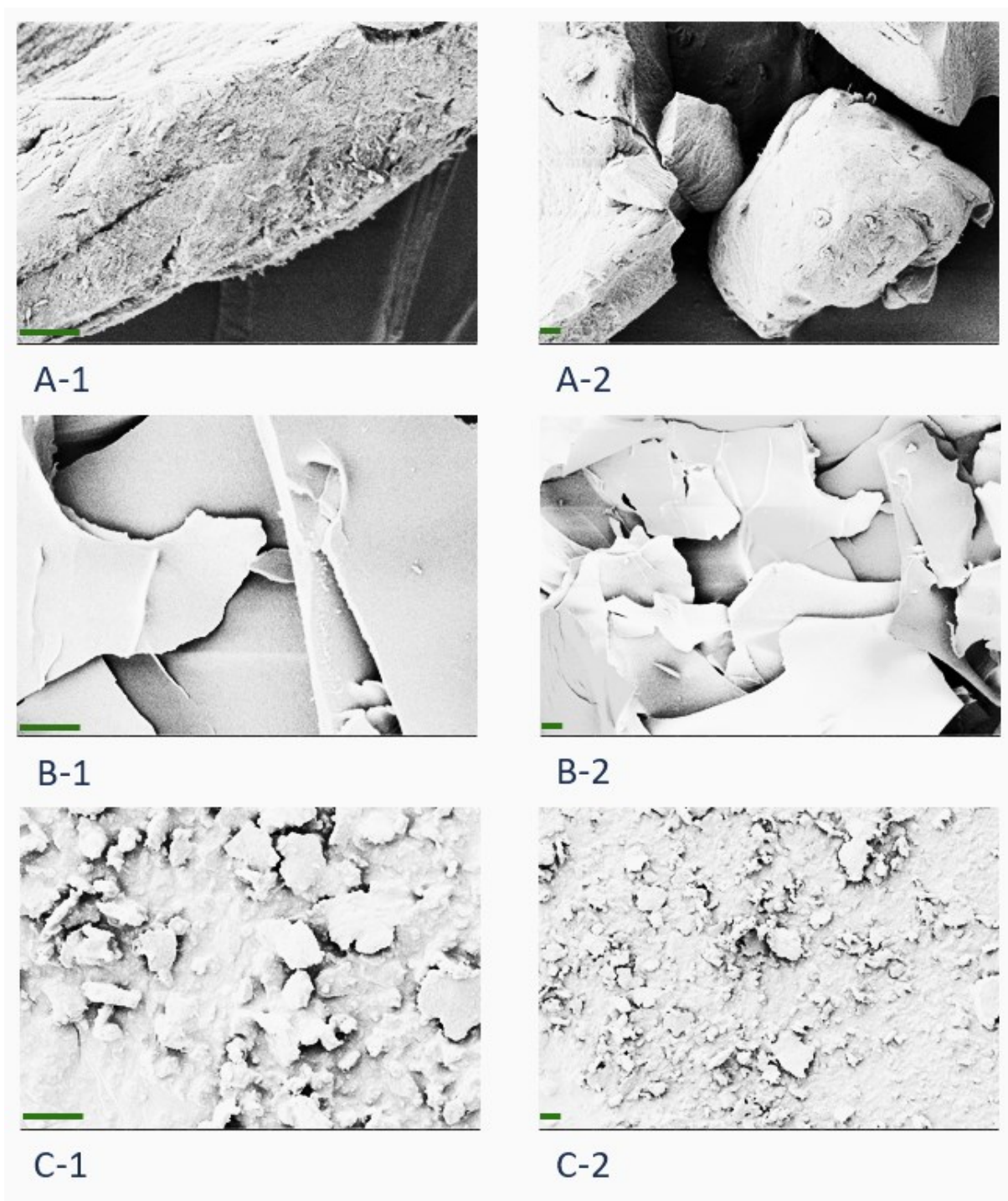


Figure 6.26 SEM images of the different gels: aerogel (A), cryogel (B) and xerogel (C) at different magnifications: 1500X (1) and 500X (2); the scale corresponds to 10 micrometres.

groups that were ensuring a certain detachment of the sheets were gone. Finally, in the case of the xerogel, no considerable difference between the states before and after pyrolysis can be noticed. Also, no or minor distinctions can be observed between the samples obtained with different carbonization temperatures

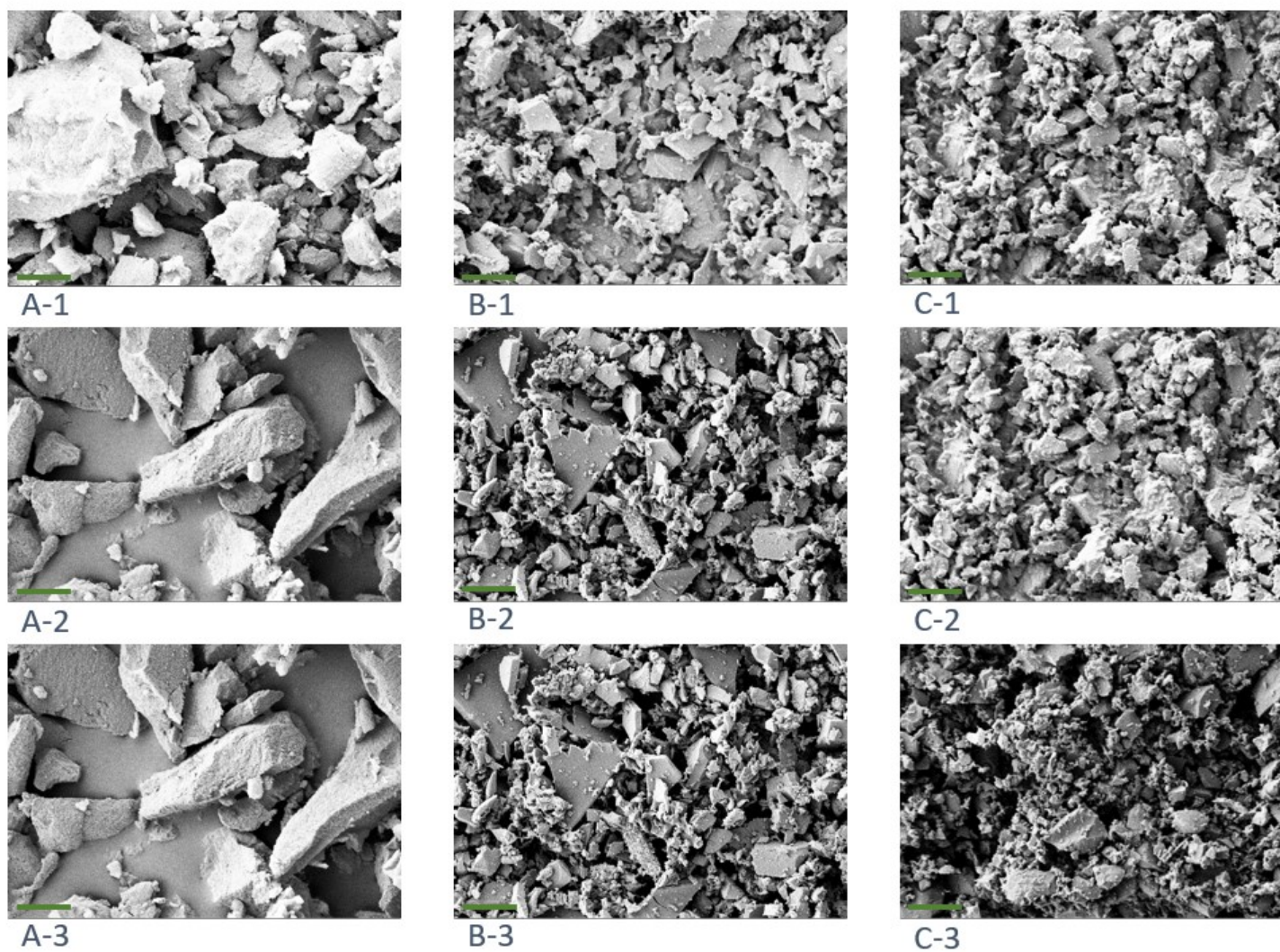


Figure 6.27 SEM images of different carbon gels: aerogel (A), cryogel (B) and xerogel (C), carbonized at different temperatures: 750°C (1), 1000°C (2), 1250°C (3); the scale corresponds to 10 micrometres

As it has already been repeatedly said, the sulphur encapsulating material for a Li-S cell has to be electrically conducting and have a high specific surface area. The analysis of the materials is, therefore, commencing with the gas sorption results (**Figure 6.28**).*

When the gel is pyrolyzed, first of all, the adsorbed water is released. Then, during the heat ramp and plateau, the organic compounds are released. Besides, the pyrolysis is accompanied by crystallization processes. According to literature¹⁴⁰, the surface area of the carbons increases until the temperature reaches 600°C, then slowly decays. In our case, such evolution can only be observed for the xerogel. The pores in this material are already collapsed, so the graphitization which takes place at high temperatures only adds to the material's density. When regarding the aerogel and cryogel, there is a raise in the specific area until 1000°C. It is possible that, even though pores are damaged, smaller pores form in their place, which increases the overall area. The specific area of the sample carbonized at 1250°C sees a strong drop in the three cases. It is due to the collapse of pores and the formation of graphitic structures.

When looking at the three materials, the carbon aerogel has the highest specific surface area, followed by the cryogel and the xerogel. Such an ordering was expected from the method characteristics and the SEM images and is confirmed by the physisorption results.

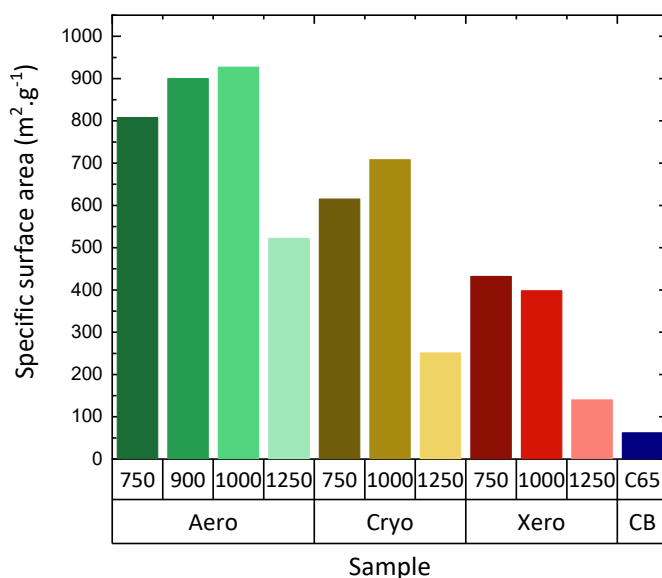


Figure 6.28 Specific surface areas of the carbon gels determined via N₂ Physisorption at 77 K and the BET equation.

* It has to be noted that the carbon aerogel powders were extremely lightweight. Therefore, during measurement, a certain amount of the particles was sucked up the tube, thus reducing the total measured area.

In the end, the specific surface area of super C65 carbon black is given for comparison. It is used as both encapsulation material and conducting additive in the standard cell. The value given by the producer had been confirmed by own measurements. Its specific surface area is significantly lower even than the ones obtained for the xerogel.

The samples have also been investigated by Raman spectroscopy. Since the analytical method is sensitive to graphitic carbon, it permits comparing the samples amongst themselves from this point of view.

To start, the organic gels have been analysed by Raman spectroscopy (**Figure 6.29**). The very strong fluorescence phenomenon does not allow to interpret the results. The beam intensity had to be set to 50 μW since the samples were damaged by higher intensities. This problem did not arise in the case of the carbon gels (**Figure 6.30**), confirming the fact that they had been entirely carbonized.

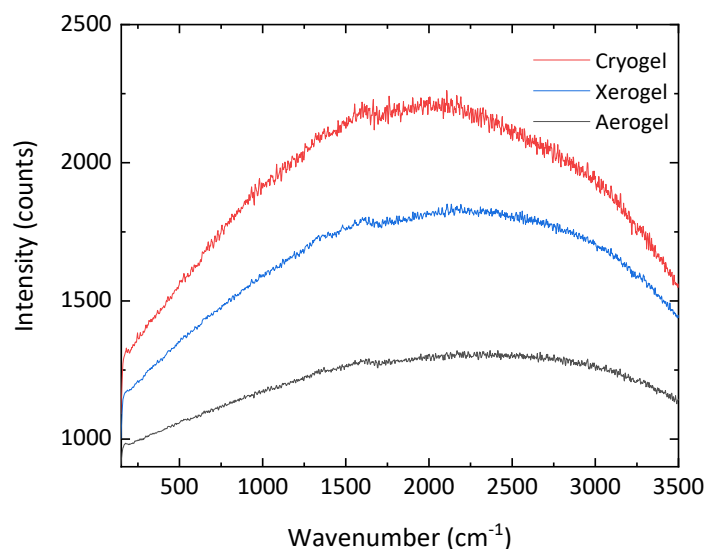


Figure 6.29 Raman spectra of the organic gels.

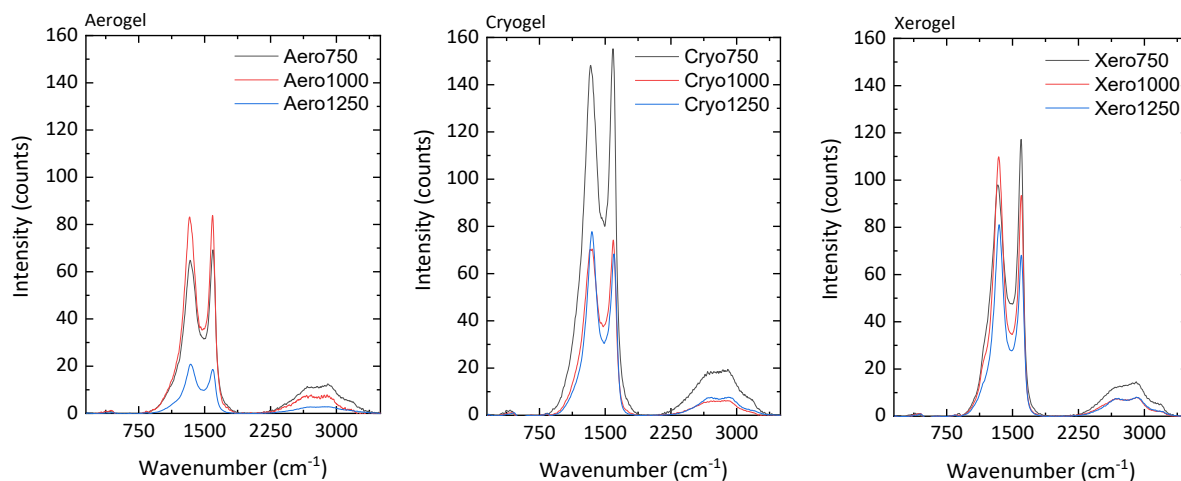


Figure 6.30 Raman spectra of the carbonized gels.

Raman spectroscopy is a powerful tool for the characterization of carbonaceous materials. It can provide information about the disorder, thickness, doping and other properties¹⁴¹ of said material. The bands one gets to deal with when analysing graphitic carbon materials are the D (1350 cm^{-1}), G (1580 cm^{-1}), 2D (2690 cm^{-1}) and, in the case of a more disordered material, D+G (2940 cm^{-1}). The G peak is the primary in-plane vibrational mode of graphene and the 2D is associated with graphitic sp² materials and is a second-order two-phonon process. The D and D+G peaks are generated by disordered carbon. When comparing the intensities of these peaks, one can conclude on the ratio of ordered graphitic structures in the material (I_D/I_G) and even on the number of graphene layers in that graphitic structure (I_{2D}/I_G) (**Table 6.2**).

The higher the ratio I_D/I_G , the higher the amount of sp²-hybridized carbon in the sample. When looking at the overall evolution for the three material kinds, we can observe the growth of the number of graphitic structures, which should lead to a higher conductivity of the carbon. The I_{2D}/I_G ratio gives information about the number of graphene layers in the structure. If the value is 2, then it is a single layer, if it is 1, it is a double layer and if it is inferior to 1 then we deal with a multilayer. Even though the differences between the values are minor, they are not non-existent, and one can draw conclusions regarding the thickness of the graphite parts. When looking into details, the transformation for each gel kind is different from the others. There is unfortunately not enough data to affirm that these discrepancies are due to individual processes and not simply to reproducibility issues.

The conductivities of the materials have then been analysed and plotted (**Figure 6.31**). The differences between the conductivities of the materials obtained at different pyrolysis temperatures being quite high, a logarithmic scale is chosen for better visibility.

There are two factors that influence the conductivity of a carbon material: the amount of conducting structures and their arrangement since they both determine how close the material is to the percolation threshold. The ratio of graphitic structures in the material may be high, but if it consists of separated graphite isles, the material will not be electrically conducting. In the same way, even a mostly amorphous material can be electrically conducting if it contains numerous graphene sheets that are well dispersed through the material.

Table 6.2 Separator Peak ratios for different carbon gels

	Aero 750	Aero 1000	Aero 1250	Cryo 750	Cryo 1000	Cryo 1250	Xero 750	Xero 1000	Xero 1250
I_D/I_G	0,93	0,99	1,13	0,84	1,17	1,18	0,95	0,94	1,15
I_{2D}/I_G	0,16	0,09	0,14	0,11	0,08	0,11	0,11	0,08	0,11

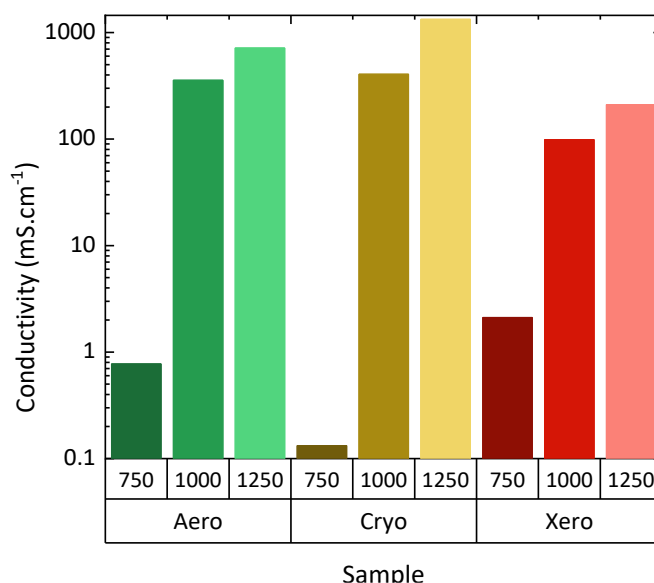


Figure 6.31 Results of the conductivity measurements for the carbonized gels.

The results obtained by Raman spectroscopy indicated that there is a rise in the amount of order inside the materials with rising carbonization temperature, which is confirmed by their conductivities. On the other hand, one would have expected the differences between conductivities to be less spectacular. This points out that a purely Raman based conclusion of the conductivities is highly prone to error and more specialised analysis methods should be conducted. The jump over several orders of magnitude seen between the sample pyrolyzed at 750°C and 1000°C can be explained by the lack of percolation. Even though the first material already contained a certain amount of graphitic structures, there were not enough to ensure the uninterrupted travel of electric current from one electrode to the other. As soon as the little missing amount was added, there was a qualitative leap in conductivity.

It is also interesting to observe the different pictures obtained for the three drying methods. The xerogel carbon is the most compact material, with the smallest specific surface area. Its electric conductivity is relatively elevated even at a small carbonization temperature. In contrast, the aerogel, a highly porous material, requires higher graphitization levels in order to be electrically conductive. The lowest conductivity at low carbonization temperature is exhibited by the cryogel, which is probably caused by its sheet-like structure. The conducting structures form preferentially within one sheet, and the current cannot properly travel between them. The order is inversed in the case of high pyrolysis temperatures. The raise for the xerogel was the least considerable for the set: little new pathways for the current have been generated. The aerogel and cryogel, in contrary, gained a lot in conductivity, overtaking the xerogel by almost an order of magnitude.

Based on their electric conductivities, all the obtained carbon materials fall in the range of semiconductors, which makes them adapted for the use in Li-S batteries. In effect, their conductivity is sufficient for routing the electrons to and from the current collector. They are, therefore, mixed with sulphur and the cathode is prepared according to the previously described method. The carbon black conductive additive (10 wt.% of active material) is still kept keep the results comparable.

After the cathode was prepared and dried, a part of the active material was removed from the current collector and analysed by TGA. This was done to make sure that no sulphur had been lost during the cathode preparation process.

For organisational reasons, only one sample for each drying method was taken, plus a standard cathode. Since the preparation method remained the same for all the cathodes, the obtained results could be easily extrapolated. The weight of the material has been plotted in function of the temperature in the chamber (**Figure 6.32** TGA results for cathode active materials containing carbon gels pyrolyzed at 1000°C, as well as for standard cathode material.).

The first portion of the curve is almost constant, the weight loss is of around 3%. It corresponds to the evaporation of the adsorbed water. The sulphur melts at 115°C, but it also sublimes easily – the strong drop that starts at 175°C corresponds to the loss of sulphur via

sublimation. One can, therefore, calculate the amount of sulphur present in the cathode material by subtracting the weight at 310°C at which all the sulphur has left the cathode from the one at 175°C. (**Table 6.3**).

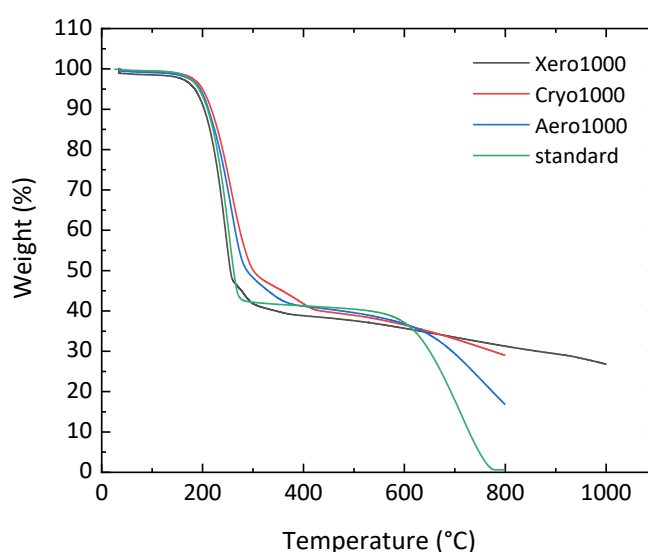


Figure 6.32 TGA results for cathode active materials containing carbon gels pyrolyzed at 1000°C, as well as for standard cathode material.

Table 6.3 Amount of sulphur in the cathode material

Sample	Xero1000	Cryo1000	Aero1000
Wt% of sulphur	56,5	54,1	55,4

The theoretical amount of sulphur in the cathode material, which is the amount of sulphur if no material is lost through the preparation steps or through sublimation is calculated at 54,7%. The slightly higher values are probably due to remaining adsorbed water in the cathode material. The second drop after 600°C corresponds to the decomposition of the guar binder.

The TGA results confirm that, for further experiments, it is reasonable to consider that the sulphur content is still around 54,7% and no major quantities have been lost due to processing.

Finally, the cells are constructed and galvanostatic charge-discharge analysis conducted. A good battery has to fulfil two tasks: have a high specific capacity and high cycling stability. All the results are given in comparison with the standard cell. It is the cell constructed with relatively cheap commercial materials. The modified cell has to be at least minorly more performant than the standard cell in order to be interesting.

One can clearly see the superiority of the gel dried by the critical point method over the other materials (**Figure 6.33**). The specific capacity of this cell is, on average, 50% higher than those of the standard cell or of the cells constructed with the other carbon gels. Even though it decreases at a higher rate, even after 500 cycles it remains considerably superior. On the other hand, the capacities of the carbon cryogel- and xerogel-based cells are comparable with that of the standard cell, although the specific surface areas of those materials are considerably higher. One can, therefore, conclude that, contrarily to what is commonly believed, the specific surface area of the carbon material is not of major importance. The parameter that leads to high performance is the shape of the pores and them being closed. If there is no physical boundary or chemically retaining element, the lithium polysulphides will not be retained by the longer path they have to cross before they end up outside of the cathode. When looking at the specific surface areas (**Figure 5.29**), the carbon cryogel shows a value over ten times higher than that of the super C65 carbon black; this fact, alas, has no influence on the performance of the cell.

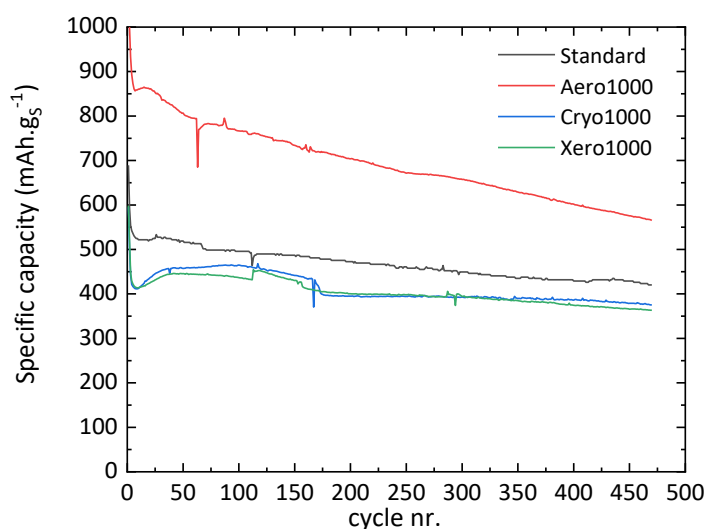


Figure 6.33 Electrochemical performance of the cells dried by three different methods in comparison with the standard cell. Measurements conducted between 1.8 and 2.6 V, with a current of 0.1C for discharge and 0.2C for charge

Next, the influence of the pyrolysis temperature is studied. The results for each drying method are given in comparison with the standard cell in **Figure 6.34**.

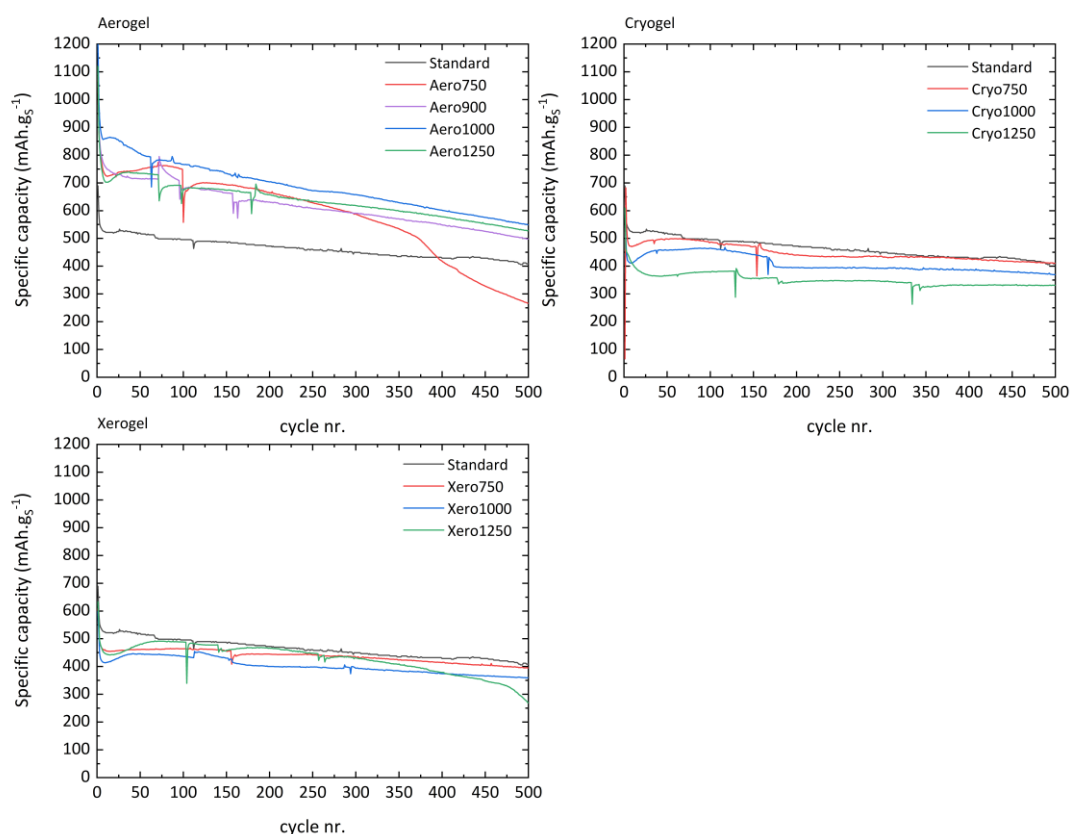


Figure 6.34 Influence of the pyrolysis temperature on the electrochemical performance of the cells. Measurements conducted between 1.8 and 2.6 V, with a current of 0.1C for discharge and 0.2C for charge

In the case of the carbon aerogel, there is a strong difference between the material carbonized at 750°C and the other materials. There is a sudden capacity drop after a certain point.

In the case of performance decay due to the consistent loss of active material, one would just observe a constant slope. The fact that the picture looks different here signifies an accident. Nonetheless, the observed picture has been reproduced in several experiments, which suggests the inferiority of the material. Although the conductivity of the material is inferior to those of the other carbon aerogels, carbonized at higher temperatures, it is not the cause of the lower performance. In effect, the conductivity should be rather seen as a threshold – the material must be capable of transporting electrons. But as soon as it copes with the task, it cannot suddenly stop doing so. The specific surface area is also an improbable candidate: it is only slightly lower than those of the other aerogel and could not be responsible for such a noticeable difference. The remaining possibility consists in the internal structure and ratio between amorphous and graphitic carbon. When looking at the other carbon aerogels and the cryo- and xerogels, no variations can be noticed in function of the pyrolysis temperature. Since higher temperatures require higher amounts of energy, it is reasonable to remain at the lowest carbonization temperature possible.

In the case of all the presented curves, the specific capacity of the first discharge does never reach the theoretical value of $1672 \text{ mAh.g}_\text{S}^{-1}$. In the case of the better performant carbon aerogel, it is around $1200 \text{ mAh.g}_\text{S}^{-1}$, while for the other samples – it always is approximately $700 \text{ mAh.g}_\text{S}^{-1}$.

The favourable geometry of the carbon aerogel, thus, not only ensures better retention of the lithium polysulphides inside the cathode, which leads to good cycling stability but also allows for better accessibility of the electric current on one side and the electrolyte on the other to a larger amount of sulphur from the start. On the other hand, the relatively low initial capacity of the other samples apparently plays a positive role in their cycling stability – the less sulphur reacts in the first cycle, the less is lost to diffusion and the more sulphur will be left for ulterior cycles.

Another interesting detail is the drop and consequent return of the capacity at the beginning of the cycling. This phenomenon has already been observed and discussed in the paragraph handling the separator choice. When looking at the overall picture, one notices that this event is particularly pronounced for the cryogel and xerogel samples. This observation goes along with the idea that only a part of sulphur reacts in the beginning, and some time is needed to render the bulk of the active material accessible.

As it has been said before, there is a wide variety of possible cathode materials and new ones keep being developed. They range between relatively simple porous materials and extremely complicated composites and matrices. One of the most well-known materials is the CMK-3⁴⁶, a carbon obtained by pyrolyzing sucrose templated on silica nanoparticles. The corresponding battery showed a capacity of approximately $800 \text{ mAh.g}_\text{S}^{-1}$ after 20 cycles. Other carbon materials

include, for example, the carbon spheres described by Zhang *et al.*¹⁴² and the mesoporous carbon developed by Li *et al.*¹⁴³. The constructed cells presented a reversible capacity of around 650 mAh.g⁻¹ after 500 cycles and, respectively, ~840 mAh. g⁻¹ after 100 cycles. Our material shows a performance comparable to the described carbons and, besides that, it is easier and safer to produce. There are other cathode materials, that have excellent performances after multiple cycles, like, for example, the composite studied by Wu *et al.*¹⁴⁴ The cell constructed in this work maintains a specific capacity of 611 mAh.g⁻¹ even after 1000 cycles at a 3C discharge rate. Nonetheless, the difficulty connected with the synthesis of the said material is such, that it is improbable to be used outside the laboratory.

6.4 SEPARATOR MODIFICATION

Another cell component which is capable of retaining the polysulphides on the cathode side of the cell, thus enhancing its performance, is the separator. It also received much less attention than the cathode.

6.4.1 Polyethersulphone as Separator Material

One way to ensure the complete retention of the lithium polysulphides by the separator membrane is to make it non-porous. This is, in fact, the functioning principle of a solid electrolytes. Then, in order for the cell to function, one has to ensure the transmittance of the lithium ions between the electrodes. If the membrane already contains Li^+ ions, they can be transmitted across the membrane following the bucket brigade principle. For example, Nafion is already used in such a manner for Li-S cells^{65,66,145,146}. Nonetheless, this material is expensive and unstable at high temperatures. As part of this work, polyethersulphones (PES) have been tested as separator materials. These polymers have been initially developed for application in fuel cells¹⁴⁷ and have high ionic conductivity, as well as good mechanic, chemical and thermal stability. The polymers were obtained from the group led by Dr J. Meier-Haak, researcher at the Leibniz Institute for Polymer Research.

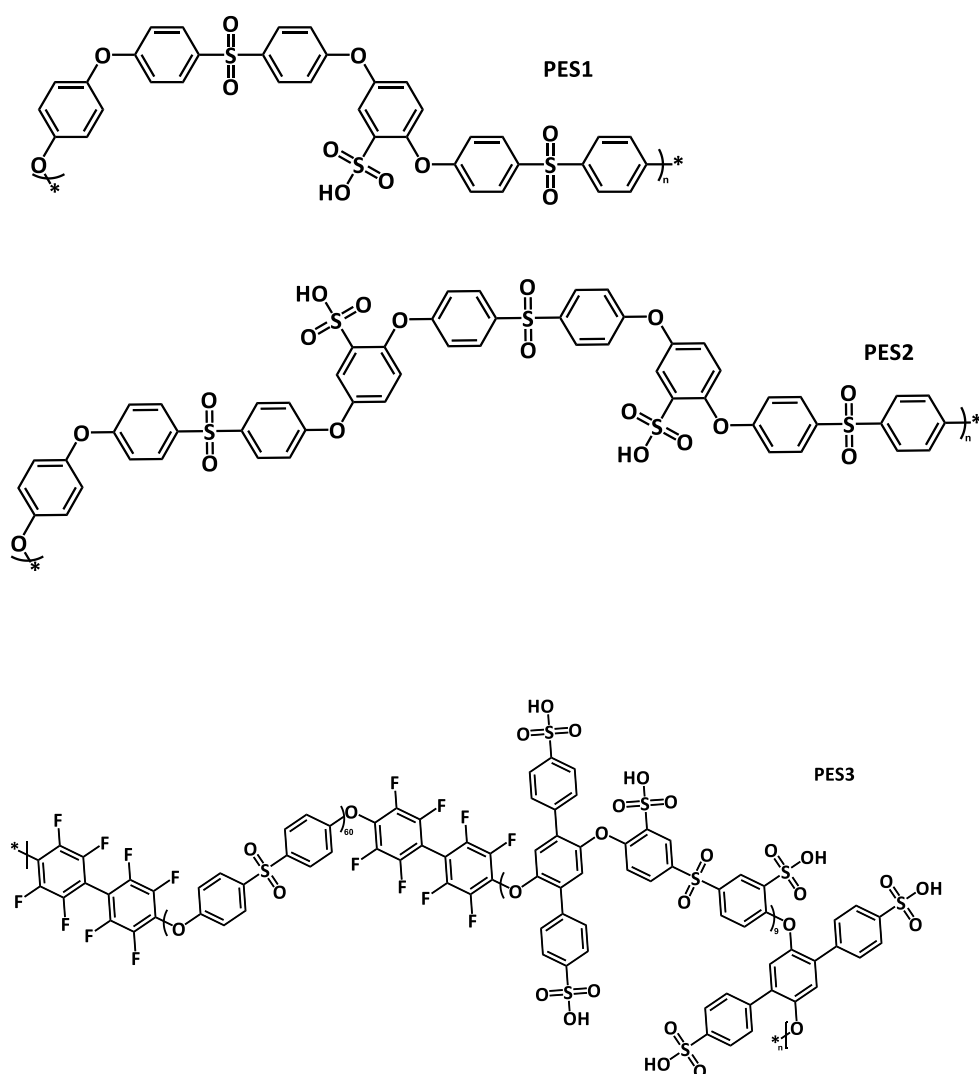
The first approach consisted of casting thin membranes, of thicknesses below 100 μm , from these polymers and lithiating them. As a result of this procedure, the proton in the $-\text{SO}_3\text{H}$ groups would be replaced by lithium ions. Unfortunately, cells built with such separators did not function. One possibility to explain this is that the available polymers had been degraded over time, so the idea had to be abandoned. Next, the decision was taken to use the polymer as additive to the commercial membrane. The $-\text{SO}_3\text{H}$ groups would then interact with the lithium polysulphides and retain them. After some preliminary tests, the approach was considered promising.

The membranes were prepared as follows. The commercial separators Celgard 2325 were cut to the coin-cell fitting size. The Celgard separator was chosen over the Freudenberg because its smooth surface allows for more control and a more even distribution of the polymer. They were then treated with O_2 plasma to ensure better adhesion of the added polymer. The PES was weighed and dissolved in a minimal amount of NMP. Then, the separator discs were placed on a smooth glass plate* and the polymer solution was dropped evenly on them. The time-lapse between plasma treatment and polymer addition was kept to be of five minutes. Special care had

* a bubble level was used to make sure that the plate was lying straight

to be taken to stay away from the edges – like this, the totality of the solution would remain on the separator and not spread on the glass plate. The prepared separators were left under the absorption hood until completely dry, then placed into a freezer at -18°C to facilitate their removal from the glass plate*. In the end, the separators were dried at 95°C for several hours, then stored in the argon-filled glovebox until cell construction.

Five different PES polymers have been tested within this work (**Figure 6.35**). They are all amorphous materials with T_g s lying highly above the room temperature. PES 1 and PES 2 do not contain the octafluorobiphenyl groups but all the polymers feature the $-\text{SO}_3\text{H}$ groups, which are one of the main points of interest. The quite rigid backbone confers mechanical stability to the whole system.



* at room temperature, the polymer easily adheres to the glass

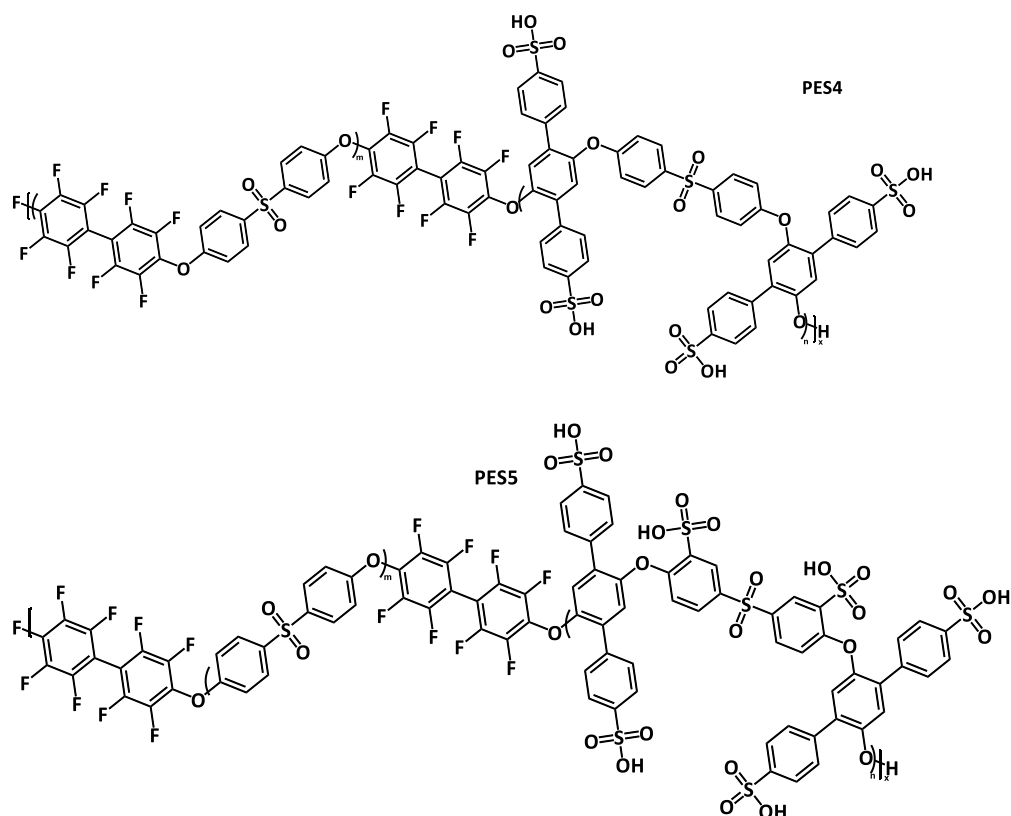


Figure 6.35 Chemical structures of polyethersulphone polymers: PES1 to PES5

To determine whether this approach is feasible and how much of the polymer is beneficial to the membrane, three different amounts of polymer have been tested: 0,25, 0,5 and 2,5 $\text{mg}\cdot\text{cm}^{-2}$. The Celgard membrane was taken as a base. This experiment has been conducted on the PES1, which is the most accessible of the five polymers (**Figure 6.36**).

The cells constructed with a PES coating on the separator are less stable than the standard cell – none of them reached even the 500 cycles threshold. Besides, all three curves show unstable behaviour even before the cell death. Nevertheless, the battery constructed using a small amount of PES1 shows an elevated capacity compared to the standard cell. Also, the character of the curve

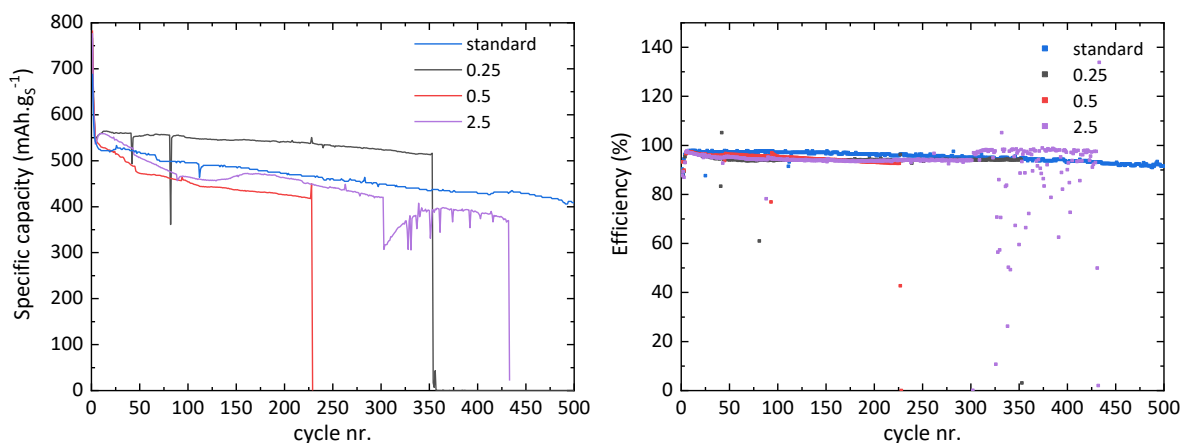


Figure 6.36 Cell performance in function of the amount of added PES. Measurements conducted between 1.8 and 2.6 V, with a current of 0.1C for discharge and 0.2C for charge

suggests that the reason for the cell's death lies in an accident such as a shortcut and not in the progressive decay. There are two possible explanations. Either the separator has been damaged during the preparation process, most likely when removing it from the glass plate, or the addition of the PES has tampered with the stability of the membrane. Even though both polymers have excellent individual chemical, thermal and mechanical stabilities, their behaviours under different conditions might not coincide, leading to a loss of the performance of the film.

To get a deeper insight into the processes during the cycling, the voltage profiles of the three samples have been plotted for three different chosen cycles (**Figure 6.37**).

Several conclusions can be drawn from these measurements. First of all, no additional artefacts are to be seen at any stage of cycling, which means that there are no side reactions taking place. On the other side, the voltages of the second plateau vary among the few chosen cycles, which has not been observed in the case of the standard cell (**Figure 6.3**). Since the second discharge plateau is associated with the reaction of formation of short molecules, a lower plateau implies a more profound barrier for the reaction to take place. There is no dependency on the cycle number – the variation of the voltage of the plateau is arbitrary. It indicates a certain instability of the cell. On the other side, when looking at the charging process, the overpotential

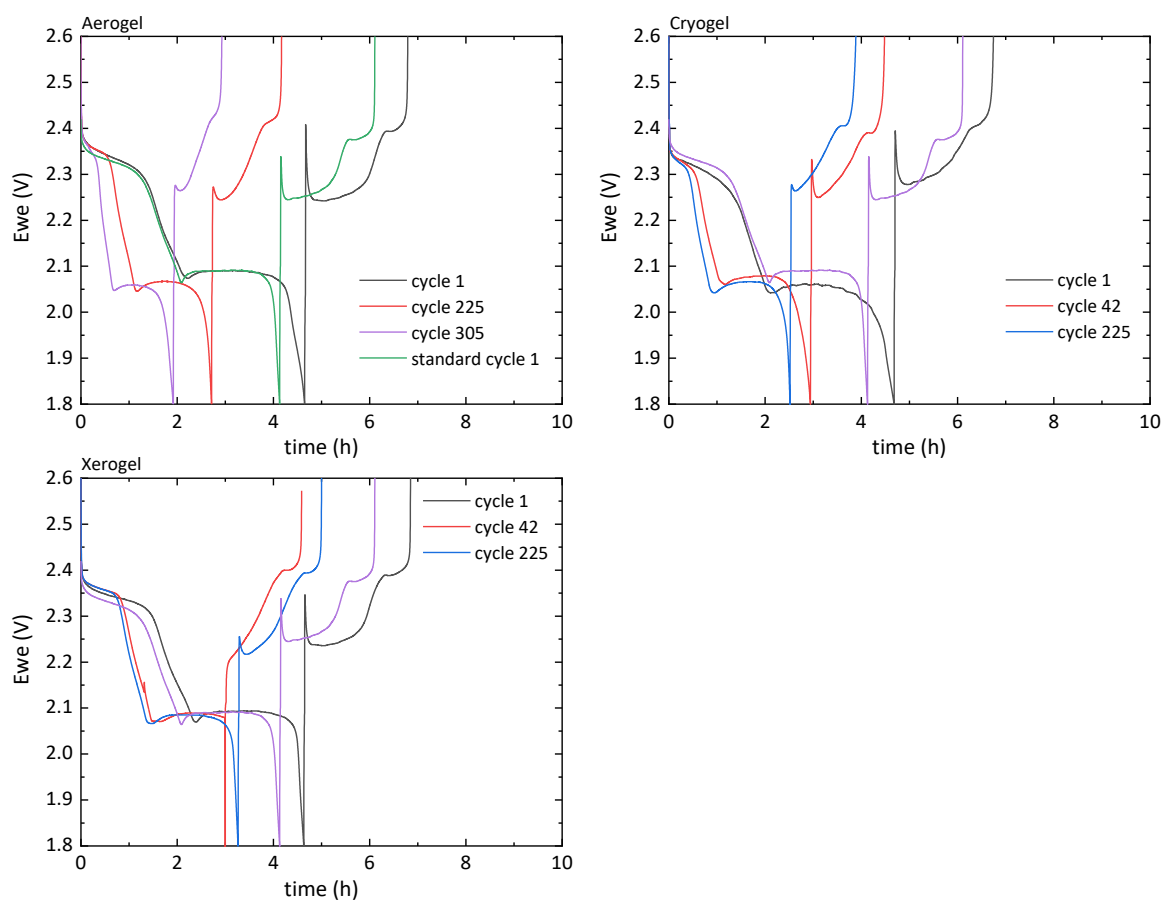


Figure 6.37 Voltage profile comparison of the different separator modifications.

phenomenon decreases throughout the cycles. When the voltage has to be raised to a level higher than the actual value at which the inverse reaction occurs, one can notice a sharp peak at the beginning of the charge. It corresponds to the effort necessary to get the reaction started. In the case of the lithium-sulphur batteries it arises from the need to react the solid Li_2S , which is harder than it is for the already dissolved salts. So, the further into the cell cycling one gets, the shorter the discharge curve becomes while the overpotential peak gets lower. Thus, the reactions in either direction are incomplete, which explains the performance loss over time.

There is the specific example of the 42nd cycle for the cell constructed with 2.5 mg.cm^{-2} of PES (**Figure 6.36**)– it corresponds to the strong capacity drop observed in **Figure 6.36**. In this case, the discharge curve does not follow the normal evolution, instead, there is a sudden voltage failure, which corresponds to an accident inside the cell. Still, the battery's functioning is re-established in the next cycle.

A small amount of PES coating is sufficient to increase the capacity of the cell. The $-\text{SO}_3\text{H}$ groups interact with the polysulphides, retaining them from migrating out of the cathode. If more PES is added, the porosity of the separator will decrease too significantly, hindering the proper execution of the electrochemical reaction. The amount of 0.25 mg.cm^{-2} is therefore retained for further experiments and consequently tested with the other polymers (**Figure 6.38**).

The performances of the test cells are overall worse than that of the standard cell: lower specific capacities and/or cycling stabilities. The exact nature of the used polymer does not play a significant role in the result: the sole fact of its addition impairs the functioning of the cell. The decisive factor lies in the uncooperative interaction between the membrane and the polymer.

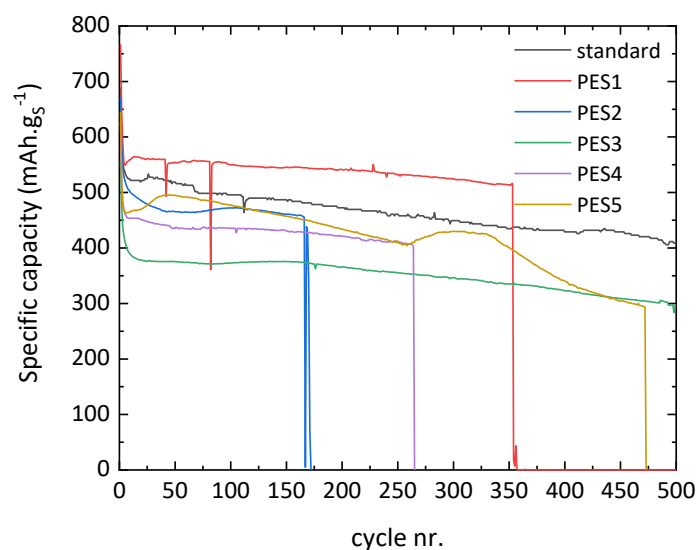


Figure 6.38 Cells constructed with separators coated with different PES polymers. Measurements conducted between 1.8 and 2.6 V, with a current of 0.1C for discharge and 0.2C for charge

Despite this failure, the idea of the separator modification to make it interact more intimately with the polysulphides and thus halt them from diffusing out of the cathode was deemed promising. A different approach was chosen, which would eliminate the issue of the interactions between the two materials, which is going to be discussed in the next chapter

6.4.2 Functionalization of the Celgard Separators

It is known that carbons functionalized with sulphur¹⁴⁸ or nitrogen^{149,150} retain the polysulphides better than pristine carbon materials, by chemisorption processes. There is less data regarding separators, and it often consists of complex and complicated structures¹⁵¹. This part of the thesis, therefore, handles the easy and scalable modification of commercially available separators.

The membranes have been made as follows. The Celgard separators were cut and treated with O₂ plasma, in order to introduce reactive groups on their surface. Polypropylene is chemically inert and, although it is the precise quality that makes it such a good material for use in batteries, it becomes a drawback when it comes to modification of the membrane. The treated polymer is immediately (in five minutes or less) placed into a glass crystallizer with concentrated sulphuric acid. Since the foil floats on the acid, it is placed with the treated face downwards. No stirring is applied since it would induce folds in the membrane. It is let to react for 18 hours. Afterwards, the foil is carefully removed from the acid and thoroughly washed with Millipore water. The washing process is conducted until the water has a neutral pH. It is then dried in the hood and in the drying oven at 95°C.

To verify the presence of sulphur-containing groups on the surface of the membrane several methods were considered. In the end EDX-analysis was chosen in order to confirm the modification (**Figure 6.39**). These results are given for two different magnifications. The sulphur and oxygen peaks are well recognisable in the modified sample. Since the Celgard membrane is composed of only polyethylene and polypropylene, these correspond to the -SO₃H groups. Still, the sulphur amount is quite low – the sulphur share is of approximately 0,1% of the total atom number. On the other hand, the measurement is performed over the total volume of the sample, so the amount of sulphur at the surface of the membrane is higher. Also, there is no significant difference between the results obtained at different magnifications: the sulphur-containing groups are evenly distributed on the surface of the sample.

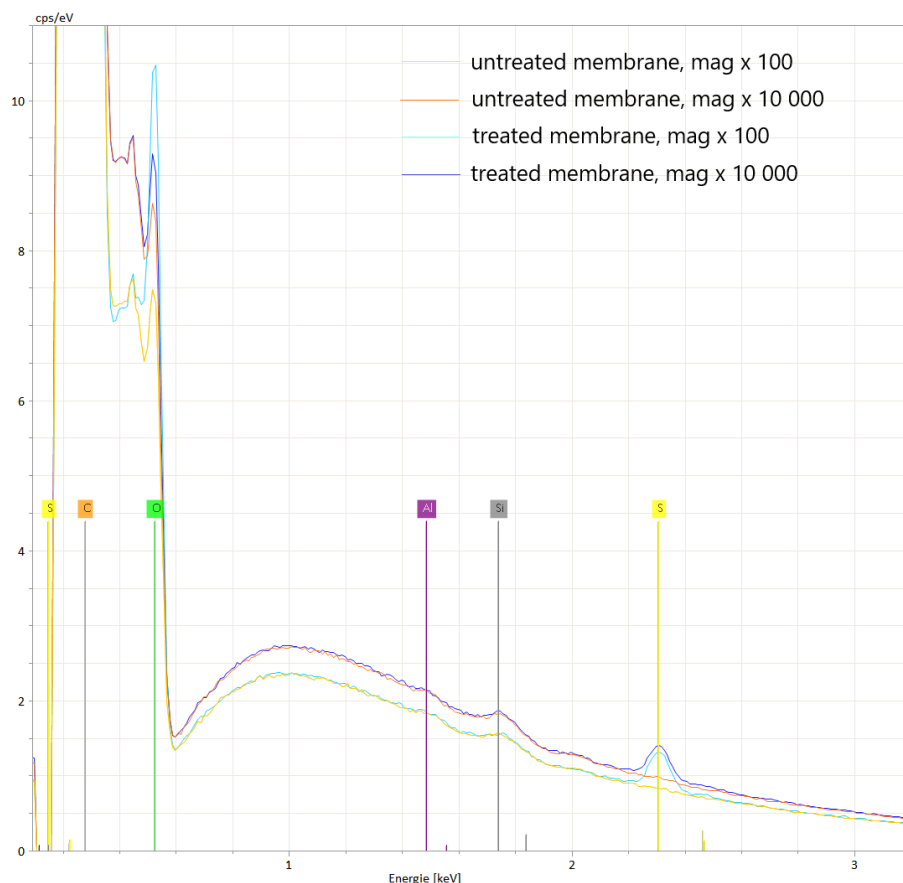


Figure 6.39 EDX spectra of untreated and treated Celgard membranes.

The effect of the functionalization of the separator membrane is studied for all the five available Celgard materials: C2320, C2325, C2340, H2512, H1612, that have been compared in 546.1.2.

EDX spectroscopy is a valuable, but time-consuming instrument, this is why it has not been used to analyse all the samples. Instead, the choice has been made in the favour of contact angle

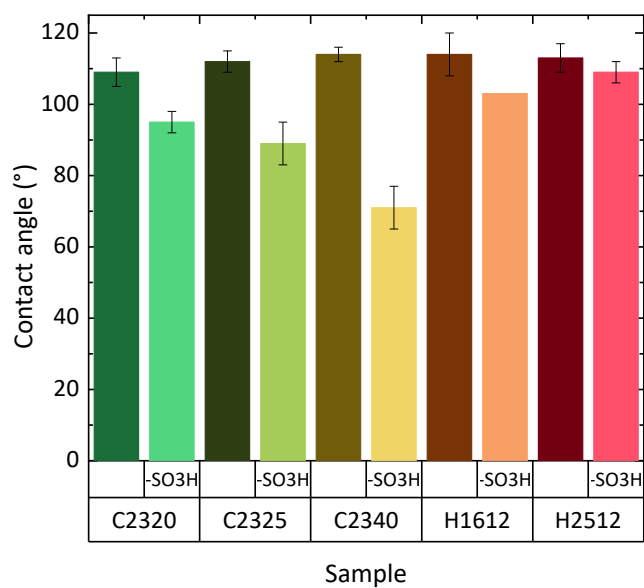


Figure 6.40 Comparison between contact angles of untreated and treated Celgard membranes.

measurements. Polypropylene is a hydrophobic material. The addition of polar groups to its surface should, therefore, raise its affinity to water and lower the contact angle. (**Figure 6.40**).

There is a striking difference between the C and the H series. The membranes featuring a lower Gurley index show an almost unchanged contact angle after the treatment. H1612 has the same porosity as C2340 while having a considerably lower thickness, while H2512 has the same thickness as C2325, but a higher porosity. Thin and porous materials have a more pronounced surface roughness, which can influence the result in two ways. On one side, it hinders the uniform plasma treatment and, therefore, functionalization, and on the other – their hydrophobic character is due both to the polymer's chemical structure and to the texture of the surface. In any case, all the membrane gained in hydrophilicity after treatment with sulphuric acid, which lends to the conclusion that all of them are functionalized.

Finally, the cells with the modified separators were constructed and cycled (**Figure 6.41**).

The capacities of the cells constructed with modified separators are at least as high as the capacities of the reference cells. In the case of C2340, exceeding the reference by approximately 10%. Regardless of the precautions taken when preparing the membranes, the treatment process introduced minor defects into the foil. The C2340 membrane is the one showing the best performance for the simple reason that, being the thickest from the lot, it is also the most robust and forgiving. In the same way, the cell constructed with the modified H1612 has the smallest cycle life, since the membrane itself is thin and extremely fragile. As a result, the addition of $-SO_3H$ groups to the surface of commercial separators has a positive effect on the performance of the cell, but the preparation method has to be better adapted to the task. One might, for instance, modify the polymers before casting the film.

When developing lithium-sulphur batteries, little attention is accorded to the separators. For this reason, the literature is relatively scarce on the subject. Nonetheless, there have been a certain number of attempts to enhance the cell's performance by working on the separator. Most of the efforts consisted in coating commercial separators with various substances¹⁵², such as Super P¹⁵³, N-doped carbon¹⁵⁴, Nafion⁶⁵, vanadium nitride¹⁵⁵ and others. The cells described in this work show results comparable to those seen in literature, even though they do not outperform them. Besides, there still is room for improvement, which means that even higher capacities and cycling stabilities could be achieved.

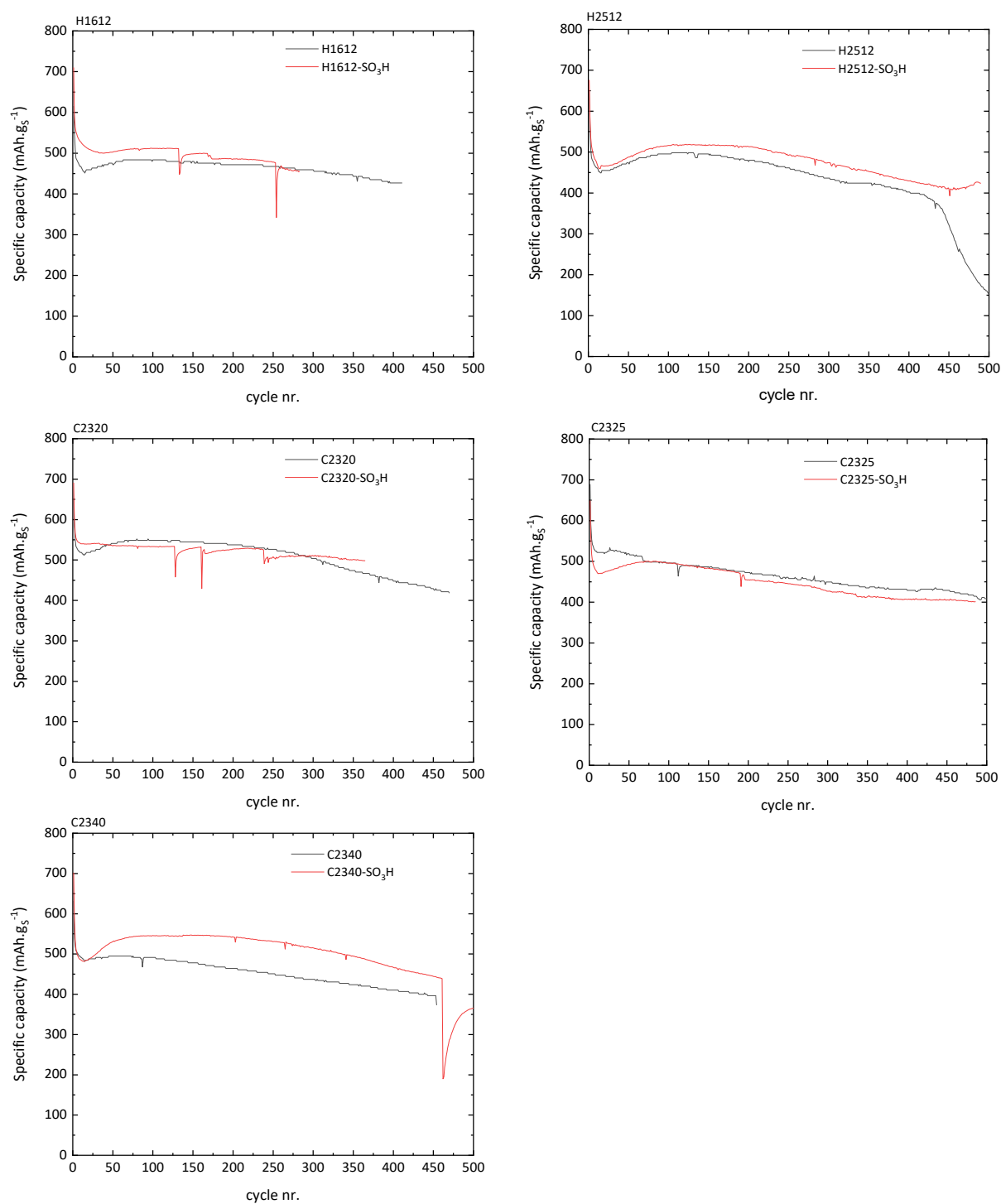


Figure 6.41 Electrochemical performance of the cells constructed with functionalized separators.

7 SUMMARY AND OUTLOOK

7.1 SUMMARY

The aim of this thesis was to analyse the electrochemical processes taking place inside a functioning Li-S cell and to modify the cell for better performance relying in part on the obtained information. The Li-S system has very promising properties, which are highly needed in the present conditions. It has a theoretical specific capacity that is six times higher than that of Li-ion batteries, and its components are cheap and non-toxic. However, although the Li-S system has been known for a long time, it is still not ready to be introduced to the market. The capacity of the experimentally prepared cells is significantly lower than the theoretic value, and it decays faster than tolerated in the case of, for example, electrical cars and portable devices. There are several reasons for such a mediocre performance, but the main one consists in the polysulphide shuttle – the dissolution of the reaction products in the electrolyte and their migration out of the cathode and through the cell. It is responsible for the loss of active material and the deactivation of the anode through the formation of an insoluble layer at its surface.

Therefore, the main topic of this work has been to observe the polysulphide shuttle processes taking place at different discharge and charge steps. For this reason, *in-operando* Raman spectroscopy analysis has been developed as part of this work. This study was meant to be a confirmation and complement to the already existing literature. Raman spectroscopy is a method that is perfectly adapted for the analysis of non-polar or slightly polar molecules, such as the lithium polysulphides. Besides, it is non-destructive, easily available and does not require any special preparations. Before any analysis could be performed, the cell had to be adapted to be penetrated by the visible light ray, while still being airtight and functioning electrochemically. The first approach consisted of the modification of a three-electrode Swagelok® cell by replacing the third electrode with a quartz window. Then, one could measure at the edge of the cell during the electrochemical cycling. The first experiment indicated that the chosen method allows observing the processes taking place inside the cell, but that several issues such as strong fluorescence and chaotic polysulphide appearance had to be addressed before the results could be deemed informative. This is why, the cell construction has been modified to stop the cathode carbon from travelling through the cell – thus the fluorescence has been strongly reduced. Also, the separators have been cut to have the same size as the electrodes, which allowed for a better orientation inside the cell via the optical microscope connected to the Raman device. Further improvements

could be made by utilizing cellulose material as separator, since its strong affinity with the polysulphides would route them to the outer edge, available to the Raman probe. All these modifications resulted in a cell in which numerous spectra characteristic of LiPS could be discerned during its cycling. Nonetheless, the main problem faced when measuring in such a cell configuration consisted of the edge effects and the poor extrapolation of the results to the interior of the cell. This is why the experiments have been continued using a modified coin cell, with a hole in the cell casing and the electrode. While one still had to rely on the diffusion of the formed entities, the reduced size of the hole and its location made the results more reliable. The experiments have been conducted on both cell sides and in parallel with analogous NEXAFS spectroscopy, performed at the BESSY II facility by project partners. In the end, we obtained a clear picture of the processes taking place inside the cell at different cycling steps and proved the good functioning of the developed test cell and method. The developed techniques could, in turn, also be applied to other systems.

Next, the study of organic gel-based carbons has been undertaken as a material for sulphur encapsulation. The carbon aerogels have been known for a longer time – they are appreciated for the very high porosity and specific surface area and the possibility to tailor the final structure by varying the synthesis conditions. Astonishingly, they did not get much attention in the context of Li-S batteries. The organic gels have been synthesized following a literature protocol, and the influence of the drying and pyrolysis conditions has been studied. An organic gel consists of a solvent trapped inside a polymeric 3D structure. The solvent has to be therefore replaced by gas before the gel is pyrolyzed and transformed into carbon. It can evidently just be left in ambient atmosphere, where the solvent would evaporate naturally but, by doing so, it damages the porous internal structure of the gel. The solvent can also be removed by freeze-drying technique: this method relies on the sublimation of a solid and is less destructive. Finally, the gentlest drying method consists of the critical point drying – the solvent is slowly replaced by CO_2 , which is a gas at normal conditions. This method is also the most time-taking. The second studied parameter was the pyrolysis temperature- the higher it is, the higher is the number of graphitic structures within the material. A variety of materials with different structures, specific surface areas and electric conductivities have been obtained and tested as encapsulation material for the sulphur cathode. The best results have been shown by the gels dried by critical point method – the initial discharge capacity was of around $1200 \text{ mAh.g}_\text{S}^{-1}$ and it remained higher than $500 \text{ mAh.g}_\text{S}^{-1}$ after 500 cycles. The materials dried by other methods showed lower performances, equivalent to that of the standard cell. This allowed deducing that the structure of the encapsulating material and not its specific surface area plays the main role in a LiS battery setup.

The polysulphide shuttle can potentially be hindered by the separator. It cannot stop their diffusion out of the cathode, but it can prevent them from reaching the anode. The third topic of this work was, therefore, the testing of several promising materials as separators for Li-S cells. First, an approach already successfully adopted within our research group has been tested, but no positive results have been obtained. Second, commercial separator foil has been coated with a polymer containing sulphonate groups, expecting these groups to interact with the polysulphides and hinder their diffusion. The resulting cells had capacities comparable to those of the standard cell but were considerably less stable. The capacity did not fade throughout the cycling but rather dropped suddenly, indicating accidents inside the cell – the interactions between polymers had a negative effect on the cell performance. It inspired the next approach, which consisted in modifying commercial separators by grafting sulphonate groups to them. This method being easy and fast, it can be easily transferred to industrial application. The obtained cells showed good performance (up to 10% higher compared to the standard cell), with one limitation: the modification process introduced folds into the separator membrane, which had a negative effect on the cell's stability. Although there are other systems with better results, the separators obtained within this work remain comparable to other developed materials.

To sum it up, this project permitted to gain deeper insight into the processes taking place inside a Li-S cell and originated materials enhancing the cell performance that are easy to manufacture industrially.

7.2 OUTLOOK

In order for the lithium-sulphur technology to take its due position amongst other accumulators, it needs higher capacities and longer cycling lives. Within this work, the processes taking place inside the cell are observed and characterized and new cathode and separator materials are investigated upon.

The polysulphide species present inside the cell at various DODs have been identified via *in-situ*, *in-operando* Raman spectroscopy. Since the available experimental data that could be used for the identification of the polysulphides is unreliable, data obtained by theoretical simulations is essential. For this reason, a logical continuation of the present work would consist in conducting own calculations. Also, more information could be potentially gathered by the spectroscopic method by lowering the cycling rate. In effect, if the reaction were kept slower, the lithium polysulphides would have more time to diffuse towards the focus point of the microscope. Besides, it is possible for the chosen rate to have an influence on the reaction by thermodynamic means.

Carbonized organic gels have been tested as possible encapsulation materials for the sulphur in the cathode and have proved themselves worthy. Among the three drying methods that have been tested, the critical point drying turned out to be optimal. Nonetheless, the freeze drying could also be appropriate if conducted using another solvent. In effect, the water expands upon freezing, thus damaging the fragile gel. A solvent whose volume remains constant could enable freeze-drying the material without causing damage to it. Since the porous structure of the material is of primary importance, the next step in this topic is to study the influence of the synthesis conditions of the organic gel on the performance of the cell. One can thus tailor the porosity and pore volumes of the material.

As far as the separator materials are concerned, only minor enhancements could be occasioned by the modification of commercial separators conducted within this work. Nevertheless, the approach proved to be promising and should, therefore, be further investigated. The main issue to be addressed consists in the macroscopic defects introduced to the commercial separators when handling them. One possible approach consists in modifying the polymers before casting the membrane. It has another advantage: polymer powder has a surface area that is much higher than that of a film, which implies that the grafted groups will be better dispersed through the membrane. The density of the sulphonate groups at the surface of the separator is quite low, which is explained by the extreme unreactivity of the polypropylene. One might, therefore,

consider applying more intense plasma treatment or pre-treat the membrane by chemical methods.

8 REFERENCES

- (1) Fossil fuels still dominate U.S. energy consumption despite recent market share decline - Today in Energy - U.S. Energy Information Administration (EIA) <https://www.eia.gov/todayinenergy/detail.php?id=26912> (accessed Sep 24, 2019).
- (2) Crutzen, P. J. *Nature* **2002**, 415 (6867).
- (3) Schlögl, R. De Gruyter: Berlin, Boston 2012.
- (4) Landrigan, P. J. *Lancet Public Heal.* **2017**, 2 (1), E4–E5.
- (5) Edenhofer, O. *Climate change 2014: mitigation of climate change*; Cambridge University Press, 2015; Vol. 3.
- (6) Fraunhofer ISE. Net public electricity generation in Germany in 2019 https://www.energy-charts.de/energy_pie.htm.
- (7) Van Asselt, A.; Reindl, D. T.; Nellis, G. F. *Sci. Technol. Built Environ.* **2018**, 24 (7), 759–769.
- (8) How batteries changed the world <https://www.tonikenergy.com/blog/how-batteries-changed-the-world/> (accessed Aug 19, 2019).
- (9) Hill, M. K. *Understanding Environmental Pollution*; Cambridge University Press: Cambridge, 2010.
- (10) Gates Energy Products. *Rechargeable Batteries Applications Handbook*; Elsevier, 1998.
- (11) Adelhelm, P.; Hartmann, P.; Bender, C. L.; Busche, M.; Eufinger, C.; Janek, J. *Beilstein J. Nanotechnol.* **2015**, 6, 1016–1055.
- (12) Planté Battery – 1859 - MagLab <https://nationalmaglab.org/education/magnet-academy/history-of-electricity-magnetism/museum/plante-battery> (accessed May 6, 2019).
- (13) Pavlov, D. *Lead-Acid Batteries: Science and Technology*; Elsevier, 2011.
- (14) Nickel Cadmium Cell Technology https://www.accutronics.co.uk/pages/nickel_cadmium_cell_technology.html (accessed May 6, 2019).
- (15) Wenham, S. R.; Green, M. A.; Watt, M. E.; Corkish, R. *Applied Photovoltaics*; Routledge, 2006.
- (16) Duraman, N. P. H.; Lim, K. L.; Chan, S. L. I. In *Advances in Batteries for Medium and Large-Scale Energy Storage*; Elsevier, 2015; pp 563–586.
- (17) Johnson, N. M. *Altern. Fuels Adv. Veh. Technol. Improv. Environ. Perform.* **2014**, 582–631.
- (18) Shukla, A. J. *Power Sources* **2001**, 100 (1–2), 125–148.
- (19) *Lithium-Ion Batteries: Science and Technologies*; Yoshio, M., Brodd, R. J., Kozawa, A., Eds.; Springer New York: New York, NY, 2009.
- (20) Goodenough, J. B.; Kim, Y. *Chem. Mater.* **2010**, 22 (3), 587–603.
- (21) Kurzweil, P.; Garche, J. In *Lead-Acid Batteries for Future Automobiles*; Elsevier, 2017; pp 27–96.
- (22) Bini, M.; Capsoni, D.; Ferrari, S.; Quartarone, E.; Mustarelli, P. In *Rechargeable Lithium Batteries*; Elsevier, 2015; pp 1–17.
- (23) Fotouhi, A.; Auger, D.; O'Neill, L.; Cleaver, T.; Walus, S. *Energies* **2017**, 10 (12).
- (24) Recharge. *The Batteries Report 2018*; 2018.
- (25) Bruce, P. G.; Freunberger, S. A.; Hardwick, L. J.; Tarascon, J.-M. *Nat. Mater.* **2012**, 11 (1), 19–29.
- (26) Balaish, M.; Kraytsberg, A.; Ein-Eli, Y. *Phys. Chem. Chem. Phys.* **2014**, 16 (7), 2801–2822.
- (27) Barchasz, C.; Molton, F.; Duboc, C.; Leprêtre, J.-C.; Patoux, S.; Alloin, F. *Anal. Chem.* **2012**, 84 (9), 3973–3980.
- (28) Song, M.-K.; Cairns, E. J.; Zhang, Y. *Nanoscale* **2013**, 5 (6), 2186–2204.
- (29) Mikhaylik, Y. V.; Akridge, J. R. *J. Electrochem. Soc.* **2004**, 151 (11), A1969–A1976.
- (30) Lowe, M. A.; Gao, J.; Abruña, H. D. *RSC Adv.* **2014**, 4 (35), 18347–18353.
- (31) Stauffer, D.; Aharony, A. *Introduction to percolation theory*; Taylor & Francis, 2014.
- (32) Nan, C.; Lin, Z.; Liao, H.; Song, M.-K.; Li, Y.; Cairns, E. J. *J. Am. Chem. Soc.* **2014**, 136 (12), 4659–4663.
- (33) Fang, X.; Peng, H. *Small* **2015**, 11 (13), 1488–1511.

- (34) Kolosnitsyn, V. S.; Karaseva, E. V. *Russ. J. Electrochem.* **2008**, *44* (5), 506–509.
- (35) Chang, H. J.; Illott, A. J.; Trease, N. M.; Mohammadi, M.; Jerschow, A.; Grey, C. P. *J. Am. Chem. Soc.* **2015**, *137* (48), 15209–15216.
- (36) Li, W.; Yao, H.; Yan, K.; Zheng, G.; Liang, Z.; Chiang, Y.-M.; Cui, Y. *Nat. Commun.* **2015**, *6* (1).
- (37) Rong, G.; Zhang, X.; Zhao, W.; Qiu, Y.; Liu, M.; Ye, F.; Xu, Y.; Chen, J.; Hou, Y.; Li, W.; Duan, W.; Zhang, Y. *Adv. Mater.* **2017**, *29* (13), 1606187.
- (38) Nelson, J.; Misra, S.; Yang, Y.; Jackson, A.; Liu, Y.; Wang, H.; Dai, H.; Andrews, J. C.; Cui, Y.; Toney, M. F. *J. Am. Chem. Soc.* **2012**, *134* (14), 6337–6343.
- (39) Zhang, S. S. *J. Power Sources* **2013**, *231*, 153–162.
- (40) Hagen, M.; Hanselmann, D.; Ahlbrecht, K.; Maça, R.; Gerber, D.; Tübke, J. *Adv. Energy Mater.* **2015**, *5* (16), 1401986.
- (41) Cheng, X.-B.; Yan, C.; Huang, J.-Q.; Li, P.; Zhu, L.; Zhao, L.; Zhang, Y.; Zhu, W.; Yang, S.-T.; Zhang, Q. *Energy Storage Mater.* **2017**, *6*, 18–25.
- (42) Cleaver, T.; Kovacic, P.; Marinescu, M.; Zhang, T.; Offer, G. *J. Electrochem. Soc.* **2018**, *165* (1), A6029–A6033.
- (43) Liang, C.; Dudney, N. J.; Howe, J. Y. *Chem. Mater.* **2009**, *21* (19), 4724–4730.
- (44) Zhang, F.; Dong, Y.; Huang, Y.; Huang, G.; Zhang, X.; Wang, L. *J. Phys. Conf. Ser.* **2012**, *339*, 012003.
- (45) Ding, B.; Shen, L.; Xu, G.; Nie, P.; Zhang, X. *Electrochim. Acta* **2013**, *107*, 78–84.
- (46) Ji, X.; Lee, K. T.; Nazar, L. F. *Nat. Mater.* **2009**, *8* (6), 500–506.
- (47) Park, M.-S.; Jeong, B. O.; Kim, T. J.; Kim, S.; Kim, K. J.; Yu, J.-S.; Jung, Y.; Kim, Y.-J. *Carbon N. Y.* **2014**, *68*, 265–272.
- (48) Chung, S.-H.; Manthiram, A. *Electrochim. Acta* **2013**, *107*, 569–576.
- (49) Choudhury, S.; Azizi, M.; Raguzin, I.; Göbel, M.; Michel, S.; Simon, F.; Willomitzer, A.; Mechtcherine, V.; Stamm, M.; Ionov, L. *Phys. Chem. Chem. Phys.* **2017**, *19* (18), 11239–11248.
- (50) Chung, S.-H.; Manthiram, A. *Electrochem. commun.* **2014**, *38*, 91–95.
- (51) He, G.; Evers, S.; Liang, X.; Cuisinier, M.; Garsuch, A.; Nazar, L. F. *ACS Nano* **2013**, *7* (12), 10920–10930.
- (52) Stoller, M. D.; Park, S.; Zhu, Y.; An, J.; Ruoff, R. S. *Nano Lett.* **2008**, *8* (10), 3498–3502.
- (53) Pandolfo, a. G.; Hollenkamp, a. F. *J. Power Sources* **2006**, *157* (1), 11–27.
- (54) Wang, Z.; Dong, Y.; Li, H.; Zhao, Z.; Bin Wu, H.; Hao, C.; Liu, S.; Qiu, J.; Lou, X. W. *Nat. Commun.* **2014**, *5* (1), 5002.
- (55) Ji, X.; Evers, S.; Black, R.; Nazar, L. F. *Nat. Commun.* **2011**, *2* (1), 325.
- (56) Xin, S.; Gu, L.; Zhao, N.-H.; Yin, Y.-X.; Zhou, L.-J.; Guo, Y.-G.; Wan, L.-J. *J. Am. Chem. Soc.* **2012**, *134* (45), 18510–18513.
- (57) Xu, C.; Wu, Y.; Zhao, X.; Wang, X.; Du, G.; Zhang, J.; Tu, J. *J. Power Sources* **2015**, *275*, 22–25.
- (58) Kim, M.; Kang, S.-H.; Manuel, J.; Zhao, X.; Cho, K. K.; Ahn, J. H. *Mater. Res. Bull.* **2015**, *69*, 29–35.
- (59) Yang, X.; Zhang, L.; Zhang, F.; Huang, Y.; Chen, Y. *ACS Nano* **2014**, *8* (5), 5208–5215.
- (60) Wang, Z.; Dou, Z.; Cui, Y.; Yang, Y.; Wang, Z.; Qian, G. *Microporous Mesoporous Mater.* **2014**, *185*, 92–96.
- (61) Liu, Y.; Guo, J.; Zhang, J.; Su, Q.; Du, G. *Appl. Surf. Sci.* **2015**, *324*, 399–404.
- (62) Zhou, W.; Xiao, X.; Cai, M.; Yang, L. *Nano Lett.* **2014**, *14* (9), 5250–5256.
- (63) Wang, H.; Yang, Y.; Liang, Y.; Robinson, J. T.; Li, Y.; Jackson, A.; Cui, Y.; Dai, H. *Nano Lett.* **2011**, *11* (7), 2644–2647.
- (64) Choi, J.-W.; Kim, J.-K.; Cheruvally, G.; Ahn, J.-H.; Ahn, H.-J.; Kim, K.-W. *Electrochim. Acta* **2007**, *52* (5), 2075–2082.
- (65) Bauer, I.; Thieme, S.; Brückner, J.; Althues, H.; Kaskel, S. *J. Power Sources* **2014**, *251*, 417–422.
- (66) Jin, Z.; Xie, K.; Hong, X.; Hu, Z.; Liu, X. *J. Power Sources* **2012**, *218*, 163–167.
- (67) Freitag, A.; Langklotz, U.; Rost, A.; Stamm, M.; Ionov, L. *Energy Storage Mater.* **2017**, *9*, 105–111.
- (68) Hassoun, J.; Scrosati, B. *Adv. Mater.* **2010**, *22* (45), 5198–5201.

- (69) Yamada, T.; Ito, S.; Omoda, R.; Watanabe, T.; Aihara, Y.; Agostini, M.; Ulissi, U.; Hassoun, J.; Scrosati, B. *J. Electrochem. Soc.* **2015**, *162* (4), A646–A651.
- (70) Gao, J.; Lowe, M. A.; Kiya, Y.; Abruña, H. D. *J. Phys. Chem. C* **2011**, *115* (50), 25132–25137.
- (71) Barchasz, C.; Leprêtre, J.-C.; Patoux, S.; Alloin, F. *Electrochim. Acta* **2013**, *89*, 737–743.
- (72) Chang, D.-R.; Lee, S.-H.; Kim, S.-W.; Kim, H.-T. *J. Power Sources* **2002**, *112* (2), 452–460.
- (73) Pang, Q.; Liang, X.; Kwok, C. Y.; Nazar, L. F. *Nat. Energy* **2016**, *1* (9), 16132.
- (74) Dominko, R.; Demir-Cakan, R.; Morcrette, M.; Tarascon, J.-M. *Electrochem. commun.* **2011**, *13* (2), 117–120.
- (75) Zhang, S.; Ueno, K.; Dokko, K.; Watanabe, M. *Adv. Energy Mater.* **2015**, *5* (16), 1500117.
- (76) Cuisinier, M.; Cabelguen, P.-E.; Adams, B. D.; Garsuch, A.; Balasubramanian, M.; Nazar, L. F. *Energy Environ. Sci.* **2014**, *7* (8), 2697–2705.
- (77) Scheers, J.; Fantini, S.; Johansson, P. *J. Power Sources* **2014**, *255*, 204–218.
- (78) Wang, L.; He, X.; Li, J.; Chen, M.; Gao, J.; Jiang, C. *Electrochim. Acta* **2012**, *72*, 114–119.
- (79) Zhang, W.; Qiao, D.; Pan, J.; Cao, Y.; Yang, H.; Ai, X. *Electrochim. Acta* **2013**, *87*, 497–502.
- (80) Krause, L. J.; Lamanna, W.; Summerfield, J.; Engle, M.; Korba, G.; Loch, R.; Atanasoski, R. *J. Power Sources* **1997**, *68* (2), 320–325.
- (81) *Lithium Batteries*; Scrosati, B., Abraham, K. M., Van Schalkwijk, W., Hassoun, J., Eds.; John Wiley & Sons, Inc.: Hoboken, NJ, USA, 2013.
- (82) Aurbach, D.; Pollak, E.; Elazari, R.; Salitra, G.; Kelley, C. S.; Affinito, J. *J. Electrochem. Soc.* **2009**, *156* (8), A694–A702.
- (83) Shin, J. H.; Cairns, E. J. *J. Electrochem. Soc.* **2008**, *155* (5), A368–A373.
- (84) Yuan, L. X.; Feng, J. K.; Ai, X. P.; Cao, Y. L.; Chen, S. L.; Yang, H. X. *Electrochem. commun.* **2006**, *8* (4), 610–614.
- (85) Kim, S.; Jung, Y.; Park, S.-J. *J. Power Sources* **2005**, *152*, 272–277.
- (86) Rao, M.; Geng, X.; Li, X.; Hu, S.; Li, W. *J. Power Sources* **2012**, *212*, 179–185.
- (87) Xiong, S.; Xie, K.; Diao, Y.; Hong, X. *J. Power Sources* **2013**, *236*, 181–187.
- (88) Zheng, J.; Gu, M.; Chen, H.; Meduri, P.; Engelhard, M. H.; Zhang, J.-G.; Liu, J.; Xiao, J. *J. Mater. Chem. A* **2013**, *1* (29), 8464–8470.
- (89) Miao, R.; Yang, J.; Feng, X.; Jia, H.; Wang, J.; Nuli, Y. *J. Power Sources* **2014**, *271*, 291–297.
- (90) Kim, H.; Lee, J. T.; Lee, D.-C.; Oschatz, M.; Cho, W. Il; Kaskel, S.; Yushin, G. *Electrochem. commun.* **2013**, *36*, 38–41.
- (91) Cheng, X.-B.; Peng, H.-J.; Huang, J.-Q.; Wei, F.; Zhang, Q. *Small* **2014**, 4257–4263.
- (92) Jeong, S.; Bresser, D.; Buchholz, D.; Winter, M.; Passerini, S. *J. Power Sources* **2013**, *235*, 220–225.
- (93) Brückner, J.; Thieme, S.; Böttger-Hiller, F.; Bauer, I.; Grossmann, H. T.; Strubel, P.; Althues, H.; Spange, S.; Kaskel, S. *Adv. Funct. Mater.* **2014**, *24* (9), 1284–1289.
- (94) Elazari, R.; Salitra, G.; Gershinsky, G.; Garsuch, A.; Panchenko, A.; Aurbach, D. *Electrochem. commun.* **2012**, *14* (1), 21–24.
- (95) Waluś, S.; Barchasz, C.; Colin, J.-F.; Martin, J.-F.; Elkaïm, E.; Leprêtre, J.-C.; Alloin, F. *Chem. Commun.* **2013**, 49 (72), 7899–7901.
- (96) Cañas, N. A.; Wolf, S.; Wagner, N.; Friedrich, K. A. *J. Power Sources* **2013**, *226*, 313–319.
- (97) Marceau, H.; Kim, C.-S.; Paolella, A.; Ladouceur, S.; Lagacé, M.; Chaker, M.; Vijh, A.; Guerfi, A.; Julien, C. M.; Mauger, A.; Armand, M.; Hovington, P.; Zaghib, K. *J. Power Sources* **2016**, *319*, 247–254.
- (98) Patel, M. U. M.; Demir-Cakan, R.; Morcrette, M.; Tarascon, J.-M.; Gaberscek, M.; Dominko, R. *ChemSusChem* **2013**, *6* (7), 1177–1181.
- (99) Cañas, N. A.; Fronczek, D. N.; Wagner, N.; Latz, A.; Friedrich, K. A. *J. Phys. Chem. C* **2014**, *118* (23), 12106–12114.
- (100) Zou, Q.; Lu, Y.-C. *J. Phys. Chem. Lett.* **2016**, *7* (8), 1518–1525.
- (101) Zheng, D.; Qu, D.; Yang, X.-Q.; Yu, X.; Lee, H.-S.; Qu, D. *Adv. Energy Mater.* **2015**, *5* (16), 1401888.
- (102) Zheng, D.; Zhang, X.; Li, C.; McKinnon, M. E.; Sadok, R. G.; Qu, D.; Yu, X.; Lee, H.-S.; Yang, X.-Q.; Qu,

- D. J. *Electrochem. Soc.* **2015**, 162 (1), A203–A206.
- (103) O'Connor, D. J.; Sexton, B. A.; Smart, R. S. C. *Surface Analysis Methods in Materials Science*; Springer Series in Surface Sciences; Springer Berlin Heidelberg, 2013.
- (104) Lewis, I. R. *Handbook of Raman Spectroscopy*; CRC Press, 2001; Vol. 35.
- (105) Smekal, A. *Naturwissenschaften* **1923**, 11 (43), 873–875.
- (106) McCreery, R. L. *Meas. Sci. Technol.* **2001**, 12 (5), 653–654.
- (107) Mohammed, A. Theoretical Studies of Raman Scattering, Royal Institute of Technology, 2011.
- (108) Abramczyk, H. *Introduction to Laser Spectroscopy*; Elsevier, 2005.
- (109) Bloembergen, N. *Am. J. Phys.* **1967**, 35 (11), 989–1023.
- (110) Lindon, J. C.; Tranter, G. E.; Holmes, J. L. (John L. *Encyclopedia of spectroscopy and spectrometry*; Academic Press, 2000.
- (111) Golcuk, K.; Mandair, G. S.; Callender, A. F.; Sahar, N.; Kohn, D. H.; Morris, M. D. *Biochim. Biophys. Acta - Biomembr.* **2006**, 1758 (7), 868–873.
- (112) Wei, D.; Chen, S.; Liu, Q. *Appl. Spectrosc. Rev.* **2015**, 50 (5), 387–406.
- (113) Lesson 2. What is Raman spectroscopy | Nanophoton corp <https://www.nanophoton.net/raman-spectroscopy/lessons/lesson-2> (accessed Sep 24, 2019).
- (114) Stevens, O. A. C.; Hutchings, J.; Gray, W.; Vincent, R. L.; Day, J. C. *J. Biomed. Opt.* **2016**, 21 (8), 087002.
- (115) Helgaker, T.; Coriani, S.; Jørgensen, P.; Kristensen, K.; Olsen, J.; Ruud, K. *Chem. Rev.* **2012**, 112 (1), 543–631.
- (116) Chivers, T. *Nature*. 1974, pp 32–33.
- (117) Daly, F. P.; Brown, C. W. *J. Phys. Chem.* **1975**, 79 (4), 350–354.
- (118) Dubois, P.; Lelieur, J. P.; Lepoutre, G. *Inorg. Chem.* **1988**, 27 (1), 73–80.
- (119) Janz, G. J.; Roduner, E.; Coutts, J. W.; Downey, J. R. *Inorg. Chem.* **1976**, 15 (8), 1751–1754.
- (120) Yeon, J.-T.; Jang, J.-Y.; Han, J.-G.; Cho, J.; Lee, K. T.; Choi, N.-S. *J. Electrochem. Soc.* **2012**, 159 (8), A1308–A1314.
- (121) Wu, H.-L.; Huff, L. A.; Gewirth, A. A. *ACS Appl. Mater. Interfaces* **2015**, 7 (3), 1709–1719.
- (122) Bethune, D. S.; Luntz, A. C.; Sass, J. K.; Roe, D. K. *Surf. Sci.* **1988**, 197 (1–2), 44–66.
- (123) Hannauer, J.; Scheers, J.; Fullenwarth, J.; Fraisse, B.; Stievano, L.; Johansson, P. *ChemPhysChem* **2015**, 16 (13), 2755–2759.
- (124) Vinayan, B. P.; Diemant, T.; Lin, X. M.; Cambaz, M. A.; Golla-Schindler, U.; Kaiser, U.; Jürgen Behm, R.; Fichtner, M. *Adv. Mater. Interfaces* **2016**, 3 (19), 1600372.
- (125) Vinayan, B. P.; Schwarzburger, N. I.; Fichtner, M. *J. Mater. Chem. A* **2015**, 3 (13), 6810–6818.
- (126) ECC-Opto-Std | EL-CELL <https://el-cell.com/products/test-cells/optical-test-cells/ecc-opto-std> (accessed Jun 24, 2019).
- (127) Hagen, M.; Schiffels, P.; Hammer, M.; Dorfner, S.; Tubke, J.; Hoffmann, M. J.; Althues, H.; Kaskel, S. *J. Electrochem. Soc.* **2013**, 160 (8), A1205–A1214.
- (128) Dörfler, S.; Hagen, M.; Althues, H.; Tübke, J.; Kaskel, S.; Hoffmann, M. J. *Chem. Commun.* **2012**, 48 (34), 4097–4099.
- (129) Scanning Electron Microscopy (SEM) https://serc.carleton.edu/research_education/geochemsheets/techniques/SEM.html (accessed Jun 18, 2019).
- (130) Scanning Electron Microscopy - Nanoscience Instruments <https://www.nanoscience.com/techniques/scanning-electron-microscopy/> (accessed Jun 18, 2019).
- (131) Sing, K. S. W. *Pure Appl. Chem.* **1985**, 57 (4), 603–619.
- (132) Thommes, M.; Kaneko, K.; Neimark, A. V.; Olivier, J. P.; Rodriguez-Reinoso, F.; Rouquerol, J.; Sing, K. S. W. *Pure Appl. Chem.* **2015**, 87 (9–10), 1051–1069.
- (133) Contact angle - DataPhysics Instruments <https://www.dataphysics->

- instruments.com/knowledge/understanding-interfaces/contact-angle/ (accessed Sep 11, 2019).
- (134) Li, Q.; Yang, H.; Xie, L.; Yang, J.; Nuli, Y.; Wang, J. *Chem. Commun.* **2016**, 52 (92), 13479–13482.
 - (135) Yu, S.-H.; Huang, X.; Schwarz, K.; Huang, R.; Arias, T. A.; Brock, J. D.; Abruña, H. D. *Energy Environ. Sci.* **2018**, 11 (1), 202–210.
 - (136) Pekala, R. W. *J. Mater. Sci.* **1989**, 24 (9), 3221–3227.
 - (137) Raventós, M.; Duarte, S.; Alarcón, R. *Food Sci. Technol. Int.* **2002**, 8 (5), 269–284.
 - (138) Beckman, E. J. *Ind. Eng. Chem. Res.* **2003**, 42 (8), 1598–1602.
 - (139) Al-Muhtaseb, S. A.; Ritter, J. A. *Adv. Mater.* **2003**, 15 (2), 101–114.
 - (140) Zhang, S. .; Wang, J.; Shen, J.; Deng, Z. .; Lai, Z. .; Zhou, B.; Attia, S. .; Chen, L. . *Nanostructured Mater.* **1999**, 11 (3), 375–381.
 - (141) Childres, I.; Jauregui, L. A.; Park, W.; Cao, H.; Chen, Y. P. *New Dev. Phot. Mater. Res.* **2013**, 1.
 - (142) Zhang, B.; Qin, X.; Li, G. R.; Gao, X. P. *Energy Environ. Sci.* **2010**, 3 (10), 1531–1537.
 - (143) Li, X.; Cao, Y.; Qi, W.; Saraf, L. V.; Xiao, J.; Nie, Z.; Mietek, J.; Zhang, J.-G.; Schwenzer, B.; Liu, J. J. *Mater. Chem.* **2011**, 21 (41), 16603–16610.
 - (144) Wu, H.; Li, Y.; Ren, J.; Rao, D.; Zheng, Q.; Zhou, L.; Lin, D. *Nano Energy* **2019**, 55, 82–92.
 - (145) Gao, J.; Sun, C.; Xu, L.; Chen, J.; Wang, C.; Guo, D.; Chen, H. *J. Power Sources* **2018**, 382 (March), 179–189.
 - (146) Tang, Q.; Shan, Z.; Wang, L.; Qin, X.; Zhu, K.; Tian, J.; Liu, X. *J. Power Sources* **2014**, 246, 253–259.
 - (147) Vogel, C.; Komber, H.; Quetschke, A.; Butwilowski, W.; Pötschke, A.; Schlenstedt, K.; Meier-Haack, J. *React. Funct. Polym.* **2011**, 71 (8), 828–842.
 - (148) See, K. A.; Jun, Y.-S.; Gerbec, J. A.; Sprafke, J. K.; Wudl, F.; Stucky, G. D.; Seshadri, R. *ACS Appl. Mater. Interfaces* **2014**, 6 (14), 10908–10916.
 - (149) Zhou, L.; Lin, X.; Huang, T.; Yu, A. *Electrochim. Acta* **2014**, 116, 210–216.
 - (150) Song, J.; Gordin, M. L.; Xu, T.; Chen, S.; Yu, Z.; Sohn, H.; Lu, J.; Ren, Y.; Duan, Y.; Wang, D. *Angew. Chemie Int. Ed.* **2015**, 54 (14), 4325–4329.
 - (151) Chen, G.; Song, X.; Wang, S.; Wang, Y.; Gao, T.; Ding, L.-X.; Wang, H. *J. Memb. Sci.* **2018**, 548, 247–253.
 - (152) Xiang, Y.; Li, J.; Lei, J.; Liu, D.; Xie, Z.; Qu, D.; Li, K.; Deng, T.; Tang, H. *ChemSusChem* **2016**, 9 (21), 3023–3039.
 - (153) Chung, S.-H.; Manthiram, A. *Adv. Funct. Mater.* **2014**, 24 (33), 5299–5306.
 - (154) Stoeck, U.; Balach, J.; Klose, M.; Wadewitz, D.; Ahrens, E.; Eckert, J.; Giebeler, L. *J. Power Sources* **2016**, 309, 76–81.
 - (155) Song, Y.; Zhao, S.; Chen, Y.; Cai, J.; Li, J.; Yang, Q.; Sun, J.; Liu, Z. *ACS Appl. Mater. Interfaces* **2019**, 11 (6), 5687–5694.
 - (156) Scrosati, B. *J. Solid State Electrochem.* **2011**, 15 (7), 1623–1630.
 - (157) MEPs ban cadmium from power tool batteries and mercury from button cells | News | European Parliament <http://www.europarl.europa.eu/news/en/press-room/20131004IPR21519/meps-ban-cadmium-from-power-tool-batteries-and-mercury-from-button-cells> (accessed May 6, 2019).
 - (158) Wu, H.; Cui, Y. *Nano Today* **2012**, 7, 414–429.

9 APPENDIX

9.1 TABLE OF FIGURES

Figure 3.1 Energy consumption of the US over time, illustrating the never-ending growth of the amount of energy necessary for the functioning of the society	2
Figure 3.2 Energy storage compared by their share on overall energy stored sorted by type	3
Figure 4.1 Schematic representation of a battery cell and the connection possibilities of several cells: (A); parallel connection (B); series connection (C).	6
Figure 4.2 Comparison of different battery technologies according to their theoretic performances and already obtained practical results	7
Figure 4.3 Illustration of the working principle of a nickel-metal hydride battery	8
Figure 4.4 Selection of electrode materials based on the thermodynamic stability of the electrolyte	10
Figure 4.5 Market shares by type of battery within the transportation sector	11
Figure 4.6 Functioning principle of the Li-S battery; (A) open circuit, (B) beginning of discharge, (C) sulphur is reduced inside the cathode and the soluble lithium polysulphides migrate into the electrolyte, (D) recharge.....	12
Figure 4.7 Typical discharge curve of a Li-S battery	13
Figure 4.8 SEM images for an in-situ plating (a-c) and stripping (d-f) experiment of lithium in a standard electrolyte for Li-S batteries. The colours are added in function of the contrasts in greyscale. Scale bar: 20 μm	16
Figure 4.9 Schematic representation of sulphur-infiltrated CMK-3 carbon, copied from ⁴⁶	19
Figure 4.10 List of possible lithium salts for Li-S batteries	21
Figure 4.11 Nanostructured anode containing free and alloyed Li metal compared to standard Li-foil ⁹¹	23
Figure 4.12 Lithium polysulfides prepared with different stoichiometric proportions of reactants	25
Figure 4.13 Spectroscopic transitions underlying several types of vibrational spectroscopy ¹⁰⁶	28
Figure 4.14 Filter comparison for Raman instrumentation, illustrating the advantages and disadvantages of each possibility	29
Figure 4.15 Schematic representation of a Raman microscope.....	31
Figure 4.16 Schematic representation of the setup for optical biopsy via Raman spectroscopy	32
Figure 5.1 Schematic representation of the steps involved in the cathode preparation.....	43
Figure 5.2 Exploded view of a coin cell, picturing its solid components	44

Figure 5.3 Modified three-electrode Swagelok [®] cell for in-situ analysis; left: optic probe, right: Raman microscope	45
Figure 5.4 Coin cell modified for in-situ measurements; left: on cathode side, right: on anode side	46
Figure 5.5 Setup for cell analysis; left: initial setup, right: enhanced setup.....	46
Figure 5.6 Different possible electron beam interactions.....	47
Figure 5.7 Contact angle at solid-liquid-gas interface	50
Figure 6.1 Cathode material delaminating from the current collector	51
Figure 6.2 Binder and current collector comparison; left: capacities, right: efficiencies.	52
Figure 6.3 Voltage profiles comparison.....	53
Figure 6.4 SEM image of FS2190.	54
Figure 6.5 Comparison of different Celgard membranes; left: capacities, right: efficiencies.	57
Figure 6.6 Raman spectra of the Li-S cell components measured each by themselves.	58
Figure 6.7 Raman spectra of lithium polysulphide solutions prepared with different stoichiometric proportions.....	59
Figure 6.8 Raman analysis using a modified Swagelok [®] cell; direction of observation	59
Figure 6.9 In-situ Raman and associated voltage profile: first cell configuration.	60
Figure 6.10 Sulphur lines manifestation.....	60
Figure 6.11 Fluorescence phenomenon throughout the cycling.....	61
Figure 6.12 Cell images obtained by optic microscopy; left to right: anode, separator layers, cathode.	62
Figure 6.13 In-situ Raman and associated voltage profile: second cell configuration.	62
Figure 6.14 Spectra from first discharge plateau and transition region.....	63
Figure 6.15 Polysulphide absorbent separator; left: cellulose, right: printing paper.....	63
Figure 6.16 In-situ Raman and associated voltage profile: second cell configuration using printing paper as separator.	64
Figure 6.17 Peak intensities at different wavenumbers (in cm^{-1}) in relation to the electrochemical discharge curve.	65
Figure 6.18 Raman analysis on the cathode (left) and anode (right) sides using a modified coin cell.....	66
Figure 6.19 Comparison of the voltage profiles between a cell with and without hole.	66
Figure 6.20 In-situ Raman and associated voltage profile: cathode side.	67
Figure 6.21 In-situ Raman and associated voltage profile: anode side.	68
Figure 6.22 Peak intensities at different wavenumbers (in cm^{-1}) in relation with the electrochemical discharge curve; left: on the cathode side, right: on the anode side	69
Figure 6.23 Total polysulphide amount at the cathode side, obtained by left: NEXAFS and right: Raman ..	72

Figure 6.24 Exemplary reaction equation and potential structure of a resorcinol-formaldehyde resin	75
Figure 6.25 Preparation of carbon gels.	77
Figure 6.26 SEM images of the different gels: aerogel (A), cryogel (B) and xerogel (C) at different magnifications: 1500X (1) and 500X (2); the scale corresponds to 10 micrometres.....	79
Figure 6.27 SEM images of different carbon gels: aerogel (A), cryogel (B) and xerogel (C), carbonized at different temperatures: 750°C (1), 1000°C (2), 1250°C (3); the scale corresponds to 10 micrometres.....	80
Figure 6.28 Specific surface areas of the carbon gels determined via N ₂ Physisorption at 77 K and the BET equation.	81
Figure 6.29 Raman spectra of the organic gels.	82
Figure 6.30 Raman spectra of the carbonized gels.	82
Figure 6.31 Results of the conductivity measurements for the carbonized gels.	84
Figure 6.32 TGA results for cathode active materials containing carbon gels pyrolyzed at 1000°C, as well as for standard cathode material.	85
Figure 6.33 Electrochemical performance of the cells dried by three different methods in comparison with the standard cell.....	87
Figure 6.34 Influence of the pyrolysis temperature on the electrochemical performance of the cells.....	87
Figure 6.35 Chemical structures of polyethersulphone polymers: PES1 to PES5	92
Figure 6.36 Cell performance in function of the amount of added PES.....	92
Figure 6.37 Voltage profile comparison of the different separator modifications.	93
Figure 6.38 Cells constructed with separators coated with different PES polymers.	94
Figure 6.39 EDX spectra of untreated and treated Celgard membranes.	96
Figure 6.40 Comparison between contact angles of untreated and treated Celgard membranes.....	96
Figure 6.41 Electrochemical performance of the cells constructed with functionalized separators.	98

9.2 TABLE OF TABLES

Table 4.1 List of lithium metal battery systems ¹⁹	9
Table 4.2 Literature concentrating on the analysis of polysulphide chains	35
Table 4.3 Raman analysis of Lithium-sulphur batteries	37
Table 5.1 List of Used Materials with their Purity	42
Table 6.1 Separator material properties as provided by the supplier	56
Table 6.2 Separator Peak ratios for different carbon gels	83
Table 6.3 Amount of sulphur in the cathode material	86

10 ERKLÄRUNG GEMÄß §5 Abs. 1 PUNKT 5

§5 Abs. 1 Punkt 5a

Versicherung

Hiermit versichere ich, dass ich die vorliegende Arbeit ohne unzulässige Hilfe Dritter und ohne Benutzung anderer als der angegebenen Hilfsmittel angefertigt habe; die aus fremden Quellen direkt oder indirekt übernommenen Gedanken sind als solche kenntlich gemacht. Die Arbeit wurde bisher weder im Inland noch im Ausland in gleicher oder ähnlicher Form einer anderen Prüfungsbehörde vorgelegt.

§5 Abs. 1 Punkt 5b

Die vorliegende Arbeit wurde am Leibniz-Institut für Polymerforschung Dresden e.V. im Zeitraum von 11/2015 bis 10/2019 als eingeschriebener Promotionsstudent und unter wissenschaftlicher Betreuung von Prof. Dr. Manfred Stamm angefertigt.

Datum, Unterschrift